ELECTROMAGNETIC MODAL ANALYSIS OF CIRCULAR - RECTANGULAR WAVEGUIDE STRUCTURES FOR COMBLINE FILTER DESIGN

By

HAIYIN WANG, M.E.

A Dissertation

Submitted to the School of Graduate Studies

in Partial Fulfillment of the Requirements

for the Degree

Doctor of Philosophy

2002

McMaster University

ELECTROMAGNETIC MODAL ANALYSIS OF C- R WAVEGUIDE STRUCTURES

DOCTOR OF PHILOSOPHY (2002) **McMaster University**

(Electrical and Computer Engineering) **Hamilton, Ontario**

TITLE: **Electromagnetic Modal Analysis of Circular-Rectangular Waveguide Structures for Combline Filter Design**

AUTHOR: **Haiyin Wang, M.E. (Memorial University of NF)**

SUPERVISOR: **Professor J. Litva**

Professor K. Wu

NUMBER OF PAGES: **xxi, 115**

Abstract

Title of Dissertation: ELECTROMAGNETIC MODAL ANALYSIS OF CIRCULAR - RECTANGULAR WAVEGUIDE STRUCTURES FOR COMBLINE FILTER DESIGN

Haiyin Wang , Doctor of Philosophy, 2002

Dissertation directed by : Professor John Litva
Department of Electrical and Computer Engineering
McMaster University
and
Professor Ke-Li Wu
Department of Electronic Engineering
The Chinese University of Hong Kong

The rapid growth in mobile and satellite communications has intensified the requirements for good performance, compact structure, high quality and low cost waveguide filters and diplexers. This dissertation is devoted to the full wave analysis and modeling of various circular-rectangular (C-R) coaxial waveguide structures which are commonly used to develop combline filters and diplexers. Specifically, models that can be cascaded to simulate the system performance of the filters and diplexers are being sought in the dissertation. The research includes three parts: (1) modal analysis of the higher-order modes in the C-R waveguide; (2) modal analysis of the TEM mode in the C-R waveguide; and (3) the scattering characteristics of the right-angle bend and the T waveguide junctions loaded with a generic post.

A rigorous analysis, which combines the orthogonal expansion method and the Galerkin method, is performed to obtain the higher-order eigenmodes in the C-R waveguide. The Bessel-Fourier series is employed to merge the circular and rectangular coordinate systems used in the analysis. The cutoff frequencies of the higher-order modes are determined using the singular value decomposition (SVD) technique.

The modal solution of the TEM mode in the C-R waveguide is obtained by superposition of the resonant modes in an equivalent rectangular cavity loaded with a conducting post. The characteristic impedance and attenuation coefficient of the waveguide are derived from the solution of the TEM mode.

Analytic models of the right-angle bend and T-junctions loaded with posts of varying heights are derived. A novel technique of the extended eigen mode functions is developed to deal with the complex boundary conditions in the junction structures. The general scattering matrices of the right-angle bend and T- junctions are obtained.

Dedication

To my family, especially my grandparents.

Acknowledgements

I would like to express sincere thanks to my supervisor, Professor John Litva for offering me a great chance to work on the electromagnetic analysis of circular-rectangular waveguide structures, and for improving my papers and thesis several times. His continued support and timely encouragement have made my study at McMaster University enjoyable.

I would like to thank my co-advisor Dr. Ke-Li Wu for his suggestion of topics, for his valuable advices and guidance, and for the financial support on both doing research and attending a conference.

I greatly appreciate Professor David Conn and Professor Patrick Yip for their service as my supervisory committee and for their advices and assistances.

I would like to thank the graduate students, professors and staff of the department for creating a pleasant work surrounding.

I would like to thank the department for several-years of financial support.

And especially, I want to thank my family, my husband Jimmy, my daughter Julia and my parents for their understanding, their trust, their love and their support during my Ph.D. study.

Table of Contents

LIST of TABLES

LIST OF FIGURES

Numbers **Pages**

List of Symbols

Chapter 2

a : the half width of the outer conductor of the circular-rectangular waveguide.

b : the half height of the outer conductor of the circular-rectangular waveguide.

b_{cmn}^{tm} : the element of matrix **B** for TM mode.

b_{smn}^{te} : the element of matrix **B** for TE mode.

c_{cmn}^{tm} : the element of matrix **C** for TM mode.

c_{smn}^{te} : the element of matrix **C** for TE mode.

d_{cmn}^{tm} : the element of matrix **D** for TM mode.

d_{smn}^{te} : the element of matrix **D** for TE mode.

e_{m}^{tm} : the element of matrix **E** for TM mode.

e_{m}^{te} : the element of matrix **E** for TE mode.

E_{zI} / E_{zII}: the z component of the electric field without the factor $e^{\pm jk_z z}$ in region I / II for TM modes.

$E_{\phi I}$ / $E_{\phi II}$: the ϕ component of the electric field without the factor $e^{\pm jk_z z}$ in region I / II for TE modes.

f_{m}^{tm} : the element of matrix **F** for TM mode.

f_{m}^{te} : the element of matrix **F** for TE mode.

H_{xI} / H_{yI}: the x / y component of the magnetic field without the factor $e^{\pm jk_z z}$ in region I for TM modes.

H_{zI} / H_{zII}: the z component of the magnetic field without the factor $e^{\pm jk_z z}$ in region I / II for TE modes.

$H_{\phi I}$ / $H_{\phi II}$: the ϕ component of the magnetic field without the factor $e^{\pm jk_z z}$ in region I / II for TM modes.

$I_m(x)$: the modified Bessel function of the first kind of order m. $I_m(x) = j^{-m} J_m(jx)$, $j = \sqrt{-1}$.

$J_m(x)$: the Bessel function of the first kind of order m.

$J'_m(x)$: the derivative of the Bessel function of the first kind of order m.

k_c : the cut-off wavenumber (eigen wavenumber) in circular-rectangular waveguide. $k_c^2 = \omega^2\varepsilon\mu - k_z^2 = k_x^2 + k_y^2 = k_y^2 - (p_n / 2a)^2$.

k_y : the eigenvalue for the y variable. $k_y = n\pi/2b$

p_n: the part of eigenvalue for the x variable. $(\frac{p_n}{2a})^2 = -k_x^2$

r_0 : the radius of the inner conductor of the circular-rectangular waveguide.

x, y, z : the rectangular coordinates. $x = \rho\cos(\phi)$, $y = \rho\sin(\phi)$, $z = z$

$Y_m(x)$: the Bessel function of the second kind of order m.

$Y'_m(x)$: the derivative of the Bessel function of the second kind of order m.

ρ, ϕ, z : the cylindrical coordinates. $\rho = (x^2 + y^2)^{1/2}$, $\phi = tg^{-1}(x/y)$

$\Phi_m(\phi) = \begin{Bmatrix} \sin(m\phi) \\ \cos(m\phi) \end{Bmatrix}$ or $\begin{Bmatrix} \cos(m\phi) \\ \sin(m\phi) \end{Bmatrix}$: eigen function of ϕ .

ψ_{In} / ψ_{IIn}: the coefficient of the eigenfields in region I / II.

Chapter 3

{**A**}, {**B**} : the coefficient vectors of the incident and reflected fields in region I and II with the reference plane at z = 0.

{**A'**} : the coefficient vector of the incident field with the reference plane at the end of cavity.

A_{mi}^{Ip}, B_{mi}^{Ip}, A_{mi}^{IIp}, B_{mi}^{IIp} : the field coefficients for the incident and reflected modes in region I and II, p = e for TM modes and p = h for TE modes.

C_{n1}^{p}, D_{n1}^{p} : the field coefficients in the cylindrical region, p = e for TM modes and p = h for TE modes.

E_z^I / E_z^{II} : the longitudinal component of the electric field in waveguide region I / II.

E_t^I / E_t^{II} : the transverse component of the electric field in waveguide region I / II.

e_{xm1}^{p}, e_{ym1}^{p}, e_{zm1}^{p}: x, y, z components of mode functions for the electric field, p = e for TM modes, p = h for TE modes.

e_{tm1}^{IIIp} : the transverse component of the mode function for the electric field in region III, p = e for TM modes and p = h for TE modes.

E_ρ^{III} : the longitudinal component of the electric field with respect to the ρ direction in the cylindrical region.

E_t^{III} : the transverse component of the electric field in the cylindrical region.

H_z^I / H_z^{II} : the longitudinal component of the magnetic field in waveguide region I / II.

H_t^I / H_t^{II} : the transverse component of the magnetic field in waveguide region I / II.

h_{zm1}^p, h_{xm1}^p, h_{ym1}^p : x, y, z components of mode functions for the magnetic field, $p = e$ for TM modes, $p = h$ for TE modes.

h_{tm1}^{IIIp} : the transverse component of the mode function for the magnetic field in region III, $p = e$ for TM modes and $p = h$ for TE modes.

H_ρ^{III} : the ρ component of the magnetic field in the cylindrical region.

H_t^{III} : the transverse component of the magnetic field in the cylindrical region.

H_ϕ^{III} : the ϕ component of the magnetic field in the cylindrical region.

I : the total current flowing on the inner conductor.

$\mathbf{J}_{ne}$: the submatrix of **W** matrix; its order is $N_e \times N_e$ and its elements are the Bessel functions of the first kind.

$\mathbf{J'}_{nh}$: the submatrix of **W** matrix; its order is $N_h \times N_h$ and its elements are the derivative of the Bessel functions of the first kind.

k_c : the cut-off wavenumber in waveguide region with respect to the z direction.

$$k_c^2 = k_{xm}^2 + k_{yl}^2 = k_0^2 + \gamma_{ml}^2.$$

k_{xm}, k_{yl} : the wavenumber along the x and y directions in region I and II.

k_{yl} : the wavenumber along the y direction in region III.

P_c : the power loss per unit length of the c-r coaxial waveguide.

P_0 : the power flowing on the line.

R_s : the surface resistance of the conductor.

S : the generalized scattering matrix of the rectangular resonator loaded with the full height post.

V : the voltage between inner and outer conductors of a C-R coaxial waveguide.

V_n^e, V_n^h : the results of integrating E_ρ^{III} for TM and TE modes in waveguide region III.

X : the matrix which connects the field coefficient vector in region III and the field coefficient vector in region I and II.

x, y, z : the rectangular coordinate system.

$\mathbf{Y}_{ne}$: the submatrix of **W** matrix; its order is $N_e \times N_e$ and its elements are the Bessel functions of the second kind.

$\mathbf{Y'}_{nh}$: the submatrix of **W** matrix; its order is $N_h \times N_h$ and its elements are the derivative of the Bessel functions of the second kind.

Z : the characteristic impedance of the C-R coaxial waveguide.

α : The attenuation coefficient of the C-R coaxial waveguide.

γ_{zm1} : the propagation/attenuation constant along the z direction in region I and II.

η_1 : the cut-off wavenumber in the cylindrical region with respect to the y direction.

$$\eta_1^2 = k_0^2 - k_{y1}^2.$$

ρ, ϕ, y : the cylindrical coordinate system.

Chapter 4

A_q^{Vp}, B_q^{Vp}: the field coefficients in region V, p = h for TE modes and p = e for TM modes.

A_q^{VIp}, B_q^{VIp}: the field coefficients in region VI, p = h for TE modes and p = e for TM modes.

$A_{p,j}^{iuv}$, $B_{p,j}^{iuv}$: the incident and reflected field coefficients of the pth normal modes for jth extended eigen mode functions, i = I, II for cavity region I and II, u = e or u = h for TM or TE modes, v = e or v = h for TM or TE incident mode.

$\mathbf{A}^{\mathrm{I}}$, $\mathbf{B}^{\mathrm{I}}$, $\mathbf{A}^{\mathrm{II}}$ and $\mathbf{B}^{\mathrm{II}}$: the coefficient matrices for incident and reflected modes respectively in region I and II.

C_j^h, C_j^e: the field coefficients in cavity region I and II for TE and TM incident modes.

D_j^h, D_j^e: the field coefficients in cavity region I' and II' for TE and TM incident modes.

$\mathbf{C}^{\mathrm{h}}$, $\mathbf{C}^{\mathrm{e}}$, $\mathbf{D}^{\mathrm{h}}$ and $\mathbf{D}^{\mathrm{e}}$: the field coefficient vectors for the extended eigen modes in cavity regions of the horizontal and vertical waveguides.

E_t^V, H_t^V: the transverse components of electric and magnetic fields in region V.

E_t^{VI}, H_t^{VI}: the transverse components of electric and magnetic fields in region VI.

$\tilde{\mathbf{E}}^{\mathrm{Iz}}$, $\tilde{\mathbf{H}}^{Iz}$: the total electric and magnetic fields in cavity region I.

$\tilde{\mathbf{E}}^{IIz}$, $\tilde{\mathbf{H}}^{IIz}$: the total electric and magnetic fields in cavity region II.

$\tilde{\mathbf{E}}^{\mathrm{I'x}}$, $\tilde{\mathbf{H}}^{I'x}$: the total electric and magnetic fields in cavity region I'.

$\tilde{\mathbf{E}}^{II'x}$, $\tilde{\mathbf{H}}^{II'x}$: the total electric and magnetic fields in cavity region II'.

e_{zq}^{ez}, $\hat{e}_{tq}^{hz}$, $\hat{e}_{tq}^{ez}$, h_{zq}^{hz}, $\hat{h}_{tq}^{hz}$ and $\hat{h}_{tq}^{ez}$: the longitudinal and transverse modes for electric and magnetic fields in the horizontal one-port waveguide. q is a pair of m, i for a mode.

e_{xq}^{ex}, $\hat{e}_{tq}^{hx}$, $\hat{e}_{tq}^{ex}$, h_{xq}^{hx}, $\hat{h}_{tq}^{hx}$ and $\hat{h}_{tq}^{ex}$: the longitudinal and transverse modes for electric and magnetic fields in the vertical one-port waveguide. q is a pair of m, i for a mode.

k_{cz} : the cut-off wavenumber with respect to the z direction. $k_{cz}^2 = k_{xm}^2 + k_{yi}^2 = \gamma_{zmi}^2 + k_0^2$

k_{xm}, k_{yi} : the wavenumber along the x and y directions. $k_{xm} = \frac{m\pi}{2a}$, $k_{yi} = \frac{i\pi}{b}$.

k_{cx} : the cut-off wavenumber with respect to the x direction. $k_{cx}^2 = k_{zm}^2 + k_{yi}^2 = \gamma_{xmi}^2 + k_0^2$

k_{zm}, k_{yi} : the wavenumber along the x and y directions. $k_{zm} = \frac{m\pi}{2a}$, $k_{yi} = \frac{i\pi}{b}$.

[M] : the matrix which connects the coefficient vectors in cavity regions and in waveguide regions V and VI by using magnetic field continuity.

$[\mathbf{S}]_2$: the general scattering matrix for a straight two-port waveguide loaded with a post. The reference plane is at z = 0.

$[\mathbf{S}']_2$: the generalized scattering matrix of two-port waveguide with one of the reference planes moved to z = -a.

$\mathbf{S}_{11}$, $\mathbf{S}_{12}$, $\mathbf{S}_{21}$ and $\mathbf{S}_{22}$: the submatrices of $[\mathbf{S}]_2$.

$\mathbf{S}'_{11}$, $\mathbf{S}'_{12}$, $\mathbf{S}'_{21}$ and $\mathbf{S}'_{22}$: the submatrices of $[\mathbf{S}']_2$.

[S] : the generalized scattering matrix for bend or T junction loaded with a varying post.

[U] : the matrix which connects the coefficient vectors in cavity regions and in waveguide regions V and VI by using electric field continuity.

γ_{xmi} : the propagation/attenuation coefficient along the x direction.

γ_{zmi} : the propagation/attenuation coefficient along the z direction.

$\vec{\phi}_j^{hI}$, $\vec{\phi}_j^{eI}$: the extended eigen mode functions for electric field in cavity region I.

The superscripts *h* / *e* mean TE / TM incident modes.

$\vec{\phi}_j^{hII}$, $\vec{\phi}_j^{eII}$: the extended eigen mode functions for electric field in cavity region II. The superscripts *h* / *e* mean TE / TM incident modes.

$\vec{\phi}_j^{hI'}$, $\vec{\phi}_j^{eI'}$: the extended eigen mode functions for electric field in cavity region I'.

The superscripts *h* / *e* mean TE / TM incident modes.

$\vec{\phi}_j^{hII'}$, $\vec{\phi}_j^{eII'}$: the extended eigen mode functions for electric field in cavity region II'. The superscripts *h* / *e* mean TE / TM incident modes.

$\vec{\psi}_j^{hI}$, $\vec{\psi}_j^{eI}$: the extended eigen mode functions for magnetic field in cavity region I. The superscripts *h* / *e* mean TE / TM incident modes.

$\vec{\psi}_j^{hII}$, $\vec{\psi}_j^{eII}$: the extended eigen mode functions for magnetic field in cavity region II.

The superscripts *h* / *e* mean TE / TM incident modes.

$\vec{\psi}_j^{hI'}$, $\vec{\psi}_j^{eI'}$: the extended eigen mode functions for magnetic field in cavity region I'. The superscripts *h* / *e* mean TE / TM incident modes.

$\vec{\psi}_j^{hII'}$, $\vec{\psi}_j^{eII'}$: the extended eigen mode functions for magnetic field in cavity region II'.

The superscripts *h* / *e* mean TE / TM incident modes.

Chapter 1

Introduction

Historical Review

Waveguide combline filters have found many applications in mobile and satellite communication systems due to their excellent electric performance, small size, high power handling capability, and low cost. Full-wave electromagnetic field analyses combined with numerical algorithms can provide an accurate and effective means of designing novel and compact filters [1][2][3].

Elliptic function combline filters with finite transmission zeros possess many desirable features such as high frequency selectivity, high stop band rejection and low pass-band loss [4][5][6]. Since evanescent modes are employed, the combline filter is more compact than other types of waveguide filters. Filled with high ε_r dielectric materials, the dimensions of the filter will be further reduced by a factor of $\sqrt{\varepsilon_r}$, so that it can be mounted on the PCB board which is used in a cellular phone [7][8][9][10][11].

In practice, the structure of the insert reentrant coaxial resonator is used to improve the power handling ability, temperature compensation and spurious performance of the filter [12][13][14]. These advantages make combline waveguide filters very attractive microwave components in today's highly competitive market place. Therefore, an accurate model for designing coaxial type filters and diplexers, based on a rigorous electromagnetic (EM) simulation, would greatly increase the state of art in this area.

Any historical review of the design methods used in combline type filters should trace its way back to the coupled transmission line model proposed by Matthaei [15]. To calculate the distributed capacitances in the filter, Cohn's approximate equations [16] were used. The extensive discussions about design procedures, formulas, relative theories, and application examples are available in reference [17]. However, the filter's characteristics often deviate from the designated response due to the approximations used in the design formulas. This problem becomes serious when the method is used for designing waveguide filters having coupling irises inside the filters. Experimental tuning is necessary to improve the filter's performance and to adjust the prototype design.

In 1966, Kurzrok reported his research on a folded combline filter, and demonstrated that the couplings between nonsuccessive cavities produced transmission zeros in the stop band of the filter's transfer function [18][19][20]. His work was mainly based on experiments and approximate design formulas.

In practice, waveguide filter design consists of two basic steps. First, an appropriate coupling matrix **M** needs to be synthesized to meet the required specification. Secondly, one has to determine the physical dimensions of the filter's resonators,

coupling irises and input and output configurations. The recent developments in electromagnetic modeling have changed the traditional method used for waveguide filter design and appear to have a bright future in an industry which is having to meet huge market demands.

The early research in electromagnetic modal analysis of coaxial resonator type filter structures were started by Liang in his analytical modeling of a cylindrical dielectric resonator in rectangular waveguides [21][22]. He used two techniques in his model: (1) The orthogonal expansion method [23] in Cartesian – cylindrical coordinate systems was extended to analyze a resonator with an inhomogeneous post region; and (2) a general three-dimensional Bessel-Fourier series was developed to calculate the mutual inner product integrations on the imaginary boundary between cylindrical and rectangular regions. Couplings between two identical cavities through a rectangular slot were also calculated using the modal analysis. Liang's work paved the way for modeling resonators and other components in combline filters.

In 1995, Yao derived a full-wave analytical model for an in-line waveguide combline resonator [24]. This resonator is one of the basic components used to build up the combline filter. Physically, it is a partial height cylindrical conducting post located in a straight rectangular waveguide. He extended Liang's orthogonal expansion method for solving the problem of conducting boundary conditions, and obtained an expression for the generalized scattering matrix (GSM) of the evanescent waveguide resonator. By cascading the scattering matrices of two non-identical adjacent resonators and the

coupling iris, the resonant frequencies and the coupling coefficient can be accurately determined [25].

Some numerical methods, such as the finite difference method (FDM) [26], the finite element method (FEM) [27], and the finite difference time domain method (FDTD) [28][29], can also be used for solving problems in filter design. They work very well when used to get solutions for component-level problems. When using these methods for a system-level EM simulation, for example, to simulate a complete waveguide combline filter, one may face serious problems from computer memories and processor speed.

On the other hand, analytical methods, such as modal analysis, have great potential for handling large system problems. As long as all the component modules are defined, one can easily perform the system simulations by simply cascading the generalized scattering matrices (GSM) for these modules [30]. Analytical methods are also attractive when people are looking for the physical interpretation behind lengthy mathematical formulas.

Many waveguide combline filters are built with folded-line configurations because it is easier to realize nonadjacent couplings. The drawing in fig. 1.1 represents such a folded combline filter. The filter consists of six waveguide resonators. Each of them consists of a partial height conducting post located inside a metal housing compartment. The two coaxial line-like structures are the input and output waveguides of the filter. The iris apertures on the walls of the metal enclosures provide the paths of electric or magnetic couplings among the resonators. In a real waveguide combline filter, the heights and the diameters of the conducting posts, and the sizes and the locations of

the irises might be different from each other, depending on the filter's performance requirements [21][24][31][32][33]. To obtain a satisfactory performance and to avoid excessive experimental adjustments, it is highly desired to have a complete electromagnetic model of the waveguide combline filter.

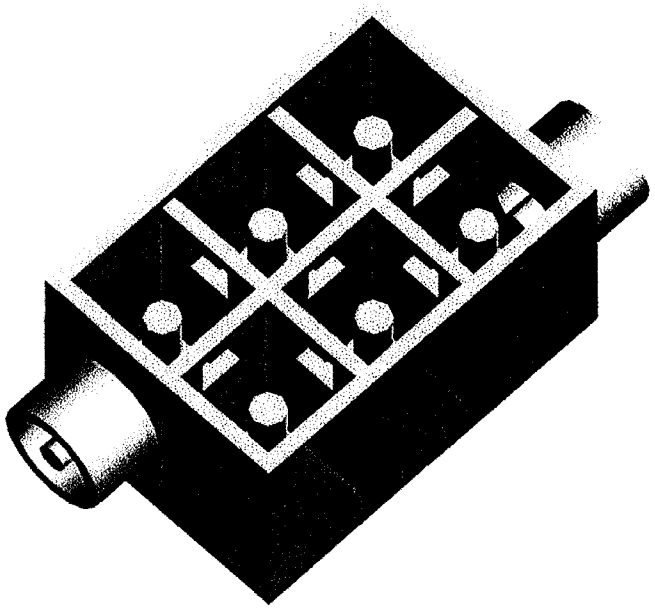

Figure 1. 1. A folded-line waveguide combline filter

Review of Mode Matching Method

Before discussing how to model the complete filter, let's have a brief review of the mode matching method and its applications in waveguide structures. The mode matching method is one of the most frequently used techniques for solving boundary - value problems [34][35]. With this method, one can model waveguide structures by finding the coefficients for the guided modes [36].

Compared to other numerical methods, one of the most significant advantages for the mode matching method is the substantial reduction in CPU time and memory size needed for calculations. This comes about because all of the integrations required for carrying inner products are available in analytical form [37][38].

Looking at figure 1.1, one can realize that the combline filter is made up of five basic waveguide components, which are shown in figure 1.2. These structures are widely used, and at first sight, appear to be simple. As a matter of fact, only one of the components, i.e. the in-line waveguide structure, as shown in figure 1.2 (b), was successfully modeled in 1995 [24], which is the time this research started.

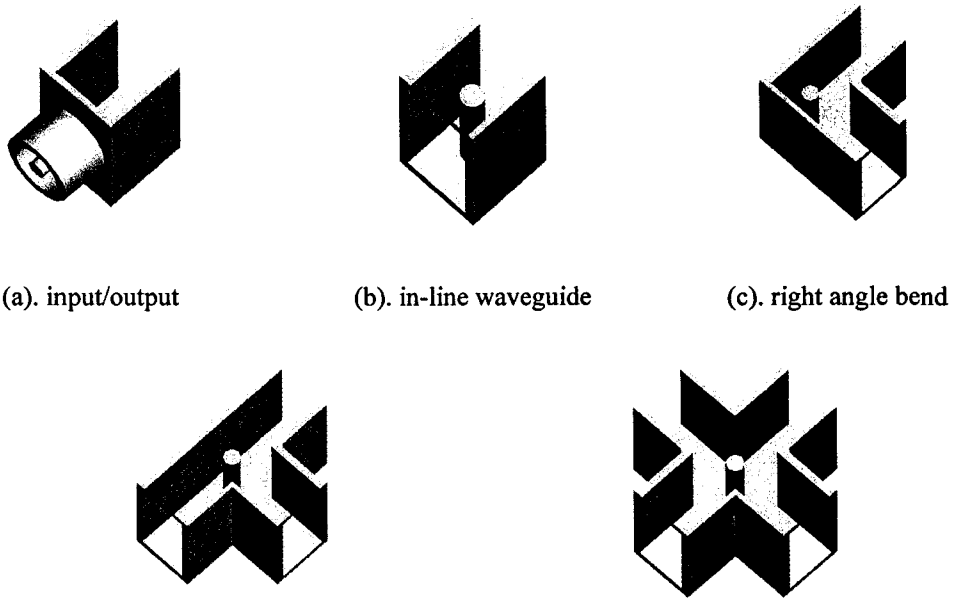

(a). input/output (b). in-line waveguide (c). right angle bend

(d) T-junction (c) cross junction

Fig. 1.2 Five types of the circular-rectangular coaxial waveguide structures

Contributions

The major contributions made in this dissertation are:

1) A rigorous modal analytical model for determining higher order modes of a circular-rectangular coaxial waveguide is given in [38] by H. Wang *et al.* This model combines the orthogonal expansion method and the Galerkin method. The resultant eigen matrix equation is solved using Singular Value Decomposition (SVD). The new method is much more efficient than the existing method which employs a single coordinate system, and reaches the same accuracy as the older method.

2) The first modal analytical model for a transverse electromagnetic wave (TEM) in a circular-rectangular coaxial waveguide was developed by H. Wang *et al* [61]. This model is based on a derived analytical expression for the electric field. Modal analysis of the waveguide junction, comprised of the circular-rectangular coaxial waveguide, can be carried out using this analytical expression. Subsequently, the analytic expressions for the characteristic impedance and the attenuation coefficient for the types of waveguides are obtained from the solution of the TEM mode.

3) A new technique for facilitating modal analysis of complex EM boundary value problems, called the method of the extended eigenmode functions, is proposed and developed. To show the power of the new technique, the generalized

scattering matrices for the waveguide bend and T- junctions, loaded with a generic post, are derived by Wu & Wang [63] using the new method.

These contributions lead to the development of key modules for electromagnetic modal analysis of combline-type filters and diplexers. This modeling is done at the system level. All the models are verified using either experimental results, or numerical results published by others. Excellent agreement is obtained in all cases.

The following is how the thesis is organized:

In Chapter 2, the TE and TM modal functions and their cutoff frequencies in circular-rectangular waveguides are obtained by using the orthogonal expansion combined with the partial region method. The Galerkin method is employed to calculate the inner products and to derive a group of linear equations for the amplitude of each mode function. The eigenmode frequency and corresponding coefficients for the modal fields are determined by solving the characteristic equation.

In Chapter 3, the TEM mode in a circular-rectangular waveguide is derived by using the modal functions in a rectangular cavity loaded with a full height circular conducting post. The resonant mode, whose wavelength is equal to twice the height of the cavity, would be TEM resonant mode. After the fields for the TEM mode are obtained, the voltage between inner and outer conductors is determined by carrying out an integration of the electric field. The analytical expressions for the characteristic impedance and attenuation coefficient are expressed in terms of the voltage and the current.

Chapter 4 discusses the scattering characteristics of the right-angle bend and T-waveguide junctions, which are shown in figure 1.2 (c) and (d). Rigorous modeling of the right angle bend and T-junctions is presented. A new method called the extended eigenmode function technique is introduced to analyze the bend junction and the T-junction. The generalized scattering matrices are obtained for the bend and T-junctions, respectively.

In Chapter 5, the research results are summarized.

Chapter 2

The Higher-Order Modal Characteristics of Circular-Rectangular Coaxial Waveguides

2.1 Introduction

Circular rectangular (C-R) coaxial waveguides have been widely used in various microwave components and circuits due to their low propagation loss. However, the community at large has a less than complete understanding of the electromagnetic characteristics involved. Many practical problems currently encountered could be better investigated if a complete knowledge of the eigenvalue spectrum of the C-R coaxial waveguide were known.

An example of a C-R coaxial transition is given by the input/output probe of a coaxial waveguide combline filter or a diplexer. The TEM mode in a circular coaxial transmission line couples with the evanescent modes in a rectangular waveguide. Since all the higher order modes in a rectangular waveguide contribute to the coupling of

evanescent modes, the effect of higher order modes in the C-R coaxial waveguide transition must be taken into account in a full electromagnetic analysis. In addition, information on higher order modes is also important for predicting the electromagnetic compatibility (EMC) characteristics of the C-R coaxial line-like structures (usually with multiple inner conductors) in high speed digital circuits. In particular, the latter is an interesting problem, where the knowledge obtained from our solutions will be useful for the development of interconnections in today's high-speed computers and switches, which are used in telecommunications.

The early work was carried out by Gruner [39], who used the Galerkin method to solve for the modes in a rectangular coaxial waveguide. The Galerkin method has also been successfully applied to the crossed rectangular waveguide problem by Tham [40]. The solutions of these basic waveguide configurations have been widely used in characterizing various complicated microwave systems. For example, they have been applied to integrated antenna beamforming networks [41] and waveguide dual mode filters [42]. Nevertheless, since all these configurations can be described using a rectangular coordinate system, it is difficult to extend the solutions to the case of C-R coaxial waveguide, where one must introduce a cylindrical coordinate system. In 1991, Omar and Schünenmann developed an approach to characterize the EM field in the C-R waveguide using summation of the eigenfunctions of a rectangular waveguide [43]. The eigenmode functions in the Cartesian coordinate system are transformed to the cylindrical coordinate system for integration along the inner circular conductor. To ensure computational accuracy, many modes (probably 50 or more) have to be used in Omar's

method. The previous work is based on a mono-coordinate system, either rectangular or cylindrical, and thereby improvement may be made by introducing a mixed C-R coordinate system for the C-R waveguide structure.

In this chapter, a general mathematical expression for the higher order modes in a C-R coaxial waveguide is given in explicit analytical form. The modal functions obtained here are in the form of a Fourier series, which can be conveniently used for further numerical manipulation. The Galerkin method is employed to formulate the problem. Because the formulation involves both rectangular and circular coordinate systems, the Bessel-Fourier series is used to merge the two different coordinate systems. In the proposed formulation, the scalar Helmholtz equations are converted into a generalized matrix eigenvalue equation. The singular value decomposition (SVD) technique [44] is then used to determine the eigenvalue spectrum, and subsequently the Fourier coefficients of the modal functions.

2.2 Basic Formulation

The purpose of the investigation presented in this chapter is to characterize the higher order modes in the C-R waveguide that is shown in Fig. 2.1. In this geometry, the inner circular conductor is concentric with the outer rectangular conductor. The waveguide is infinitely long with perfect conducting walls. There are three kinds of modes that can be supported by this structure. They are TEM mode, TE modes and TM modes. TEM mode is the dominant mode in the C-R coaxial waveguide and will be

investigated in the next chapter. The TE modes and TM modes are the higher-order modes in the C-R waveguide.

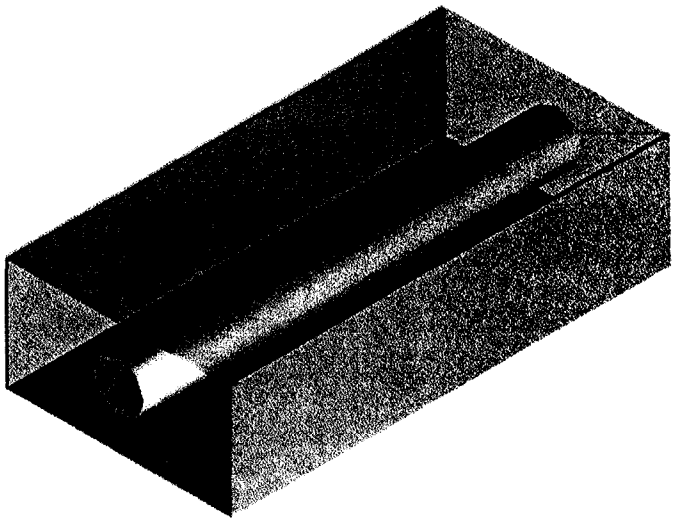

Fig.2.1 A circular-rectangular coaxial waveguide.

Fig. 2.2 shows the cross section of the waveguide, where the inner conductor has a radius of r_o, and the size of the outer conductor is $2a \times 2b$.

To analyze the C-R waveguide, the cross section is divided into two regions, the rectangular region I and the cylindrical region II as shown in Fig. 2.2. The coordinate system for each region should have its axis parallel to the boundary of the region such that the fields in each region can be expressed as summations of eigenmode functions in the region. We use rectangular coordinates in region I, and cylindrical coordinates in region II. Both coordinate systems have the same point of origin, which is located at the

center of the inner conductor. The dashed line represents the imaginary boundary consisting of a cylindrical surface with radius b, which separates the two regions.

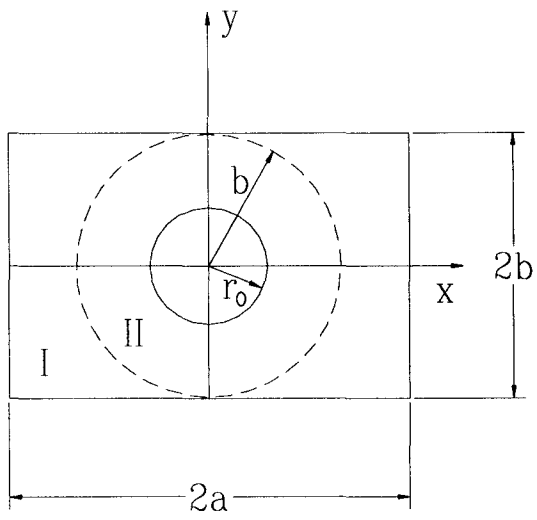

Fig. 2.2 Cross section of the C-R coaxial waveguide

The fields in region I and region II are expressed in terms of eigenmode functions that satisfy partial boundary conditions for each of the corresponding regions. To represent the field distributions, we choose trigonometric functions and hyperbolic functions in region I, Bessel functions and trigonometric functions in region II.

Since the structure of the waveguide is symmetrical with respect to the x and y axes, only one quadrant needs to be analyzed. Based on various boundary conditions which are assigned to the x and y axes for TM and TE modes, the eigenvalue problem can be divided into four distinct groups shown in Table 2.1.

In Table 2.1, the first/second subscript of the mode corresponds to the boundary conditions, which have been applied to the y/x axis, respectively.

Table 2.1 Eigenmode Patterns

Mode	X-axis	Y-axis
$TM_{odd,\ odd}$, $TE_{odd,\ odd}$	magnetic wall	magnetic wall
$TM_{odd,\ even}$, $TE_{odd,\ even}$	electric wall	magnetic wall
$TM_{even,\ odd}$, $TE_{even,\ odd}$	magnetic wall	electric wall
$TM_{even,\ even}$, $TE_{even,\ even}$	electric wall	electric wall

In later sections, the eigenvalue spectrum and the mode functions of each group are solved separately. By separating the modes into four groups, the mode spectrum becomes sparse for each group. Therefore, the determination of the eigenvalues of the problem becomes much easier. The degenerate modes shared by different groups are derived separately so that no degenerate mode is missed.

2.2.1 Field Expressions and Boundary Conditions of TM Modes

In order to analyze the TM modes, the boundary conditions require the z component of the electric field strength E_z to vanish along the outer and inner conductor surfaces. We solve the Helmholtz equation for E_z using separation of variables in the rectangular coordinates. Then applying the boundary conditions along the waveguide wall to the equation, E_z in region I of the third quadrant can be expressed as:

$$E_{zI} = \sum_{n=1,2,\cdots}^{\infty} \psi_{In} \sinh\left[p_{In}\frac{(x+a)}{2a}\right]\sin\left[\frac{n\pi(y+b)}{2b}\right],$$
$$-a \le x \le 0, \quad -b \le y \le 0, \quad \rho > b, \tag{2.1}$$

with the dispersion relation

$$p_{In}^2 = -4k_c^2 a^2 + \left(\frac{n\pi a}{b}\right)^2. \tag{2.2}$$

Here, ψ_{In} is the complex coefficient of the eigen field, k_c is the cutoff wavenumber of the waveguide and is given as:

$$k_c^2 = \omega^2 \varepsilon\mu - k_z^2, \tag{2.3}$$

where k_z is the propagation wavenumber in the z-direction, ω is the radian frequency, ε and μ are the permittivity and permeability, respectively.

Because cylindrical coordinates are used in region II, we express E_z in terms of the Bessel functions, i.e.,

$$E_{zII} = \sum_{m=0,1,\cdots}^{\infty} \psi_{II,m}\left[J_m(k_c\rho)Y_m(k_c r_o) - J_m(k_c r_o)Y_m(k_c\rho)\right]\Phi_m(\phi),$$
$$r_0 \le \rho \le b, \quad \pi \le \phi \le \frac{3\pi}{2}, \tag{2.4}$$

where $\psi_{II,m}$ is the complex coefficient, $J_m(k_c\rho)$ and $Y_m(k_c\rho)$ are the Bessel functions of the first and the second kinds of order m, respectively. For a certain eigenmode, all the field components have a common factor $e^{\pm jk_z z}$. To simplify expressions, E and H are used to express the electric and magnetic field components without factor $e^{\pm jk_z z}$ in this chapter.

The ϕ components of the magnetic fields in regions I and II can therefore be written as

$$
\begin{aligned}
H_{\phi I} &= H_{yI}\cos\phi - H_{xI}\sin\phi \\
&= -j\frac{\omega\varepsilon}{k_c^2}\sum_{n=1,2,\cdots}^{\infty}\psi_{In}\left\{\frac{p_{In}}{2a}\cosh\left[p_{In}\frac{(x+a)}{2a}\right]\sin\left[\frac{n\pi(y+b)}{2b}\right]\cos\phi\right. \\
&\qquad \left. +\frac{n\pi}{2b}\sinh\left[p_{In}\frac{(x+a)}{2a}\right]\cos\left[\frac{n\pi(y+b)}{2b}\right]\sin\phi\right\}, \\
&\qquad -a\le x\le 0, \quad -b\le y\le 0, \quad \rho > b,
\end{aligned}
\tag{2.5}
$$

and

$$
\begin{aligned}
H_{\phi II} &= -j\frac{\omega\varepsilon}{k_c^2}\sum_{m=0,1,\cdots}^{\infty}\psi_{II,m}|k_c|\left[J'_m(k_c\rho)Y_m(k_c r_o) - J_m(k_c r_o)Y'_m(k_c\rho)\right]\Phi_m(\phi), \\
&\qquad r_0\le\rho\le b, \quad \pi\le\phi\le\frac{3\pi}{2},
\end{aligned}
\tag{2.6}
$$

where H_{xI} and H_{yI} are the x and y components of the magnetic field in region I, $J'_m(k_c\rho)$ and $Y'_m(k_c\rho)$ are the derivatives of the Bessel functions of the first and the second kinds with respect to ρ, and

$$
\Phi_m(\phi) = \begin{Bmatrix}\cos(m\phi)\\ \sin(m\phi)\end{Bmatrix}. \tag{2.7}
$$

in which $\cos(m\phi)$ corresponds to $TM_{odd,\ odd}$ and $TM_{even,\ odd}$ modes and $\sin(m\phi)$ corresponds to $TM_{odd,\ even}$ and $TM_{even,\ even}$ modes, determined by using Table 2.1 and the periodicities of $\cos(m\phi)$ and $\sin(m\phi)$. The continuity of E_z and H_ϕ implies that

$$
\begin{aligned}
E_{zI} &= E_{zII}, \\
H_{\phi I} &= H_{\phi II},
\end{aligned}
\tag{2.8}
$$

at the imaginary boundary ρ = b.

After substituting the field expressions (2.1), and (2.4)-(2.6) into (2.8), we multiply both sides with the eigen function $\Phi_k(\phi)$ in region II and then integrate from π to

$3\pi/2$. The trigonometric functions in each group of the eigenmodes have the same symmetry as the eigenfields. When eigenfields are extended to the whole region, the trigonometric functions are extended to the range of 0 to 2π. Therefore, the orthogonality of the trigonometric functions can be used in region π to $3\pi/2$. Because of the orthogonality of the trigonometric functions, the following equations are obtained:

$$\begin{aligned}\sum_{n=1,3,\cdots}^{N}\psi_{In}b_{\Phi kn}^{tm}&=\psi_{II,k}e_{k}^{tm},\\ \sum_{n=1,3,\cdots}^{N}\psi_{In}\left(c_{\Phi kn}^{tm}+d_{\Phi kn}^{tm}\right)&=\psi_{II,k}f_{k}^{tm},\end{aligned}\tag{2.9}$$

where

$$b_{\Phi kn}^{tm}=\int_{\pi}^{\frac{3\pi}{2}}\sinh\left[p_{In}\frac{(b\cos\phi+a)}{2a}\right]\sin\left[\frac{n\pi(\sin\phi+1)}{2}\right]\Phi_{k}(\phi)d\phi,\tag{2.10}$$

$$c_{\Phi kn}^{tm}=\int_{\pi}^{\frac{3\pi}{2}}\frac{p_{In}}{2a}\cosh\left[p_{In}\frac{(b\cos\phi+a)}{2a}\right]\sin\left[\frac{n\pi(\sin\phi+1)}{2}\right]\cos\phi\,\Phi_{k}(\phi)d\phi,\tag{2.11}$$

$$d_{\Phi kn}^{tm}=\int_{\pi}^{\frac{3\pi}{2}}\frac{n\pi}{2b}\sinh\left[p_{In}\frac{(b\cos\phi+a)}{2a}\right]\cos\left[\frac{n\pi(\sin\phi+1)}{2}\right]\sin\phi\,\Phi_{k}(\phi)d\phi,\tag{2.12}$$

$$e_{k}^{tm}=\left[J_{k}(k_{c}b)Y_{k}(k_{c}r_{o})-J_{k}(k_{c}r_{o})Y_{k}(k_{c}b)\right]\Delta_{k},\tag{2.13}$$

$$f_{k}^{tm}=\left|k_{c}\right|\left[J'_{k}(k_{c}b)Y_{k}(k_{c}r_{o})-J_{k}(k_{c}r_{o})Y'_{k}(k_{c}b)\right]\Delta_{k},\tag{2.14}$$

when $\Phi_{k}(\phi)=\cos(k\phi)$, $\qquad \Delta_{k}=\begin{cases}\dfrac{\pi}{2}, & k=0,\\ \dfrac{\pi}{4}, & k\neq 0,\end{cases}$ (2.15)

when $\Phi_k(\phi) = \sin(k\phi)$, $\Delta_k = \frac{\pi}{4}$ (2.16)

In these equations, n = 1, 2, ···, 2N, and k = m = 0, 1, ···, 2M where N and M are the numbers of modes used in regions I and region II, respectively.

After eliminating ψ_{In} from (2.9), the above equations can be written in matrix form

$$\mathbf{A}^{tm}\psi_{II} = \mathbf{0}, \tag{2.17}$$

where ψ_{II} is the coefficient vector of the eigen fields in the cylindrical region and

$$\mathbf{A}^{tm} = \mathbf{E}^{tm} - \mathbf{B}^{tm}\left(\mathbf{C}^{tm} + \mathbf{D}^{tm}\right)^{-1}\mathbf{F}^{tm}. \tag{2.18}$$

In (2.18), the superscript tm of each matrix means the TM modes and the superscript -1 means the inverse of the matrix. The elements of each matrix are given by the corresponding lower-case letters defined in equations (2.10)-(2.16). To ensure the existence of the inverse matrix, the number of the modes used in region I should be the same as that in region II, i.e. M = N.

From equation (2.9), the field coefficient vector in region I can be determined by

$$\psi_I = \mathbf{B}^{tm^{-1}}\mathbf{E}^{tm}\psi_{II}. \tag{2.19}$$

To have a nontrivial solution of (2.17), the determinant of matrix $\mathbf{A}^{tm}$ has to be equal to zero. A group of eigenvalues k_c's that satisfy the characteristic equation $\det[\mathbf{A}^{tm}] = 0$ can be obtained. Each eigenvalue corresponds to a cutoff wavenumber for a TM mode in the C-R waveguide. Consequently, the eigenmodes can be obtained from the solutions for ψ_{In} and ψ_{IIn}.

The boundary conditions for TM modes on the x and y axes include: the tangential components of a magnetic field should be zero on the magnetic wall and the tangential components of an electric field should be zero on the electric wall. It means that $\partial E_z / \partial n$ needs to be zero along the x and y axes for $TM_{odd, odd}$. We choose $\Phi_k(\phi) = \cos(k\phi)$ in equations (2.9) – (2.16), with m= 0, 2, … and n = 1, 3, 5, …. These satisfy the boundary conditions of the perfect magnetic wall along the x and y axes. For $TM_{even, odd}$ modes, we use the same $\Phi_k(\phi)$ with m = 1, 3, 5, …, n = 1, 3, 5, ….

Similarly, we can obtain the matrix equations for $TM_{odd, even}$ and $TM_{even, even}$ modes using (2.9) – (2.16) with $\Phi_k(\phi) = \sin(k\phi)$, where m = 1, 3, 5, ···, and n = 2, 4, 6, ··· for $TM_{odd, even}$ modes, and m =2, 4, 6, ··· and n = 2, 4, 6, ··· for $TM_{even, even}$ modes.

The other components of the electric fields, E_x, E_y, E_ρ, E_ϕ, and the magnetic field components can be derived from E_z by using Maxwell's equations.

2.2.2 Field Expressions and Cutoff Frequencies of TE Modes

For TE modes, the fields $H_z \neq 0$ and $E_z = 0$. The magnetic field components for the TE modes in region I and region II are given by

$$H_{zI} = \sum_{n=1,2,\cdots}^{\infty} \psi_{In} \cosh\left[p_{In}\frac{(x+a)}{2a}\right]\cos\left[\frac{n\pi(y+b)}{2b}\right], \qquad -a \le x \le 0, \quad -b \le y \le 0, \quad \rho > b \tag{2.20}$$

$$H_{zII} = \sum_{m=0,1,\cdots}^{\infty} \psi_{II,m}\left[J_m(k_c\rho)Y'_m(k_c r_o) - J'_m(k_c r_o)Y_m(k_c\rho)\right]\Phi_m(\phi), \qquad r_0 \le \rho \le b, \quad \pi \le \phi \le \frac{3\pi}{2}. \tag{2.21}$$

The ϕ components of the electric fields in regions I and II can be written as

$$E_{\phi I} = j\frac{\omega\mu}{k_c^2}\sum_{n=1,2,\cdots}^{\infty}\psi_{In}\left\{\frac{p_{In}}{2a}\sinh\left[p_{In}\frac{(x+a)}{2a}\right]\cos\left[\frac{n\pi(y+b)}{2b}\right]\cos\phi\right.$$
$$\left.-\frac{n\pi}{2b}\cosh\left[p_{In}\frac{(x+a)}{2a}\right]\sin\left[\frac{n\pi(y+b)}{2b}\right]\sin\phi\right\}, \qquad (2.22)$$

$$-a\le x\le 0,\quad -b\le y\le 0,\quad \rho>b$$

and

$$E_{\phi II} = j\frac{\omega\mu}{k_c^2}\sum_{m=0,1,\cdots}^{\infty}\psi_{II,m}|k_c|\left[J'_m(k_c\rho)Y'_m(k_c r_o)-J'_m(k_c r_o)Y'_m(k_c\rho)\right]\Phi_m(\phi), \qquad (2.23)$$
$$r_0\le\rho\le b,\quad \pi\le\phi\le\frac{3\pi}{2},$$

where

$$\Phi_m(\phi)=\begin{Bmatrix}\sin(m\phi)\\ \cos(m\phi)\end{Bmatrix}, \qquad (2.24)$$

in which $\sin(m\phi)$ is for $TE_{odd,\ odd}$ and $TE_{evevn,\ odd}$ modes and $\cos(m\phi)$ is for $TE_{odd,\ even}$ and $TE_{even,\ even}$ modes, determined by using Table 2.1 and the periodicities of $\sin(m\phi)$ and $\cos(m\phi)$.

Using $\Phi_k(\phi)$ for the inner product with $H_{zI} = H_{zII}$ and $E_{\phi I} = E_{\phi II}$, the following equations, which are similar to equation (2.9), are obtained

$$\sum_{n=1,3,\cdots}^{N}\psi_{In}b_{\Phi kn}^{te}=\psi_{II,k}e_{kk}^{te},\quad \text{and}$$
$$\sum_{n=1,3,\cdots}^{N}\psi_{In}\left(c_{\Phi kn}^{te}-d_{\Phi kn}^{te}\right)=\psi_{II,k}f_{kk}^{tm}. \qquad (2.25)$$

After eliminating ψ_{In} from these equations, we have the matrix equation

$$\mathbf{A}^{te}\psi_{II}=\mathbf{0}, \qquad (2.26)$$

where

$$\mathbf{A}^{te} = \mathbf{E}^{te} - \mathbf{B}^{te}\left(\mathbf{C}^{te} - \mathbf{D}^{te}\right)^{-1}\mathbf{F}^{te}. \tag{2.27}$$

The field coefficient vector ψ_I in the rectangular region can be obtained from the matrix equation

$$\psi_I = \mathbf{B}^{te^{-1}}\mathbf{E}^{te}\psi_{II}. \tag{2.28}$$

In the above equations, the superscript te means the TE modes. In equation (2.25) and the matrix equations, the elements are given by

$$b^{te}_{\Phi mn} = \int_{\pi}^{\frac{3\pi}{2}} \cosh\left[p_{In}\frac{(b\cos\phi + a)}{2a}\right]\cos\left[\frac{n\pi(\sin\phi + 1)}{2}\right]\Phi_m(\phi)d\phi, \tag{2.29}$$

$$c^{te}_{\Phi mn} = \int_{\pi}^{\frac{3\pi}{2}} \frac{p_{In}}{2a}\sinh\left[p_{In}\frac{(b\cos\phi + a)}{2a}\right]\cos\left[\frac{n\pi(\sin\phi + 1)}{2}\right]\cos(\phi)\,\Phi_m(\phi)d\phi, \tag{2.30}$$

$$d^{te}_{\Phi mn} = \int_{\pi}^{\frac{3\pi}{2}} \frac{n\pi}{2b}\cosh\left[p_{In}\frac{(b\cos\phi + a)}{2a}\right]\sin\left[\frac{n\pi(\sin\phi + 1)}{2}\right]\sin(\phi)\,\Phi_m(\phi)d\phi, \tag{2.31}$$

$$e^{te}_{mm} = \left[J_m(k_c b)Y'_m(k_c r_o) - J'_m(k_c r_o)Y_m(k_c b)\right]\Delta_k, \tag{2.32}$$

$$f^{te}_{mm} = |k_c|\left[J'_m(k_c b)Y'_m(k_c r_o) - J'_m(k_c r_o)Y'_m(k_c b)\right]\Delta_k. \tag{2.33}$$

We use $\Phi_k(\phi) = \sin(k\phi)$ for $TE_{odd,\ odd}$ modes and $TE_{even,\ odd}$ modes. In addition, m = 2, 4, 6, ··· , n = 1, 3, 5, ··· for $TE_{odd,\ odd}$ modes, and m = 1, 3, 5, ···, n = 1, 3, 5, ··· for $TE_{even,\ odd}$ modes.

Similarly, $\Phi_k(\phi) = \cos(k\phi)$ is used for $TE_{odd,\ even}$ modes and $TE_{even,\ even}$ modes with m = 1, 3, 5, ··· , n = 0, 2, 4, ··· for $TE_{odd,\ even}$ modes, and m = 0, 2, 4, ··· , n = 0, 2, 4, ··· for $TE_{even,\ even}$ modes.

The values of Δ_k in equation (2.32) and (2.33) are also given by equations (2.15) and (2.16).

2.2.3 Bessel-Fourier Series

When we calculate the elements for matrices **B**, **C**, **D** and **E**, the integrands are the products of hyperbolic functions and trigonometric functions. Using the relations

$$\sinh(x) = (e^{x} - e^{-x})/2,$$

$$\cosh(x) = (e^{x} + e^{-x})/2 \tag{2.34}$$

and $\Phi_k(\phi) = \cos(k\phi)$, equations (2.10) and (2.29) can be rewritten as

$$b_{ckn}^{tm} = \int_{\pi}^{\frac{3\pi}{2}} \left\{ \frac{1}{2} e^{p_{ln}\left(\frac{b\cos\phi + a}{2a}\right)} \sin\left[\frac{n\pi(\sin\phi + 1)}{2}\right] \cos(k\phi) - \frac{1}{2} e^{-p_{ln}\left(\frac{b\cos\phi + a}{2a}\right)} \sin\left[\frac{n\pi(\sin\phi + 1)}{2}\right] \cos(k\phi) \right\} d\phi \tag{2.35}$$

and

$$b_{ckn}^{te} = \int_{\pi}^{\frac{3\pi}{2}} \left\{ \frac{1}{2} e^{p_{ln}\left(\frac{b\cos\phi + a}{2a}\right)} \cos\left[\frac{n\pi(\sin\phi + 1)}{2}\right] \cos(k\phi) + \frac{1}{2} e^{-p_{ln}\left(\frac{b\cos\phi + a}{2a}\right)} \cos\left[\frac{n\pi(\sin\phi + 1)}{2}\right] \cos(k\phi) \right\} d\phi . \tag{2.36}$$

The Bessel-Fourier series [22] is then used to calculate the above integrals analytically. The Bessel-Fourier series is given here for completeness:

$$\sin\left[\frac{n\pi(1+\sin\phi)}{2}\right]e^{\mp\frac{p_{In}}{2a}b\cos\phi}=\sum_{k=-\infty}^{\infty}\sin\left(\frac{n\pi}{2}+k\phi\right)\begin{cases}J_k[T(b)]e^{\mp jk\left[\arctan\left(\frac{b|p_{In}|}{an\pi}\right)\right]}, & \\ & p_{In}^2<0; \\ J_k[T(b)]\left[\frac{an\pi+bp_{In}}{an\pi-bp_{In}}\right]^{\mp\frac{k}{2}}, & \\ & an\pi>b|p_{In}|, \quad p_{In}^2>0; \\ (-1)^{\frac{k}{2}}I_k[|T(b)|]\left[\frac{an\pi+bp_{In}}{an\pi-bp_{In}}\right]^{\mp\frac{k}{2}}, & \\ & an\pi<b|p_{In}|, \quad p_{In}^2>0;\end{cases} \tag{2.37}$$

and

$$\cos\left[\frac{n\pi(1+\sin\phi)}{2}\right]e^{\mp\frac{p_{In}}{2a}b\cos\phi}=\sum_{k=-\infty}^{\infty}\cos\left(\frac{n\pi}{2}+k\phi\right)\begin{cases}J_k[T(b)]e^{\mp jk\left[\arctan\left(\frac{b|p_{In}|}{an\pi}\right)\right]}, & \\ & p_{In}^2<0; \\ J_k[T(b)]\left[\frac{an\pi+bp_{In}}{an\pi-bp_{In}}\right]^{\mp\frac{k}{2}}, & \\ & an\pi>b|p_{In}|, \quad p_{In}^2>0; \\ (-1)^{\frac{k}{2}}I_k[|T(b)|]\left[\frac{an\pi+bp_{In}}{an\pi-bp_{In}}\right]^{\mp\frac{k}{2}}, & \\ & an\pi<b|p_{In}|, \quad p_{In}^2>0;\end{cases} \tag{2.38}$$

where p_{ln} is given in equation (2.2), and

$$T(b) = \frac{1}{2}\sqrt{(n\pi)^2 - (2b\gamma_{xn})^2}\,, \tag{2.39}$$

with $$\gamma_{xn}^2 = \left(\frac{n\pi}{2b}\right)^2 - k_c^2, \tag{2.40}$$

we have $T(b) = bk_c$.

By using the Bessel-Fourier series, the first integration on the right side of equation (2.35) can be written as

$$b_{cknl}^{tm} = e^{\frac{P_{ln}}{2}} \int_{\pi}^{3\pi/2} e^{\frac{p_{ln}}{2a} b\cos(\phi)} \sin[\frac{n\pi}{2}(\sin(\phi)+1)]\cos(n\phi)d\phi \tag{2.41}$$

$$= \sum_{k=-K}^{K} e^{\frac{P_{ln}}{2}} \left(\int_{\pi}^{3\pi/2} \sin(\frac{n\pi}{2} + k\phi)\cos(n\phi)d\phi \right) \begin{cases} J_k[T(b)]e^{-j\arctan(\frac{b|p_{ln}|}{an\pi})}, & p_{ln}^2 < 0, \\ J_k[T(b)][\frac{an\pi + bp_{ln}}{an\pi - bp_{ln}}]^{k/2}, & p_{ln}^2 > 0, \\ & an\pi > b\,|\,p_{ln}\,|, \\ (-1)^{k/2} I_k[T(b)][\frac{an\pi + bp_{ln}}{an\pi - bp_{ln}}]^{k/2}, & p_{ln}^2 > 0, \\ & an\pi < b\,|\,p_{ln}\,|. \end{cases}$$

The integrations for the different k's in the summation can be calculated analytically so that the integration in (2.41) is calculated by the summation of series. To ensure the accuracy of the summation, the number of the terms for the truncated series must be at least as large as [22]

$$K = 15 + 3n. \tag{2.42}$$

2.3 Numerical Results and Discussions

In order to verify the modeling approach and demonstrate its application, a C-R waveguide is investigated in detail. The waveguide has dimensions of a = 2.54 cm and b = 1.27 cm. The cutoff frequencies are obtained by mapping the complete frequency range of interest for each mode. The SVD technique is used to determine the image points that satisfy the equation det (**A**) = 0 [44], where **A** is either $\mathbf{A}^{tm}$ or $\mathbf{A}^{te}$. The advantage of the SVD technique is that it is able to improve the efficiency and reliability in the zero point searching procedure.

Using the SVD technique, matrix **A** is expressed as $\mathbf{U}\Sigma\mathbf{V}^{\mathrm{T}}$, where **U** and **V** are unitary matrices of the left and right singular vectors of matrix **A**, respectively. det(**U**) = 1 and det(**V**) = 1. Σ is a real diagonal matrix with singular values σ_{ii} in a descending order, where i = 1, 2, ..., n. If the minimum element σ_{nn} of the matrix Σ is equal to zero, we have det(**A**) = 0.

The values of the minimum element σ_{nn} of matrix Σ versus eigen wavenumber k_c for $TE_{odd,\ even}$ modes and $TE_{even,\ even}$ modes are given in figures 2.3 and 2.4, respectively. In fig. 2.3, the value of k_c is 0.511249 for H_{10} mode at the first zero point of σ_{nn}. The value of k_c at the first zero point of σ_{nn} is 1.3253987 for H_{20} mode in fig. 2.4.

Figures 2.5 and 2.6 show the cutoff wavenumbers k_c versus the normalized inner conductor radius r_o / a. It can be seen that the k_c of each TE or TM mode in the C-R waveguide approaches the value of a hollow rectangular waveguide of the same dimensions as r_o approaches a value of zero [65]. Therefore, the hollow rectangular

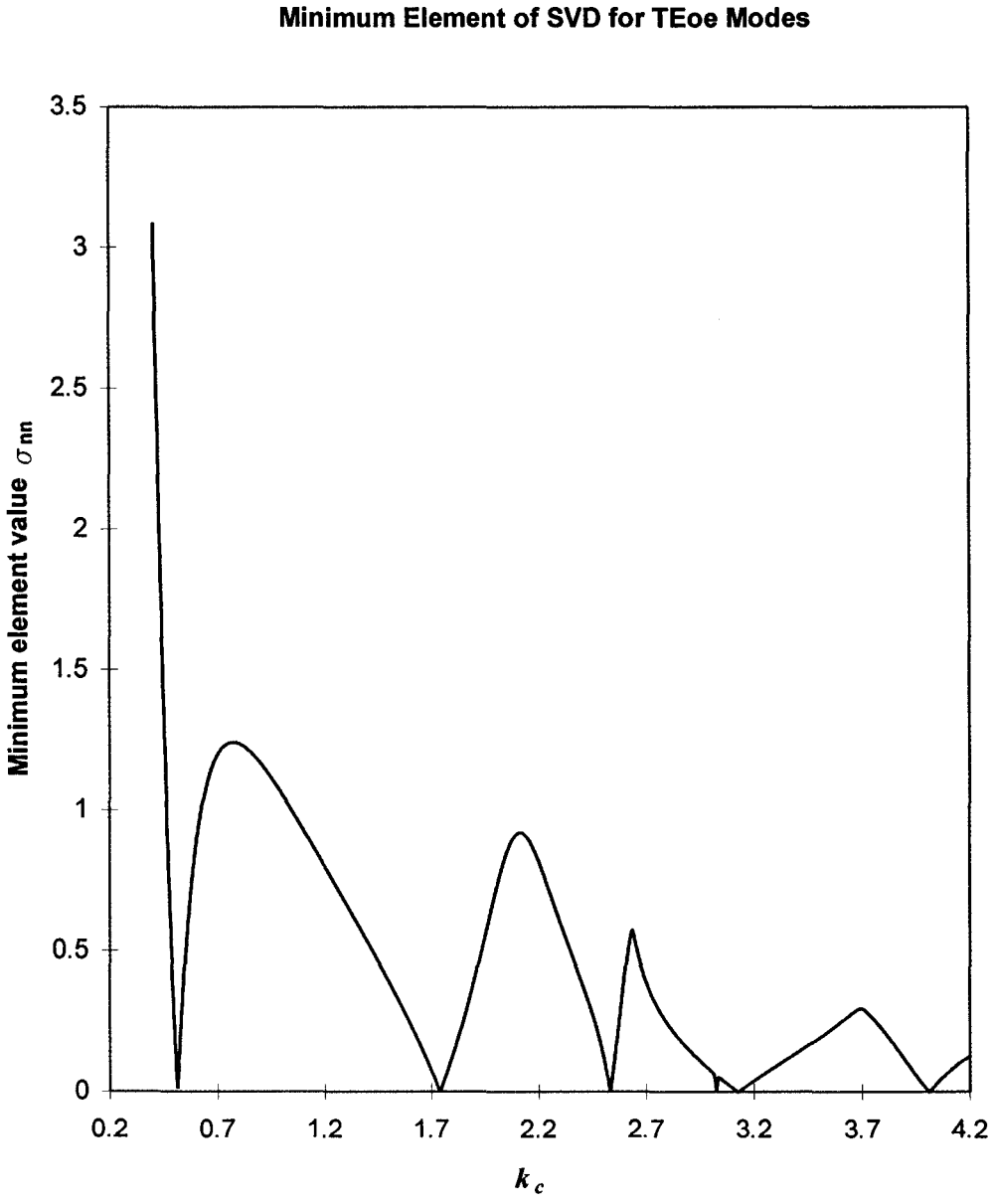

Fig. 2.3 The value of σ_{nn} vs. cutoff wavenumber k_c for $TE_{odd, even}$ modes

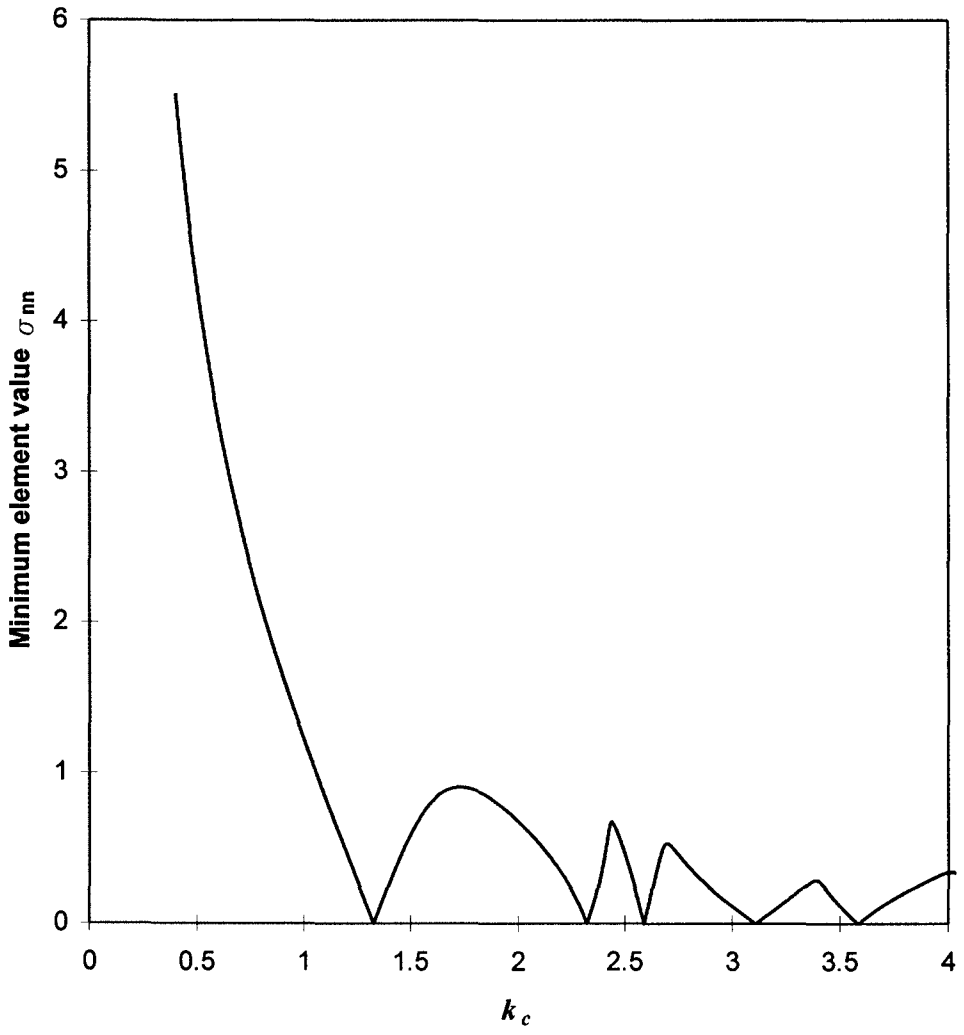

Fig. 2.4 The value of σ_{nn} vs. cutoff wavenumber k_c for $TE_{even,even}$ Modes

waveguide may be viewed as a special case in the C-R waveguide modeling. There are a number of degenerate modes that share the same cutoff frequencies for $r_o = 0$. The degenerate modes split as the radius of the inner conductor is increased (TE_{01}, TE_{20}, and TE_{02}, TE_{40} in Fig. 2.6, TM_{41}, TM_{22} in Fig. 2.5).

Fig. 2.5 shows another interesting phenomenon of the TM modes in C-R waveguides: pairs of cutoff wavenumbers converge as one increases the dimension r_o of the inner conductor. This phenomenon indicates the potential for the different TM modes being combined together, or combined modes being split up into individual ones, simply by adjusting the r_o / a ratio. A possible explanation for this is that the two TM modes sharing the same second subscript, TM_{21} and TM_{11} for instance, are subject to the same x-axis boundary conditions but different y-axis conditions. Furthermore, one of the modes has the y-axis as an electric wall while the other has the y-axis as an magnetic wall. As r_o increases, the boundary along the y-axis becomes shorter and shorter until eventually, the two modes merge into one mode.

Another interesting observation in Fig. 2.5 is that the cutoff wavenumbers for the $TM_{odd, odd}$ modes have a discontinuity when r_0 tends to zero. Figures 2.7 and 2.8 present the field distributions for the TM_{11} mode for the two cases, $r_0 = 0$ and $r_0 \neq 0$. In Fig. 2.7, the radius of the inner conductor is zero. This figure gives the field distribution for the TM_{11} mode in a hollow rectangular waveguide. The maximum value of the field occurs at the center of the waveguide, where the inner conductor would normally be located. In

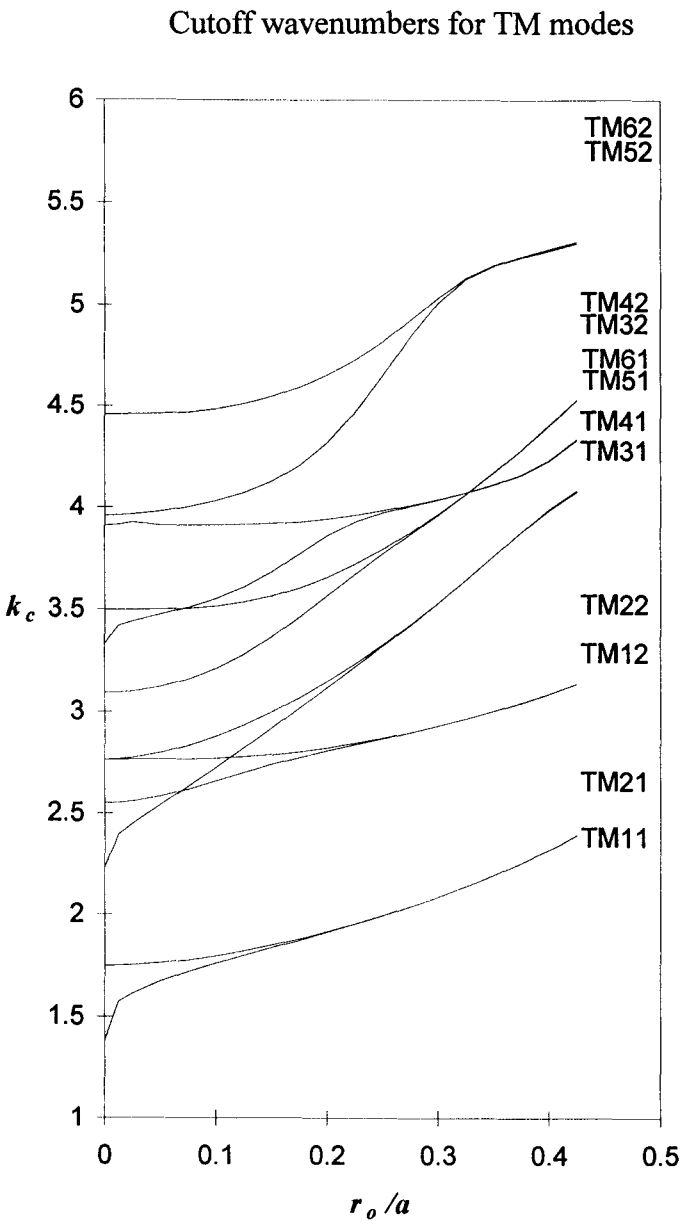

Fig. 2.5 Typical TM mode characteristics of C-R coaxial waveguide (b/a = 0.5).

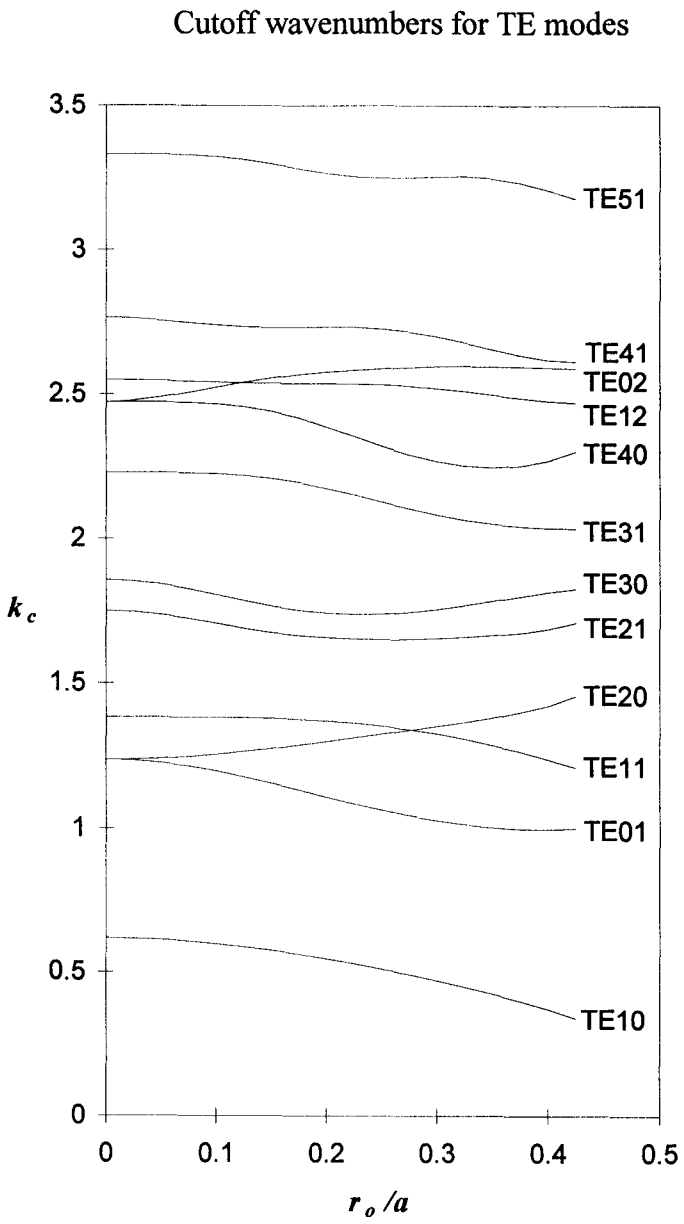

Fig. 2.6 Typical TE mode characteristics of C-R coaxial waveguide (b/a = 0.5).

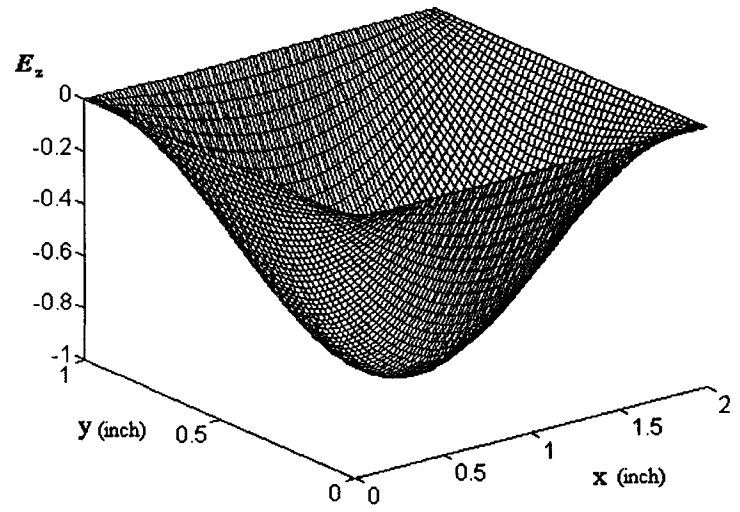

Fig. 2.7 E_z distribution of TM_{11} mode in a hollow waveguide

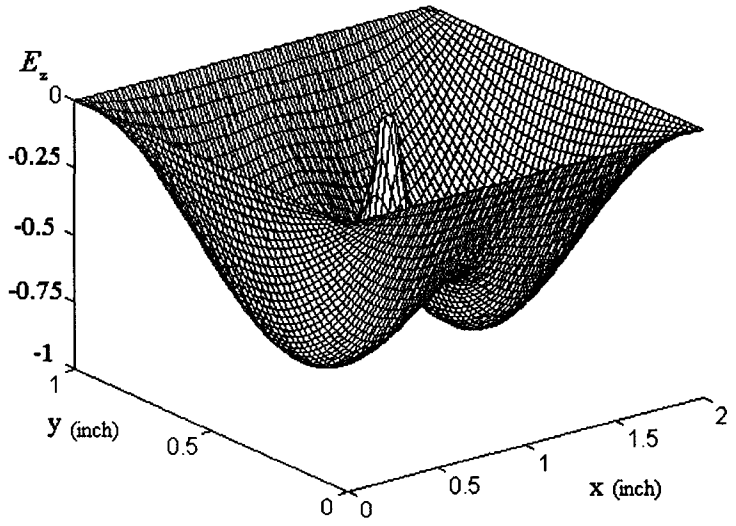

Fig. 2.8 E_z distribution of TM_{11} mode in a C-R coaxial waveguide

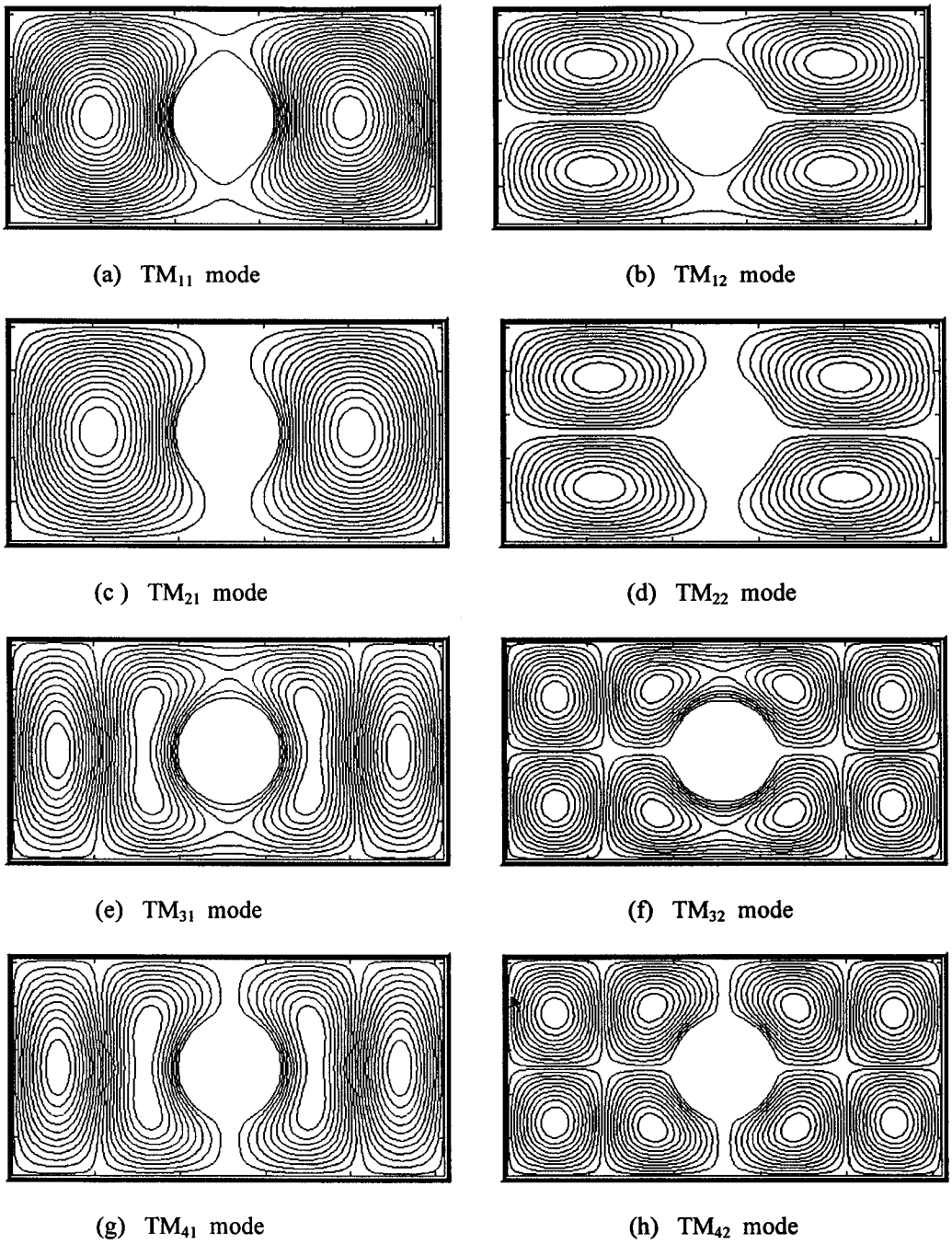

(a) TM_{11} mode (b) TM_{12} mode

(c) TM_{21} mode (d) TM_{22} mode

(e) TM_{31} mode (f) TM_{32} mode

(g) TM_{41} mode (h) TM_{42} mode

Fig. 2.9 E_z mode field for first eight TM modes in a C-R coaxial waveguide

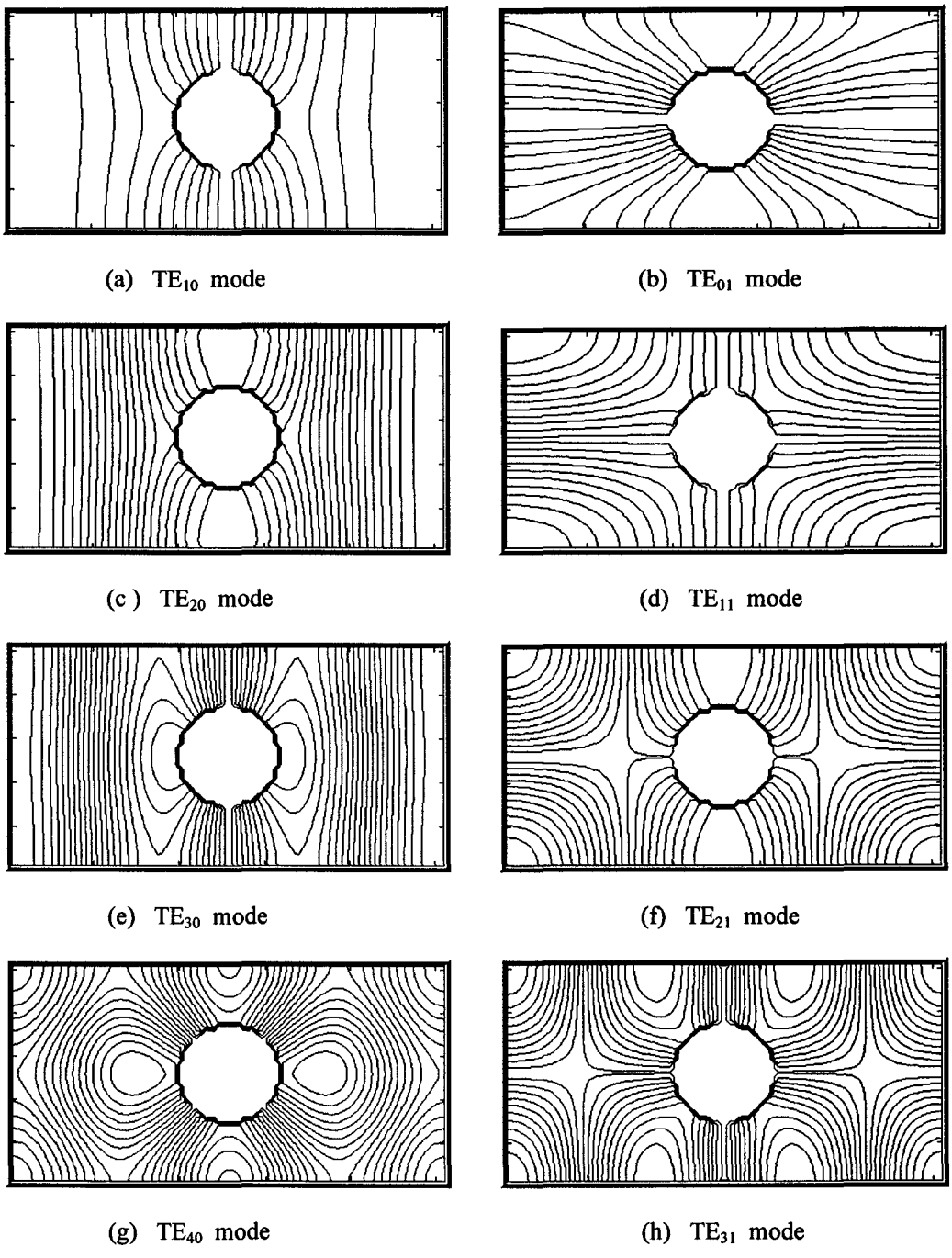

(a) TE_{10} mode (b) TE_{01} mode

(c) TE_{20} mode (d) TE_{11} mode

(e) TE_{30} mode (f) TE_{21} mode

(g) TE_{40} mode (h) TE_{31} mode

Fig. 2.10 H_z mode field for the first eight TE modes in a C-R coaxial waveguide

Fig. 2.8, the radius of inner conductor is very small but not equal to zero. The field at the surface of the inner conductor is zero. The field distribution has a discontinuous change as r_0 changes from zero to nonzero. The discontinuity in the field causes a discontinuous change in the wave numbers.

Fig. 2.9 and Fig. 2.10 present the contours of the eight typical TM and TE modes in the C-R waveguide, where $r_o / a = 0.225$. In Fig. 2.9, the z components of the electric field for the TM modes are plotted. In Fig. 2.10, we plot the contours of the z components of the magnetic fields for the TE modes.

In order to further verify the validity of this analytical method, we compared the results of k_c with the values calculated using a finite element technique. The waveguide size is $a = 2.54$ cm, $b = 1.27$ cm, and $r_o = 0.635$ cm. The average element size in the finite element method is 0.1016 cm. Table II gives the comparison for each mode in the waveguide, and, as can be seen, the relative error between the two methods is less than 9.85×10^{-4}.

Table II. Comparisons of the values of k_c obtained using the present technique and the finite element technique

Modes	k_c (1 / cm) by present method	k_c (1 / cm) by finite element method	Relative errors between the two methods
TE_{10}	0.51124951	0.51147162	4.34×10^{-4}
TE_{01}	1.0637058	1.06394546	2.25×10^{-4}
TE_{20}	1.3253987	1.32524321	1.17×10^{-4}
TE_{11}	1.3535700	1.3537048	9.95×10^{-5}
TE_{21}	1.6493145	1.6493224	4.78×10^{-6}
TE_{30}	1.7379933	1.7379533	2.30×10^{-5}
TE_{31}	2.1282537	2.1285580	1.42×10^{-4}
TE_{40}	2.3222497	2.3226796	1.85×10^{-4}
TE_{12}	2.5335094	2.5335731	2.51×10^{-5}
TE_{02}	2.5892876	2.5892433	1.71×10^{-5}
TM_{11}	1.9948099	1.9935818	6.16×10^{-4}
TM_{21}	1.9953650	1.9946881	3.39×10^{-4}
TM_{12}	2.8694867	2.8691664	1.11×10^{-4}
TM_{22}	2.8721777	2.8718947	9.85×10^{-4}
TM_{31}	3.3197261	3.3178141	5.74×10^{-4}
TM_{41}	3.3264943	3.3247878	5.13×10^{-4}
TM_{32}	3.7715987	3.7705847	2.68×10^{-4}
TM_{42}	3.7941012	3.7933216	2.05×10^{-4}
TM_{13}	3.9728472	3.9723368	1.28×10^{-4}
TM_{23}	3.9843494	3.9838875	1.15×10^{-4}

Chapter 3

Modal Analysis of the TEM Mode in A Circular-Rectangular Coaxial Waveguide

3.1 Introduction

The transverse electromagnetic (TEM) mode is found to be the dominant mode in circular-rectangular coaxial waveguides. This waveguide structure has been widely used in transitions between circular coaxial waveguides and rectangular waveguides in various microwave communication systems. Many critical parameters in general microwave circuit design, such as the characteristic impedance, attenuation coefficient and power loss, can be derived by carrying out TEM-mode based analysis. Therefore, to completely understand the electromagnetic characteristics involved, it is of primary importance to obtain the solution of the TEM mode in the C-R coaxial waveguide.

Numerical methods can be used to calculate the TEM mode distribution and the characteristic impedance of the C-R coaxial waveguide. Among the popular numerical techniques are the finite difference method [45] and the finite element method [46]. Although numerical techniques offer considerable flexibility for dealing with complicated structures, their dynamic range and accuracy may be limited by discretization and round-off errors. In addition, numerical methods usually require a considerable amount of computer memory and CPU time. Analytical solutions, on the other hand, offer the advantages of accuracy, efficiency and an embedded physical understanding. This is particularly true when one carries out the analysis of the junction between a C-R waveguide and a rectangular waveguide. It is found that an analytically derived model greatly facilitates the electromagnetic simulation of the structure. Therefore, researchers have put a great deal of effort into obtaining an analytical solution for the problem of modeling a C-R coaxial waveguide [43][38].

Analytical expressions have been reported by previous authors for deriving the characteristic impedance of a limited class of C-R coaxial waveguides. For example, Frankel employed the method of conformal transformation and the method of images jointly to deduce the characteristic impedance of two-conductor and three-conductor lines in a rectangular conducting enclosure [47]. The characteristic impedance of a circular-square coaxial structure was derived in the same paper, although the radius of the inner conductor is limited to some fraction of the size of its enclosure. Chisholm used a variational method to develop expressions for the characteristic impedance of a "trough line" and a "slab line" [48]. A trough line is a circular cylinder within a semi-infinite

rectangular waveguide. A slab line is a post in an infinite rectangular waveguide. Modified terms were introduced into the expression so that it could be used for a greater value of r_0, the radius of the inner conductor. Similar methods were used in [49], [50] and [51] for simulating some special cases of C-R coaxial waveguides. However, in each case, the mode field distribution was not available in analytical form. Therefore, a more general method is desired for modeling the TEM mode in a circular-rectangular coaxial waveguide.

In this chapter, a novel modal analysis is presented to describe the TEM mode in a C-R waveguide. Instead of formulating the problem by a two-dimensional solution as was done for higher-order modes in chapter 2, the solution for the TEM mode is obtained by superposition of the TE and TM modes, defined in a three-dimensional waveguide cavity loaded with a full-height conducting post. The eigensolution of the cavity corresponding to the TEM resonant frequency determines the coefficients of the series expression of the TEM solution. In order to formulate the eigenmatrix equation, the total electromagnetic field in the waveguide region, as well as in an artificial cylindrical region, is expanded using the orthogonal eigenmodes of TE and TM type waves in each region. Continuity of the tangential components of the electric and magnetic fields on the artificial cylindrical boundary is used to derive the general scattering matrix for a cylindrical conductor post situated in a rectangular waveguide. We then apply the boundary conditions at the two shorting planes, which are located at the two ends of the post-loaded waveguide, to derive the eigenmatrix equation. Since the resonant frequency for the TEM mode is determined

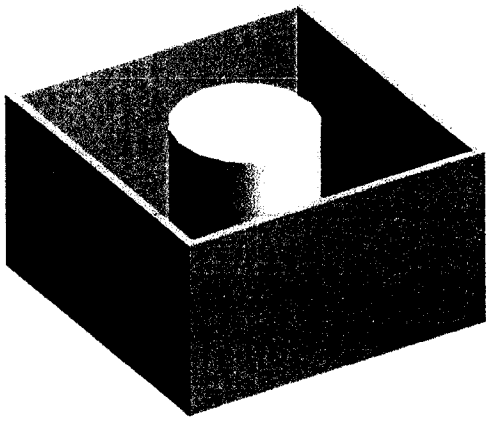

Fig.3.1.1 A rectangular waveguide cavity loaded with a full height conducting post

only by the given height of the resonator, the eigen vector for the TEM mode can be solved without having to search for the eigenvalue.

A number of practical problems are solved based on the formulas that are derived in this chapter. First, we calculate the characteristic impedance of C-R waveguides with various aspect ratios. The results are compared with those calculated using the finite element method (FEM) and other closed form approximations. Excellent agreement is observed in all of these cases. Then, the attenuation coefficient versus the characteristic impedance of the C-R coaxial waveguides for a typical coaxial waveguide is investigated. The results reveal some useful guidelines that can be used for designing coaxial-type

combline filters, interdigital filters and diplexers, which are widely used in wireless communications. The method can also be applied to analyzing other structures as shown in Fig. 3.2.

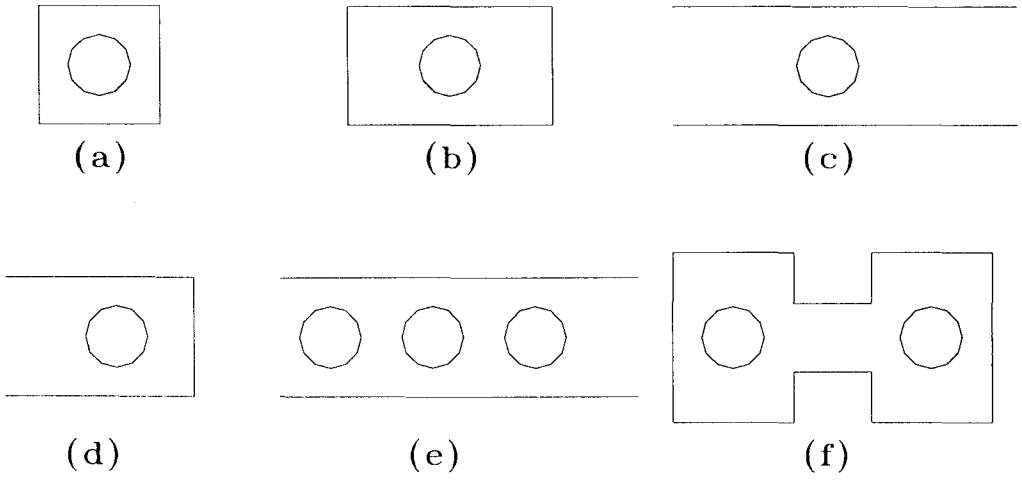

Fig.3.2 The structures for which TEM mode can be analyzed with the proposed method: (a) circular-square coaxial waveguide, (b) circular-rectangular coaxial waveguide, (c) Slab line waveguide, (d) Trough line waveguide, (e) Multiple cylinders in a waveguide, (f) Double-ridged waveguide with circular center conductors.

3.2 Formulation

The characteristics of the TEM mode in a circular rectangular waveguide are different from those of higher-order modes. The TEM mode is a special case of the TM modes, where the cutoff frequency of the TEM mode is equal to zero[64]. Therefore, the scalar Helmholtz equation for the TEM mode reduces to a Laplace's equation on the cross section of the waveguide

$$\nabla_t^2 \varphi = 0 . \tag{3.1}$$

where ∇_t^2 is the Laplacian operator in the two transverse dimensions. φ stands for the transverse electric fields and the transverse magnetic fields. Because the cutoff wavenumber $k_c = 0$, the solution given in chapter 2 cannot be directly applied to the TEM mode solution in a circular rectangular waveguide.

In this section, a new resonant approach is used to characterize a rectangular waveguide resonator loaded with a full height cylindrical post. The standing wave of the TEM_{010} resonant mode in the resonator can be considered to consist of two TEM waves traveling in opposite directions along the coaxial waveguide. The field distribution of the standing wave over the cross section would be the mode function of the corresponding TEM mode.

The eigen-mode solution for the C-R waveguide can be derived by considering the structure shown in Fig. 3.3 (a), in which a rectangular waveguide cavity is loaded with a

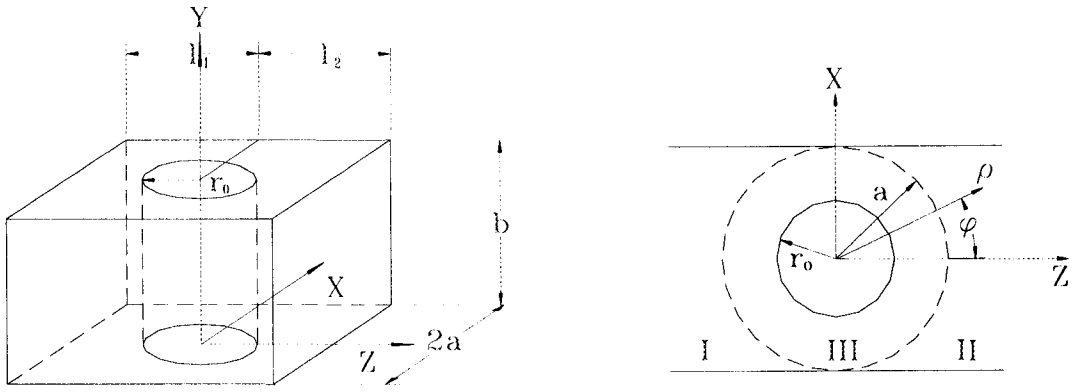

(a) The structure of a C-R cavity **(b) An infinite rectangular waveguide loaded with a full height post**

Fig. 3.3 Structure of a circular-rectangular coaxial waveguide cavity

full height conducting post. The width of the cavity is 2a, the length of the cavity is $l_1+l_2 \geq 2a$, the height of the cavity is b and the radius of the post is r_0. The discontinuity in Fig. 3.3 (b) is divided into the following three regions: (1) rectangular region I; (2) rectangular region II; and (3) cylindrical region III.

The imaginary boundary that separates three regions is a cylindrical surface with radius of $\rho = a$.

3.2.1. Field Expressions and Boundary Conditions

First, an infinitely long rectangular waveguide loaded with a conducting post is considered. The axis of the post coincides with the y-axis of the Cartesian coordinate system used in the waveguide regions. A cylindrical coordinate system used in the post region is defined by $\rho^2 = x^2 + z^2$ and $\tan\phi = \frac{x}{z}$. For the post region, $\rho \le a$. For the waveguide regions, $-a \le x \le a$, $0 \le y \le b$ and $\rho > a$. For region I, z < 0 and for region II, z ≥ 0.

After the Helmholtz equations in the Cartesian coordinates are solved, the components of the electromagnetic fields with respect to the z-direction in the rectangular waveguide region I and II are expressed as

$$\begin{Bmatrix} E_z^I \\ E_z^{II} \end{Bmatrix} = \sum_m \sum_i \left[\begin{Bmatrix} A_{mi}^{Ie} \\ B_{mi}^{IIe} \end{Bmatrix} e^{-\gamma_{mi} z} - \begin{Bmatrix} B_{mi}^{Ie} \\ A_{mi}^{IIe} \end{Bmatrix} e^{\gamma_{mi} z} \right] e_{zmi}^{e}, \tag{3.2}$$

$$\begin{Bmatrix} E_t^I \\ E_t^{II} \end{Bmatrix} = \sum_{p=h,e} \sum_m \sum_i \left[\begin{Bmatrix} A_{mi}^{Ip} \\ B_{mi}^{IIp} \end{Bmatrix} e^{-\gamma_{mi} z} + \begin{Bmatrix} B_{mi}^{Ip} \\ A_{mi}^{IIp} \end{Bmatrix} e^{\gamma_{mi} z} \right] \hat{e}_{tmi}^{p}, \tag{3.3}$$

$$\begin{Bmatrix} H_z^I \\ H_z^{II} \end{Bmatrix} = \sum_m \sum_i \left[\begin{Bmatrix} A_{mi}^{Ih} \\ B_{mi}^{IIh} \end{Bmatrix} e^{-\gamma_{mi} z} + \begin{Bmatrix} B_{mi}^{Ih} \\ A_{mi}^{IIh} \end{Bmatrix} e^{\gamma_{mi} z} \right] h_{zmi}^{h}, \tag{3.4}$$

$$\begin{Bmatrix} H_t^I \\ H_t^{II} \end{Bmatrix} = \sum_{p=h,e} \sum_m \sum_i \left[\begin{Bmatrix} A_{mi}^{Ip} \\ B_{mi}^{IIp} \end{Bmatrix} e^{-\gamma_{mi} z} - \begin{Bmatrix} B_{mi}^{Ip} \\ A_{mi}^{IIp} \end{Bmatrix} e^{\gamma_{mi} z} \right] \hat{h}_{tmi}^{p}, \tag{3.5}$$

where the subscript z indicates the longitudinal field components, the subscript t indicates the transverse field components with respect to the z direction. A_{mi}'s and B_{mi}'s are the coefficients of the waveguide modes incident on and reflected from the post region. e_{mi}^{p}

and h_{mi}^{p} are components of mode functions for electric and magnetic fields. γ_{mi} is the propagation/attenuation constants in the z-direction for each mode, and the subscripts m and i are the mode indices in the x- and y- directions. The superscripts p= e and p = h correspond to the TM and TE modes with respect to the z-direction, respectively. Since the lowest TEM resonant mode in the circular rectangular waveguide cavity is the TEM_{010} mode, only the modal functions with i =1 need to be considered. Based on the above perception, the mode functions are given by

$$e_{zm1}^{p} = \begin{cases} \sin[k_{xm}(x+a)]\sin(k_{y1}y), & for\ \ p=e, \\ 0, & for\ \ p=h, \end{cases} \tag{3.6}$$

$$j\omega\mu_0 h_{zm1}^{p} = \begin{cases} 0, & for\ \ p=e, \\ \cos[k_{xm}(x+a)]\cos(k_{y1}y), & for\ \ p=h, \end{cases} \tag{3.7}$$

$$e_{xm1}^{p} = \frac{1}{k_c^2}\begin{Bmatrix} -\gamma_{m1}k_{xm}, & for\ \ p=e \\ k_{y1}, & for\ \ p=h \end{Bmatrix} \cos[k_{xm}(x+a)]\sin(k_{y1}y), \tag{3.8}$$

$$e_{ym1}^{p} = \frac{1}{k_c^2}\begin{Bmatrix} -\gamma_{m1}k_{y1}, & for\ \ p=e \\ -k_{xm}, & for\ \ p=h \end{Bmatrix} \sin[k_{xm}(x+a)]\cos(k_{y1}y), \tag{3.9}$$

$$j\omega\mu_0 h_{xm1}^{p} = \frac{1}{k_c^2}\begin{Bmatrix} -k_0^2 k_{y1}, & for\ \ p=e \\ \gamma_{m1}k_{xm}, & for\ \ p=h \end{Bmatrix} \sin[k_{xm}(x+a)]\cos(k_{y1}y), \tag{3.10}$$

$$j\omega\mu_0 h_{ym1}^{p} = \frac{1}{k_c^2}\begin{Bmatrix} k_0^2 k_{xm}, & for\ \ p=e \\ \gamma_{m1}k_{y1}, & for\ \ p=h \end{Bmatrix} \cos[k_{xm}(x+a)]\sin(k_{y1}y), \tag{3.11}$$

where

$$k_c^2 = k_{xm}^2 + k_{y1}^2 = \gamma_{m1}^2 + k_0^2. \tag{3.12}$$

In the expressions, $j=\sqrt{-1}$, ω is the angular frequency, μ_0 is the permeability of the air, and k_0 is the wave number in the free space. The wavenumbers along the x and y directions are

$$k_{xm}=\frac{m\pi}{2a}, \qquad k_{y1}=\frac{\pi}{b}, \qquad k_0^2=\omega^2\mu_0\varepsilon_0. \tag{3.13}$$

The field components in the post region are described in terms of the TE and TM modes with respect to the y direction, which are the solutions of the Helmholtz equations in a ρ, ϕ, y cylindrical coordinate system. Since the artificial boundaries in region III are vertical to the ρ direction, the electromagnetic fields are expressed as the transverse and the longitudinal components with respect to the ρ direction by

$$\vec{E}_t^{III}=\sum_n[C_{n1}^e J_n(\eta_1^e\rho)+D_{n1}^e Y_n(\eta_1^e\rho)]\,\hat{e}_{tn1}^{IIIe}+\sum_n[C_{n1}^h J'_n(\eta_1^h\rho)+D_{n1}^h Y'_n(\eta_1^h\rho)]\,\eta_1^h\,\hat{e}_{tn1}^{IIIh}, \tag{3.14}$$

$$E_\rho^{III}=\sum_n[C_{n1}^e J'_n(\eta_1^e\rho)+D_{n1}^e Y'_n(\eta_1^e\rho)]\,\eta_1^e\,e_{\rho n1}^{IIIe}+\sum_n[C_{n1}^h J_n(\eta_1^h\rho)+D_{n1}^h Y_n(\eta_1^h\rho)]\,e_{\rho n1}^{IIIh}, \tag{3.15}$$

$$\vec{H}_t^{III}=\sum_n[C_{n1}^e J'_n(\eta_1^e\rho)+D_{n1}^e Y'_n(\eta_1^e\rho)]\,\eta_1^e\,\hat{h}_{tn1}^{IIIe}+\sum_n[C_{n1}^h J_n(\eta_1^h\rho)+D_{n1}^h Y_n(\eta_1^h\rho)]\,\hat{h}_{tn1}^{IIIh}, \tag{3.16}$$

$$H_\rho^{III}=\sum_n[C_{n1}^e J_n(\eta_1^e\rho)+D_{n1}^e Y_n(\eta_1^e\rho)]\,h_{\rho n1}^{IIIe}+\sum_n[C_{n1}^h J'_n(\eta_1^h\rho)+D_{n1}^h Y'_n(\eta_1^h\rho)]\,\eta_1^h\,h_{\rho n1}^{IIIh}, \tag{3.17}$$

where C_{n1}^{e}, D_{n1}^{e}, C_{n1}^{h} and D_{n1}^{h} are complex coefficients of the eigenfields. η_1^e and η_1^h are cut-off wavenumbers for the TM and TE modes, respectively. The mode functions are given by

$$\hat{e}_{tn1}^{IIIe} = \hat{y}\begin{Bmatrix}\sin(n\phi)\\ \cos(n\phi)\end{Bmatrix}\cos(k_{y1}y) + \hat{\phi}\begin{Bmatrix}-\cos(n\phi)\\ \sin(n\phi)\end{Bmatrix}\frac{nk_{y1}}{\rho\eta_1^{e2}}\sin(k_{y1}y), \tag{3.18}$$

$$\hat{e}_{tn1}^{IIIh} = \hat{\phi}\begin{Bmatrix}\cos(n\phi)\\ -\sin(n\phi)\end{Bmatrix}\frac{1}{\eta_1^{h2}}\sin(k_{y1}y), \tag{3.19}$$

$$j\omega\mu h_{tn1}^{IIIe} = \hat{\phi}\begin{Bmatrix}\sin(n\phi)\\ \cos(n\phi)\end{Bmatrix}\frac{k_0^2}{\eta_1^{e2}}\cos(k_{y1}y), \tag{3.20}$$

$$j\omega\mu h_{tn1}^{IIIh} = \hat{y}\begin{Bmatrix}\cos(n\phi)\\ -\sin(n\phi)\end{Bmatrix}\sin(k_{y1}y) - \hat{\phi}\begin{Bmatrix}\sin(n\phi)\\ \cos(n\phi)\end{Bmatrix}\frac{nk_{y1}}{\rho\eta_1^{h2}}\cos(k_{y1}y), \tag{3.21}$$

where $\hat{y}$ and $\hat{\phi}$ are the unit vectors in the y and ϕ directions, and $\eta_1^2 = k_0^2 - k_{y1}^2$, $k_{y1} = \dfrac{\pi}{b}$ with $\eta_1 = \eta_1^h$ or $\eta_1 = \eta_1^e$.

The boundary conditions to be satisfied are: (1) the tangential components of the electromagnetic fields with respect to the ρ direction in both the waveguide regions and the post region are continuous across the imaginary boundary $\rho = a$, and can be written as

$$\vec{E}_t^{III}\,|_{\rho=a} = \begin{cases}\hat{y}E_y^I + \hat{\phi}(E_x^I\cos\phi - E_z^I\sin\phi)|_{\rho=a}, & \pi/2 \le \phi \le 3\pi/2,\\ \hat{y}E_y^{II} + \hat{\phi}(E_x^{II}\cos\phi - E_z^{II}\sin\phi)|_{\rho=a}, & -\pi/2 \le \phi < \pi/2,\end{cases} \tag{3.22}$$

$$\bar{H}_t^{III}|_{\rho=a}=\begin{cases}\hat{y}H_y^I+\hat{\phi}(H_x^I\cos\phi-H_z^I\sin\phi)|_{\rho=a}, & \pi/2\le\phi\le 3\pi/2,\\ \hat{y}H_y^{II}+\hat{\phi}(H_x^{II}\cos\phi-H_z^{II}\sin\phi)|_{\rho=a}, & -\pi/2\le\phi<\pi/2;\end{cases} \tag{3.23}$$

(2) the tangential components of the electric field disappear on the surface of the inner conductor, which is

$$\bar{E}_t^{III}|_{\rho=r_0}=0. \tag{3.24}$$

Since a full height conducting post is considered, the boundary condition on the inner post conductor is easily satisfied by taking inner products of equation (3.24) with mode functions $\hat{h}_{tk1}^{IIIe}$ and $\hat{h}_{tk1}^{IIIh}$ at $\rho=r_0$, that is

$$<\bar{E}_t^{III},\hat{h}_{tk1}^{IIIe}>=0 \qquad \text{and} \qquad <\bar{E}_t^{III},\hat{h}_{tk1}^{IIIh}>=0. \tag{3.25}$$

Substituting (3.14) into (3.25) leads to

$$[C_{k1}^e J_k(\eta_1^e r_0)+D_{k1}^e Y_k(\eta_1^e r_0)]<\hat{e}_{tk1}^{IIIe},\hat{h}_{tk1}^{IIIe}>=0,$$

$$[C_{k1}^h J'_k(\eta_1^h r_0)+D_{k1}^h Y'_k(\eta_1^h r_0)]|\eta_1^h|<\hat{e}_{tk1}^{IIIh},\hat{h}_{tk1}^{IIIh}>=0. \tag{3.26}$$

where the inner product is defined as [22]

$$<\hat{e},\ \hat{h}>_{\rho=a}=\iint_S(\hat{e}\times\hat{h})_{\rho=a}\cdot\hat{n}dS=\int_0^b dy\int_{\phi_1}^{\phi_2}(e_\phi h_y-e_y h_\phi)_{\rho=a}ad\phi$$

The matrix expression can be derived from the above equations

$$\begin{bmatrix} \mathbf{J}_{ne}(\eta_1^e r_0) & \mathbf{Y}_{ne}(\eta_1^e r_0) & \mathbf{0} & \mathbf{0} \\ \mathbf{0} & \mathbf{0} & \mathbf{J'}_{nh}(\eta_1^h r_0) & \mathbf{Y'}_{nh}(\eta_1^h r_0) \end{bmatrix} \begin{bmatrix} \mathbf{C}^e \\ \mathbf{D}^e \\ \mathbf{C}^h \\ \mathbf{D}^h \end{bmatrix} = [\mathbf{W}] \begin{bmatrix} \mathbf{C}^e \\ \mathbf{D}^e \\ \mathbf{C}^h \\ \mathbf{D}^h \end{bmatrix} = \{\mathbf{0}\}, \qquad (3.27)$$

where $\mathbf{J}_{ne}$, $\mathbf{Y}_{ne}$, $\mathbf{J'}_{nh}$ and $\mathbf{Y'}_{nh}$ are submatrices. The elements in $\mathbf{J}_{ne}$ and $\mathbf{Y}_{ne}$ are the Bessel functions of the first and second kinds respectively. The elements in $\mathbf{J'}_{nh}$ and $\mathbf{Y'}_{nh}$ are the derivatives of the Bessel functions of first and second kinds with respect to ρ respectively. The orders of matrices $\mathbf{J}_{ne}$ and $\mathbf{Y}_{ne}$ are $N_e \times N_e$, the orders of matrices $\mathbf{J'}_{nh}$ and $\mathbf{Y'}_{nh}$ are $N_h \times N_h$. N_e is the total number of TM modes used, and N_h is the total number of TE modes used. The **W** matrix for a full height post is given by

$$[\mathbf{W}] = \begin{bmatrix} \mathbf{W}_{11} & \mathbf{W}_{12} & \mathbf{W}_{13} & \mathbf{W}_{14} \\ \mathbf{W}_{21} & \mathbf{W}_{22} & \mathbf{W}_{23} & \mathbf{W}_{24} \end{bmatrix} = \begin{bmatrix} \mathbf{J}_{ne} & \mathbf{Y}_{ne} & \mathbf{0} & \mathbf{0} \\ \mathbf{0} & \mathbf{0} & \mathbf{J'}_{nh} & \mathbf{Y'}_{nh} \end{bmatrix}. \qquad (3.28)$$

The **W** matrix shows the relation between the coefficients of the electromagnetic fields in post region III and the boundary conditions at the surface of the inner conductor.

3.2.2 General Scattering Matrix and Field Coefficients

The other boundary conditions at $\rho = a$ are taken into account by taking inner products of equation (3.22) with $\hat{h}_{tk1}^{IIIe}$ and $\hat{h}_{tk1}^{IIIh}$, and (3.23) with $\hat{e}_{tk1}^{IIIe}$ and $\hat{e}_{tk1}^{IIIh}$, the left sides of the equations become

$$< \vec{E}_t^{III}, \hat{h}_{tm1}^{IIIe} >= C_{n1}^e J_n(\eta_1^e a) < \hat{e}_{tm1}^{IIIe}, \hat{h}_{tm1}^{IIIe} > + D_{n1}^e Y_n(\eta_1^e a) < \hat{e}_{tm1}^{IIIe}, \hat{h}_{tm1}^{IIIe} >, \qquad (3.29a)$$

$$< \hat{e}_{tm1}^{IIIe}, \vec{H}_t^{III} >= C_{n1}^e J'_n(\eta_1^e a) \,|\, \eta_1^e \,| < \hat{e}_{tm1}^{IIIe}, \hat{h}_{tm1}^{IIIe} > + D_{n1}^e Y'_n(\eta_1^e a) \,|\, \eta_1^e \,| < \hat{e}_{tm1}^{IIIe}, \hat{h}_{tm1}^{IIIe} >, \qquad (3.29b)$$

$$< \vec{E}_t^{III}, \hat{h}_{tm1}^{IIIh} >= C_{n1}^h J'_n(\eta_1^h a) |\eta_1^h| < \hat{e}_{tm1}^{IIIh}, \hat{h}_{tm1}^{IIIh} > + D_{n1}^h Y'_n(\eta_1^h a) |\eta_1^h| < \hat{e}_{tm1}^{IIIh}, \hat{h}_{tm1}^{IIIh} >, \qquad (3.29c)$$

$$< \hat{e}^{h}_{tm1}, \vec{H}^{III}_{t} >= C^{h}_{n1} J_n(\eta^{h}_{1} a) < \hat{e}^{IIIh}_{tm1}, \hat{h}^{IIIh}_{tm1} > + D^{h}_{n1} Y_n(\eta^{h}_{1} a) < \hat{e}^{IIIh}_{tm1}, \hat{h}^{IIIh}_{tm1} >, \tag{3.29d}$$

and the right sides of the equations are written as

$$< \hat{y}E^{I}_{y} + \hat{\phi}E^{I}_{\phi} + \hat{y}E^{II}_{y} + \hat{\phi}E^{II}_{\phi}, \hat{h}^{IIIe}_{tm1} >= [\mathbf{u}_{11}\ \mathbf{u}_{12}\ \cdots\ \mathbf{u}_{18}]\begin{bmatrix}\mathbf{A}\\ \mathbf{B}\end{bmatrix}, \tag{3.30a}$$

$$< \hat{e}^{IIIe}_{tm1}, \hat{y}H^{I}_{y} + \hat{\phi}H^{I}_{\phi} + \hat{y}H^{II}_{y} + \hat{\phi}H^{II}_{\phi} >= [\mathbf{u}_{21}\ \mathbf{u}_{22}\ \cdots\ \mathbf{u}_{28}]\begin{bmatrix}\mathbf{A}\\ \mathbf{B}\end{bmatrix}, \tag{3.30b}$$

$$< \hat{y}E^{I}_{y} + \hat{\phi}E^{I}_{\phi} + \hat{y}E^{II}_{y} + \hat{\phi}E^{II}_{\phi}, \hat{h}^{IIIh}_{tm1} >= [\mathbf{u}_{31}\ \mathbf{u}_{32}\ \cdots\ \mathbf{u}_{38}]\begin{bmatrix}\mathbf{A}\\ \mathbf{B}\end{bmatrix}, \tag{3.30c}$$

$$< \hat{e}^{IIIh}_{tm1}, \hat{y}H^{I}_{y} + \hat{\phi}H^{I}_{\phi} + \hat{y}H^{II}_{y} + \hat{\phi}H^{II}_{\phi} >= [\mathbf{u}_{41}\ \mathbf{u}_{42}\ \cdots\ \mathbf{u}_{48}]\begin{bmatrix}\mathbf{A}\\ \mathbf{B}\end{bmatrix}. \tag{3.30d}$$

The following matrix equation is derived,

$$[\mathbf{Q}]\begin{bmatrix}\mathbf{C}^{e}\\ \mathbf{D}^{e}\\ \mathbf{C}^{h}\\ \mathbf{D}^{h}\end{bmatrix} = \begin{bmatrix}\mathbf{u}_{11} & \mathbf{u}_{12} & \cdots & \mathbf{u}_{18}\\ \mathbf{u}_{21} & \mathbf{u}_{22} & \cdots & \mathbf{u}_{28}\\ \mathbf{u}_{31} & \mathbf{u}_{32} & \cdots & \mathbf{u}_{38}\\ \mathbf{u}_{41} & \mathbf{u}_{42} & \cdots & \mathbf{u}_{48}\end{bmatrix}\begin{bmatrix}\mathbf{A}^{Ie}\\ \mathbf{A}^{Ih}\\ \mathbf{A}^{IIe}\\ \mathbf{A}^{IIh}\\ \mathbf{B}^{Ie}\\ \mathbf{B}^{Ih}\\ \mathbf{B}^{IIe}\\ \mathbf{B}^{IIh}\end{bmatrix}, \tag{3.31}$$

where the elements of **Q** consist of Bessel functions only, and the elements of $\mathbf{u}_{ij}$ have the form of the inner product $< \hat{e}^{IIIp}_{tm1}, \pm e^{\pm\gamma_m z}\hat{h}^{I,IIp}_{tm1} >_{\rho=a}$ or $< \pm e^{\pm\gamma_m z}\hat{e}^{I,IIp}_{tm1}, \hat{h}^{IIIp}_{tm1} >_{\rho=a}$ with $p = e$ or $p = h$.

Therefore, we have found that the relationship between the coefficients of the fields in the waveguide region and the post region is given by

$$\begin{bmatrix} \mathbf{C}^e \\ \mathbf{D}^e \\ \mathbf{C}^h \\ \mathbf{D}^h \end{bmatrix} = \begin{bmatrix} \mathbf{X}_{11} & \mathbf{X}_{12} & \cdots & \mathbf{X}_{18} \\ \mathbf{X}_{21} & \mathbf{X}_{22} & \cdots & \mathbf{X}_{28} \\ \mathbf{X}_{31} & \mathbf{X}_{32} & \cdots & \mathbf{X}_{38} \\ \mathbf{X}_{41} & \mathbf{X}_{42} & \cdots & \mathbf{X}_{48} \end{bmatrix} \begin{bmatrix} \mathbf{A}^{Ie} \\ \mathbf{A}^{Ih} \\ \mathbf{A}^{IIe} \\ \mathbf{A}^{IIh} \\ \mathbf{B}^{Ie} \\ \mathbf{B}^{Ih} \\ \mathbf{B}^{IIe} \\ \mathbf{B}^{IIh} \end{bmatrix}, \tag{3.32}$$

with $[\mathbf{X}] = [\mathbf{Q}]^{-1}[\mathbf{U}]$. The expressions for the elements of [Q] and [U] matrices are given in the appendix of this chapter. Substituting (3.32) into (3.27) results in

$$[\mathbf{W}]\begin{Bmatrix} \mathbf{C}^e \\ \mathbf{D}^e \\ \mathbf{C}^h \\ \mathbf{D}^h \end{Bmatrix} = [\mathbf{W}][\mathbf{X}]\begin{Bmatrix} \mathbf{A} \\ \mathbf{B} \end{Bmatrix} = [\mathbf{W}][\mathbf{X}_A \mathbf{X}_B]\begin{Bmatrix} \mathbf{A} \\ \mathbf{B} \end{Bmatrix} = \{\mathbf{0}\}, \tag{3.33}$$

where the elements in the **W** matrix contain only the Bessel functions of the first and the second kinds. The elements in the **X** matrix involve the inner products of the eigenmode functions in the post region and waveguide regions. $\mathbf{X}_A$ corresponds to the wave incident onto the post region, while $\mathbf{X}_B$ corresponds to the wave reflected from the post region. The matrix [X] connects the fields in the waveguide regions and the post region.

To align with the definition of the general scattering matrix, we rearrange equation (3.33) and obtain the following expression

$$\{\mathbf{B}\} = [\mathbf{S}]\{\mathbf{A}\} = -([\mathbf{W}][\mathbf{X}_B])^{-1}[\mathbf{W}][\mathbf{X}_A]\{\mathbf{A}\}, \tag{3.34}$$

with respect to the reference plane at z = 0. [S] is the general scattering matrix with the reference plane at the center of the post. {A} and {B} are coefficient vectors of the

incident and reflected field in rectangular waveguide regions, respectively. Then, by applying the boundary condition of the two conducting planes at the ends of the cavity, we obtain the matrix expression given by

$$([\mathbf{D}][\mathbf{S}][\mathbf{D}]+[\mathbf{I}])\{\mathbf{A}'\}=\{\mathbf{0}\} \quad \text{and} \quad [\mathbf{D}]=\begin{bmatrix}\mathbf{D}_1 & \mathbf{0}\\ \mathbf{0} & \mathbf{D}_2\end{bmatrix} \tag{3.35}$$

where the submatrix $\mathbf{D}_k$ is a diagonal transmission matrix with $d_{ii}=e^{-\gamma_i l_k}$, **[I]** is the identity matrix, and **{A′}** is the coefficient vector of the incident wave with reference to planes that have been shifted to the ends of the cavity. The characteristic equation det([D][S][D]+[I])=0 must be satisfied to ensure existence of the eigensolution of equation (3.35).

Intuitively, it is known that the resonant mode of the cavity corresponding to the TEM mode in the transverse direction comes with a wavelength equal to twice the height of the cavity. In other words, the eigen vector **{A′}** can be determined from equation (3.35), using the known eigenvalue (resonant frequency). **{A}** is given by shifting the reference plane back to the center of the post,

$$\{\mathbf{A}\}=[\mathbf{D}]\{\mathbf{A}'\} \tag{3.36}$$

After the coefficient vectors **{A}**, and then **{B}** are obtained for the waveguide regions, using equations (3.36) and (3.34), the coefficient vectors in the post region can be easily determined using equation (3.32). The field distribution in the cavity therefore can be obtained.

3.2.3 Characteristic Impedance of a C-R Waveguide

Once the eigenmode field distributions are found, the characteristic impedance for a C-R coaxial waveguide can be calculated by

$$Z = \frac{V}{I} = \frac{\int_{r_0}^{a} E_\rho^{III}(\phi = \pi/2)d\rho}{\oint H_\phi^{III}(\rho = \rho_0)\rho_0 d\phi}, \qquad r_0 \le \rho_0 \le a, \tag{3.37}$$

where V is the voltage between the inner and outer conductors, and I is the total current flowing on the inner conductor. To calculate the voltage V, the electric field E_ρ needs to be integrated from the inner conductor to the outer conductor along any path. A judicious choice is the path along $\phi = \pi/2$, since only the field expression in the post region is needed. The integration of E_ρ^{III} is carried out by integrating each term of E_ρ^{III} in equation (3.15), which gives

$$\begin{aligned}
&\int_{r_0}^{a} E_\rho^{III}(\phi = \pi/2)d\rho \\
&= \sum_n \int_{r_0}^{a} [C_{n1}^e J'_n(\eta_1^e \rho) + D_{n1}^e Y'_n(\eta_1^e \rho)]\eta_1^e e_{\rho n1}^{IIIe}(\phi = \frac{\pi}{2})d\rho \\
&\quad + \sum_n \int_{r_0}^{a} [C_{n1}^h J_n(\eta_1^h \rho) + D_{n1}^h Y_n(\eta_1^h \rho)]e_{\rho n1}^{IIIh}(\phi = \frac{\pi}{2})d\rho \qquad (3.38) \\
&= \sum_{n=0}^{N_e} V_n^e + \sum_{n=0}^{N_h} V_n^h,
\end{aligned}$$

where V_n^e and V_n^h are results of integrating E_ρ^{III} for TM and TE modes, respectively.

They are given by

$$V_n^e = \{C_{n1}^e[J_n(\eta_1^e a) - J_n(\eta_1^e r_0)] + D_{n1}^e[Y_n(\eta_1^e a) - Y_n(\eta_1^e r_0)]\}\Phi_n^e \frac{(-\pi)}{b\eta_1^{e2}} \sin(\frac{\pi}{b} y_0), \qquad (3.39a)$$

$$V_n^h = C_{n1}^h \begin{cases} J_n(\eta_1^h a) - J_n(\eta_1^h r_0) - 2\sum_{k=1}^{n/2}[J_{2k}(\eta_1^h a) - J_{2k}(\eta_1^h r_0)] - J_0(\eta_1^h a) + J_0(\eta_1^h r_0) \\ \qquad n = 0, 2, 4, \ldots \\ J_n(\eta_1^h a) - J_n(\eta_1^h r_0) - 2\sum_{k=0}^{(n-1)/2}[J_{2k+1}(\eta_1^h a) - J_{2k+1}(\eta_1^h r_0)] + \eta_1^h \int_{r_0}^{a} J_0(\eta_1^h r) dr \\ \qquad n = 1, 3, 5, \ldots \end{cases}$$

$$\cdot \Phi_n^h \frac{1}{\eta_1^{h2}} \sin(\frac{\pi}{b} y_0)$$

$$+ D_{n1}^h \begin{cases} Y_n(\eta_1^h a) - Y_n(\eta_1^h r_0) - 2\sum_{k=1}^{n/2}[Y_{2k}(\eta_1^h a) - Y_{2k}(\eta_1^h r_0)] - Y_0(\eta_1^h a) + Y_0(\eta_1^h r_0) \\ \qquad n = 0, 2, 4, \ldots \\ Y_n(\eta_1^h a) - Y_n(\eta_1^h r_0) - 2\sum_{k=0}^{(n-1)/2}[Y_{2k+1}(\eta_1^h a) - Y_{2k+1}(\eta_1^h r_0)] + \eta_1^h \int_{r_0}^{a} Y_0(\eta_1^h r) dr \\ \qquad n = 1, 3, 5, \ldots \end{cases}$$

$$\cdot \Phi_n^h \frac{1}{\eta_1^{h2}} \sin(\frac{\pi}{b} y_0) \quad , \qquad (3.39b)$$

where $y_0 = \lambda_0 / 8$, λ_0 is the wavelength at the working frequency and

$$\Phi_n^e = \Phi_n^h = \begin{cases} \sin(\frac{n\pi}{2}) & n = 1, 3, 5, \ldots \\ \cos(\frac{n\pi}{2}) & n = 0, 2, 4, \ldots \end{cases}. \qquad (3.39c)$$

The analytic expression for the total current is given by

$$\oint H_{\phi}^{III}(\rho=\rho_0)\rho_0 d\phi = [C_{01}^{e} J_0'(\eta_1^{e}\rho_0) + D_{01}^{e} Y_0'(\eta_1^{e}\rho_0)]\frac{k_0^2}{\eta_1^2} 2\pi\cos(\frac{\pi}{b}y_0)\rho_0 . \qquad (3.40)$$

Here, the total current on the inner conductor is a constant with respect to the parameter ρ_0. H_{ϕ}^{III} is obtained from equations (3.16), (3.20) and (3.21) by taking the ϕ component of H_t^{III}. After the voltage and current are obtained, one can easily calculate the characteristic impedance with equation (3.37).

3.2.4 Power Loss and Attenuation Coefficient

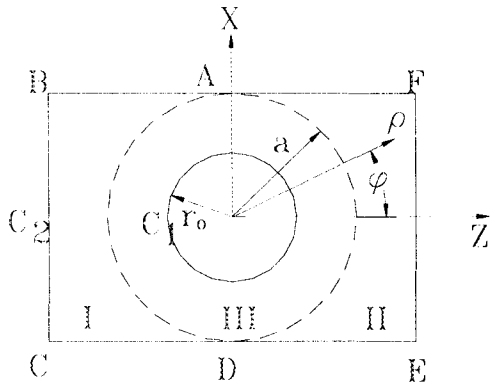

Fig. 3.4 The integration circle on the inner and outer conductor boundaries

By using the definition of the power loss per unit length of the waveguide due to the finite conductivity of the metallic conductors, we have

$$P_c = \frac{R_s}{2}\int_{C_1+C_2} \overline{H}\cdot\overline{H}^{*}\, dl , \qquad (3.41)$$

where R_s is the surface resistance of the conductors, C_1 and C_2 represent the integration paths over the inner and outer conductor boundaries shown in Fig. 3.4. $\overline{H}$ is the component of the magnetic field parallel to C_1 and C_2. $\overline{H} = H_\phi^{III}$ is on the inner conductor surface. On the outer conductor surface, $\overline{H} = H_z^I$ is on AB and CD, $\overline{H} = H_x^I$ on BC, $\overline{H} = H_z^{II}$ on DE and AF, and $\overline{H} = H_x^{II}$ on EF. Because of the symmetric distribution of the magnetic field, we can calculate P_c using the following equation:

$$P_c = 2R_s[\int_{-l_1}^{0}(H_z^I \cdot H_z^{I*})_{x=a}\,dz + \int_{0}^{a}(H_x^I \cdot H_x^{I*})_{z=-a}\,dx + \frac{1}{4}\oint_{C_1}(H_\phi^{III} \cdot H_\phi^{III*})_{\rho=r_0}\,r_0 d\phi]. \quad (3.42)$$

The attenuation coefficient is given by

$$\alpha = \frac{P_c}{2P_0} = \frac{P_c}{\int_{r_0}^{a} E_\rho^{III}(\phi = \frac{\pi}{2})d\rho \oint H_\phi^{III*}(\rho = \rho_0)\rho_0 d\phi}, \quad (3.43)$$

where P_0 is the power that flows along the conductors, and the integrals of E_ρ^{III} and H_ϕ^{III} are calculated using equations (3.38) and (3.40), respectively .

3.3 Numerical Results and Discussion

To verify the accuracy of the solution, the field distribution in a C-R coaxial waveguide and related parameters are calculated by using our new technique. The frequency chosen for computation is 9.836 GHz. It is found that when 4 TE and 4 TM symmetric modes in the rectangular waveguide and 8 TE and 8 TM symmetric modes in

the cylindrical region are used, the numerically determined frequency is accurate to four decimal places.

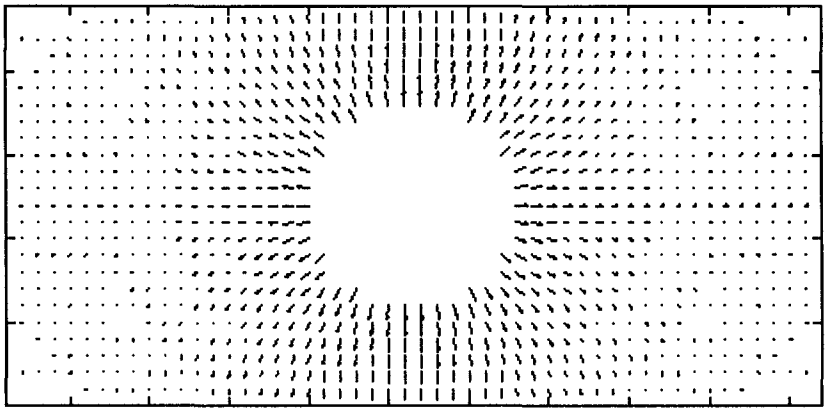

Fig. 3.5 (a) Field distribution of the TEM mode in a C-R waveguide.

$b/a = 1.2$, $r_0/a = 0.47$, $l_1/a = l_2/a = 2$.

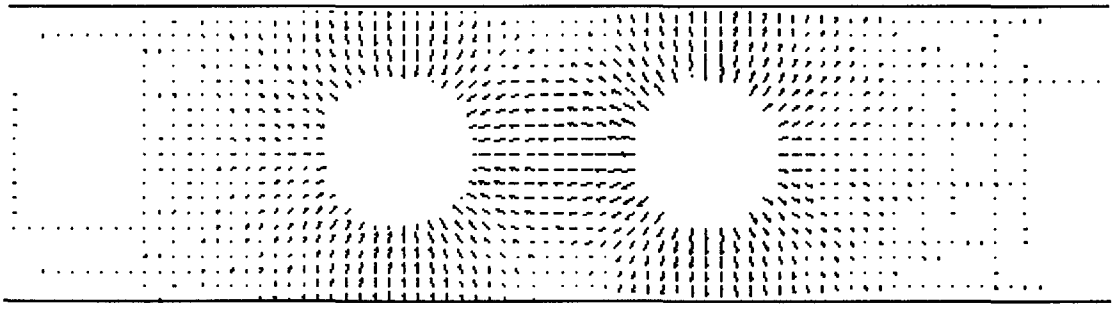

Fig. 3.5 (b) Field distribution of the TEM mode in a twin line structure.

$r_0/a = 0.47$, $l_1/a = l_2/a = \infty$, $b/a = 1.2$, $d/a = 2$.

The vector fields in a C-R waveguide and in a twin line structure are shown in Fig.3.5 (a) and (b), respectively. The field lines appear to converge either into or out of the region occupied by the post. In the vicinity of the post, the field lines are approximately aligned along radials, which extend outwards from the center of these posts. The field lines are perpendicular to the surfaces of inner and outer conductors.

The even- and odd- mode impedances, Z_e and Z_o, of the multiple inner conductor structure vs. the ratio of r_0 /a are presented in Fig. 3.8. Perfect electric walls are used at the two sides of an inner conductor for calculating Z_o, and perfect magnetic walls are used for calculating Z_e. Excellent agreement is observed between the calculated results and those published in [52]. The Z_e and Z_o of the multiple inner conductor coaxial line are important parameters in designing the coaxial-line interdigital filters.

It is worth mentioning that in all the examples calculated in this section, the value of the impedance increases as r_0 decreases or as l_1 and l_2 increase. When l_1 and l_2 are greater than $3a$, the value of the impedance tends towards a constant.

Fig. 3.6 shows the characteristic impedance of a C-R coaxial waveguide versus the ratio r_0/a. The result is compared with that obtained using the commercial finite element package (Ansoft's HFSS). Fig. 3.7 gives a comparison of the calculated value using a proposed formulation for the characteristic impedance of a slab line with the results reported in [48]. In both cases, excellent agreement is obtained.

The attenuation due to conductor loss versus the characteristic impedance for different ratios of l_1/a is plotted in fig. 3.9, where $l_1 = l_2$. The attenuation reaches its minimum between the values of 70 ohm and 90 ohm on the impedance scale. In this

region, the attenuation varies smoothly in a very limited range. When the value of l_1/a increases, the attenuation decreases for the same impedance of the C-R coaxial waveguides. The attenuation of a circular coaxial waveguide is also plotted in the same figure. The inner conductor of the circular coaxial waveguide has the same radius as that of the C-R waveguides. The radius of the outer conductor is chosen such that the value of the area covered by the outer conductor of the circular coaxial waveguide is the same as that of the circular- square coaxial waveguide ($l_1/a = 1$). The minimum attenuation is achieved for an impedance value of around 75 ohm in the case of the circular coaxial waveguide. It can be seen that it is a good approximation to estimate the conductor loss of C-R waveguides using the formulation for circular coaxial lines.

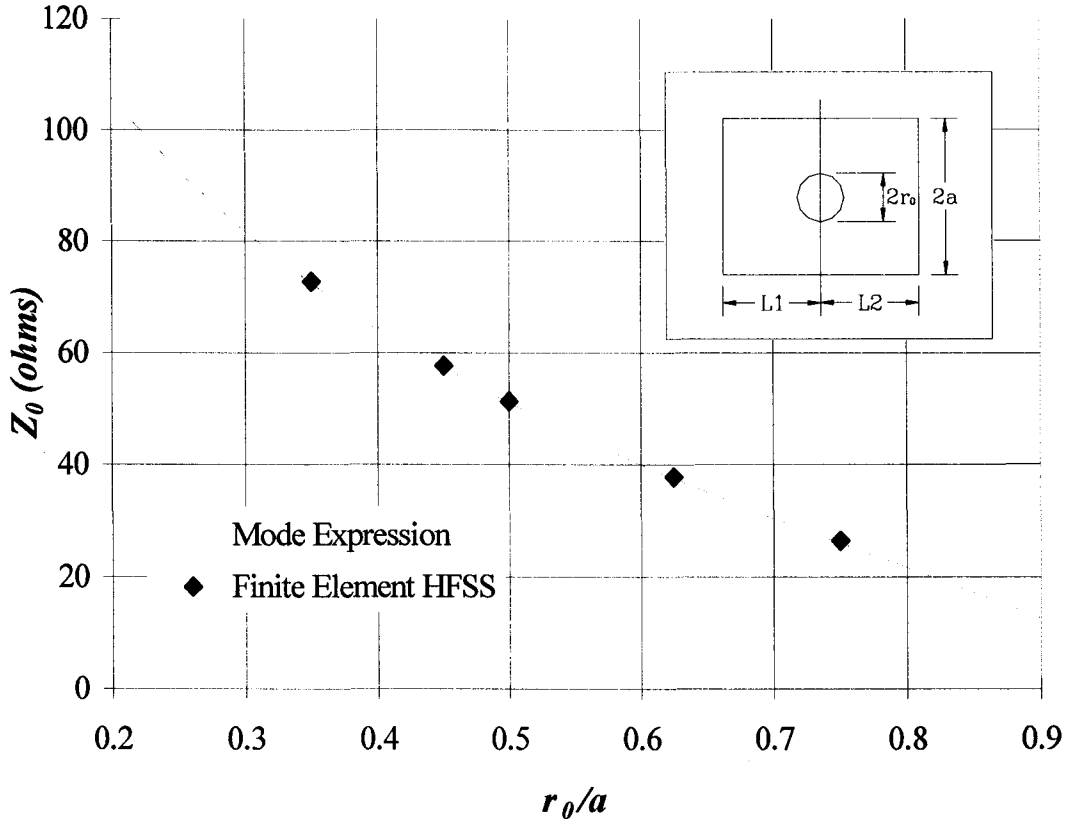

Fig. 3.6 The characteristic impedance of a C-R waveguide vs. r_0/a

b/a=1.2, $l_1/a = l_2/a$ =1.25, a=0.5in, f=9.836 GHz.

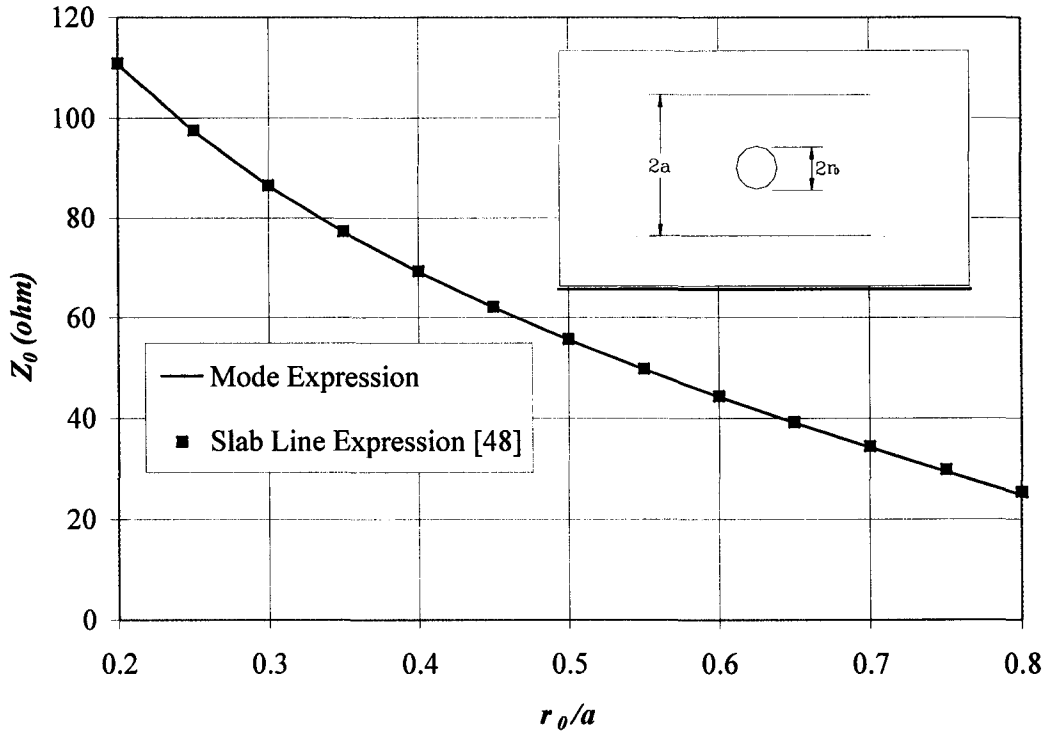

Fig. 3.7 The characteristic impedance of the slab line.

a=0.5in, $l_1=l_2=\infty$.

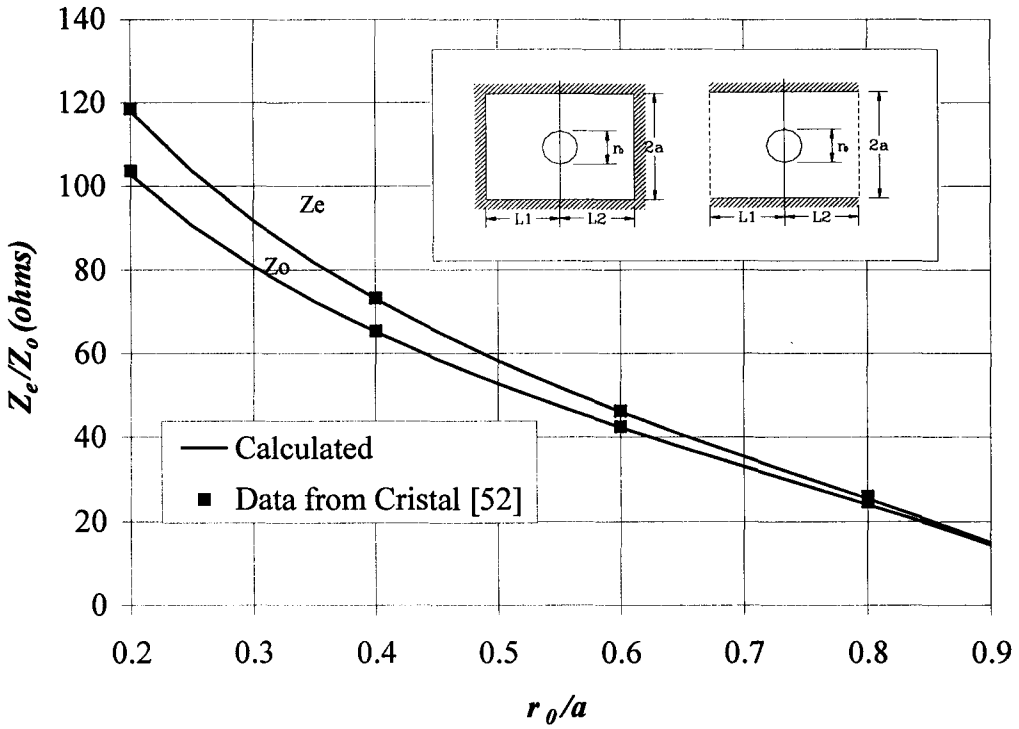

Fig. 3.8 The even and odd mode impedance of the multiple inner conductors.

$l_1/a = l_2/a = 0.9 + r_0/a$, $d/a = 2l_1/a$.

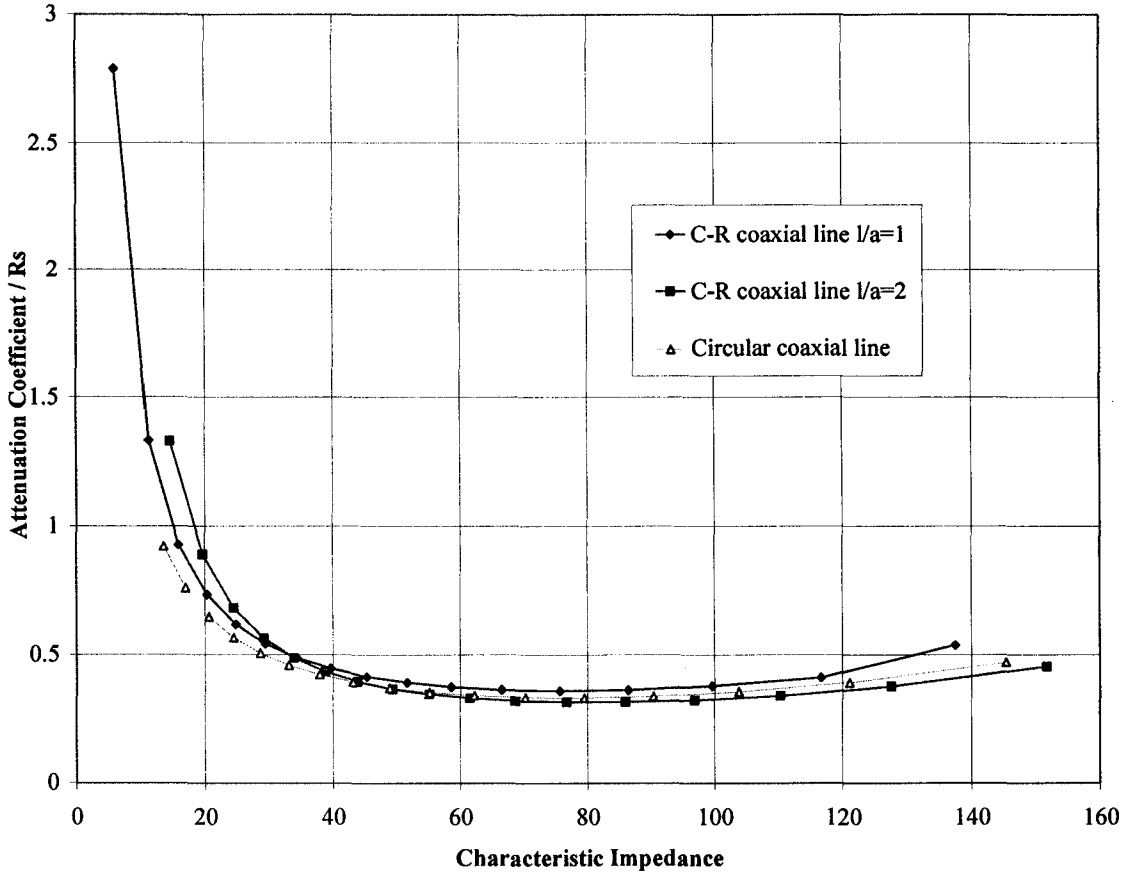

Fig. 3.9 The attenuation coefficient of the C-R waveguide vs. characteristic impedance

a=0.5 inches.

3.4 Appendix

3.4.1 Element Expressions of Matrix [Q]

Elements of the matrix Q in equation (3.31) are given by

$$q_{11} = J_n(\eta_1^e a) < \hat{e}_{tm1}^{IIIe}, \hat{h}_{tm1}^{IIIe} >, \qquad q_{13} = 0, \tag{3.44 a}$$

$$q_{12} = Y_n(\eta_1^e a) < \hat{e}_{tm1}^{IIIe}, \hat{h}_{tm1}^{IIIe} >, \qquad q_{14} = 0, \tag{3.44 b}$$

$$q_{21} = J'_n(\eta_1^e a)|\eta_1^e| < \hat{e}_{tm1}^{IIIe}, \hat{h}_{tm1}^{IIIe} >, \qquad q_{23} = 0, \tag{3.44 c}$$

$$q_{22} = Y'_n(\eta_1^e a)|\eta_1^e| < \hat{e}_{tm1}^{IIIe}, \hat{h}_{tm1}^{IIIe} >, \qquad q_{24} = 0, \tag{3.44 d}$$

$$q_{31} = 0, \qquad q_{33} = J'_n(\eta_1^h a)|\eta_1^h| < \hat{e}_{tm1}^{IIIh}, \hat{h}_{tm1}^{IIIh} >, \tag{3.44 e}$$

$$q_{32} = 0, \qquad q_{34} = Y'_n(\eta_1^h a)|\eta_1^h| < \hat{e}_{tm1}^{IIIh}, \hat{h}_{tm1}^{IIIh} >, \tag{3.44 f}$$

$$q_{41} = 0, \qquad q_{43} = J_n(\eta_1^h a) < \hat{e}_{tm1}^{IIIh}, \hat{h}_{tm1}^{IIIh} >, \tag{3.44 g}$$

$$q_{42} = 0, \qquad q_{44} = Y_n(\eta_1^h a) < \hat{e}_{tm1}^{IIIh}, \hat{h}_{tm1}^{IIIh} >, \tag{3.44 h}$$

3.4.2 Element Expressions of Matrix [U]

$$u_{11} = \int_{\frac{\pi}{2}}^{\frac{3\pi}{2}} d\phi \int_0^b dy \left[-e^{-\gamma_{m1}z} e^e_{ym1} \begin{Bmatrix} \sin(n\phi) \\ \cos(n\phi) \end{Bmatrix} \frac{k_0^2}{\eta_1^{e2}} \cos(k_{y1}y) \right] \tag{3.45}$$

$$u_{12} = \int_{\frac{\pi}{2}}^{\frac{3\pi}{2}} d\phi \int_0^b dy \left[-e^{-\gamma_{m1}z} e^h_{ym1} \begin{Bmatrix} \sin(n\phi) \\ \cos(n\phi) \end{Bmatrix} \frac{k_0^2}{\eta_1^{e2}} \cos(k_{y1}y) \right] \tag{3.46}$$

$$u_{13} = \int_{-\frac{\pi}{2}}^{\frac{\pi}{2}} d\phi \int_0^b dy \left[-e^{\gamma_{m1}z} e^e_{ym1} \begin{Bmatrix} \sin(n\phi) \\ \cos(n\phi) \end{Bmatrix} \frac{k_0^2}{\eta_1^{e2}} \cos(k_{y1}y) \right] \tag{3.47}$$

$$u_{14} = \int_{-\frac{\pi}{2}}^{\frac{\pi}{2}} d\phi \int_0^b dy \left[-e^{\gamma_{m1}z} e^h_{ym1} \begin{Bmatrix} \sin(n\phi) \\ \cos(n\phi) \end{Bmatrix} \frac{k_0^2}{\eta_1^{e2}} \cos(k_{y1}y) \right] \tag{3.48}$$

$$u_{15} = \int_{\frac{\pi}{2}}^{\frac{3\pi}{2}} d\phi \int_0^b dy \left[-e^{\gamma_{m1}z} e^e_{ym1} \begin{Bmatrix} \sin(n\phi) \\ \cos(n\phi) \end{Bmatrix} \frac{k_0^2}{\eta_1^{e2}} \cos(k_{y1}y) \right] \tag{3.49}$$

$$u_{16} = \int_{\frac{\pi}{2}}^{\frac{3\pi}{2}} d\phi \int_0^b dy \left[-e^{\gamma_{m1}z} e^h_{ym1} \begin{Bmatrix} \sin(n\phi) \\ \cos(n\phi) \end{Bmatrix} \frac{k_0^2}{\eta_1^{e2}} \cos(k_{y1}y) \right] \tag{3.50}$$

$$u_{17} = \int_{-\frac{\pi}{2}}^{\frac{\pi}{2}} d\phi \int_0^b dy \left[-e^{-\gamma_{m1}z} e^e_{ym1} \begin{Bmatrix} \sin(n\phi) \\ \cos(n\phi) \end{Bmatrix} \frac{k_0^2}{\eta_1^{e2}} \cos(k_{y1}y) \right] \tag{3.51}$$

$$u_{18} = \int_{-\frac{\pi}{2}}^{\frac{\pi}{2}} d\phi \int_0^b dy \left[-e^{-\gamma_{m1}z} e^h_{ym1} \begin{Bmatrix} \sin(n\phi) \\ \cos(n\phi) \end{Bmatrix} \frac{k_0^2}{\eta_1^{e2}} \cos(k_{y1}y) \right] \tag{3.52}$$

$$u_{21} = \int_{\frac{\pi}{2}}^{\frac{3\pi}{2}} d\phi \int_0^b dy e^{-\gamma_{m1}z} [h_{ym1}^e \begin{Bmatrix} -\cos(n\phi) \\ \sin(n\phi) \end{Bmatrix} \frac{nk_{y1}}{a\eta_1^{e2}} \sin(k_{y1}y) - h_{xm1}^e \cos(\phi) \begin{Bmatrix} \sin(n\phi) \\ \cos(n\phi) \end{Bmatrix} \cos(k_{y1}y)] \tag{3.53}$$

$$u_{22} = \int_{\frac{\pi}{2}}^{\frac{3\pi}{2}} d\phi \int_0^b dy e^{-\gamma_{m1}z} [h_{ym1}^h \begin{Bmatrix} -\cos(n\phi) \\ \sin(n\phi) \end{Bmatrix} \frac{nk_{y1}}{a\eta_1^{e2}} \sin(k_{y1}y) - (h_{xm1}^h \cos(\phi) - h_{zm1}^h \sin(\phi)) \begin{Bmatrix} \sin(n\phi) \\ \cos(n\phi) \end{Bmatrix} \cos(k_{y1}y)] \tag{3.54}$$

$$u_{23} = \int_{-\frac{\pi}{2}}^{\frac{\pi}{2}} d\phi \int_0^b dy e^{\gamma_{m1}z} [-h_{ym1}^e \begin{Bmatrix} -\cos(n\phi) \\ \sin(n\phi) \end{Bmatrix} \frac{nk_{y1}}{a\eta_1^{e2}} \sin(k_{y1}y) + h_{xm1}^e \cos(\phi) \begin{Bmatrix} \sin(n\phi) \\ \cos(n\phi) \end{Bmatrix} \cos(k_{y1}y)] \tag{3.55}$$

$$u_{24} = \int_{-\frac{\pi}{2}}^{\frac{\pi}{2}} d\phi \int_0^b dy e^{\gamma_{m1}z} [-h_{ym1}^h \begin{Bmatrix} -\cos(n\phi) \\ \sin(n\phi) \end{Bmatrix} \frac{nk_{y1}}{a\eta_1^{e2}} \sin(k_{y1}y) + (h_{xm1}^h \cos(\phi) + h_{zm1}^h \sin(\phi)) \begin{Bmatrix} \sin(n\phi) \\ \cos(n\phi) \end{Bmatrix} \cos(k_{y1}y)] \tag{3.56}$$

$$u_{25} = \int_{\frac{\pi}{2}}^{\frac{3\pi}{2}} d\phi \int_0^b dy e^{\gamma_{m1}z} [-h_{ym1}^e \begin{Bmatrix} -\cos(n\phi) \\ \sin(n\phi) \end{Bmatrix} \frac{nk_{y1}}{a\eta_1^{e2}} \sin(k_{y1}y) + h_{xm1}^e \cos(\phi) \begin{Bmatrix} \sin(n\phi) \\ \cos(n\phi) \end{Bmatrix} \cos(k_{y1}y)] \tag{3.57}$$

$$u_{26} = \int_{\frac{\pi}{2}}^{\frac{3\pi}{2}} d\phi \int_0^b dy e^{\gamma_{m1} z} [-h^h_{ym1} \begin{Bmatrix} -\cos(n\phi) \\ \sin(n\phi) \end{Bmatrix} \frac{nk_{y1}}{a\eta_1^{e2}} \sin(k_{y1} y) + (h^h_{xm1} \cos(\phi) + h^h_{zm1} \sin(\phi)) \begin{Bmatrix} \sin(n\phi) \\ \cos(n\phi) \end{Bmatrix} \cos(k_{y1} y)] \tag{3.58}$$

$$u_{27} = \int_{-\frac{\pi}{2}}^{\frac{\pi}{2}} d\phi \int_0^b dy e^{-\gamma_{m1} z} [h^e_{ym1} \begin{Bmatrix} -\cos(n\phi) \\ \sin(n\phi) \end{Bmatrix} \frac{nk_{y1}}{a\eta_1^{e2}} \sin(k_{y1} y) - h^e_{xm1} \cos(\phi) \begin{Bmatrix} \sin(n\phi) \\ \cos(n\phi) \end{Bmatrix} \cos(k_{y1} y)] \tag{3.59}$$

$$u_{28} = \int_{-\frac{\pi}{2}}^{\frac{\pi}{2}} d\phi \int_0^b dy e^{-\gamma_{m1} z} [h^h_{ym1} \begin{Bmatrix} -\cos(n\phi) \\ \sin(n\phi) \end{Bmatrix} \frac{nk_{y1}}{a\eta_1^{e2}} \sin(k_{y1} y) - (h^h_{xm1} \cos(\phi) - h^h_{zm1} \sin(\phi)) \begin{Bmatrix} \sin(n\phi) \\ \cos(n\phi) \end{Bmatrix} \cos(k_{y1} y)] \tag{3.60}$$

$$u_{31} = \int_{\frac{\pi}{2}}^{\frac{3\pi}{2}} d\phi \int_0^b dy e^{-\gamma_{m1} z} [(e^e_{xm1} \cos(\phi) - e^e_{zm1} \sin(\phi)) \begin{Bmatrix} \cos(n\phi) \\ -\sin(n\phi) \end{Bmatrix} \sin(k_{y1} y) + e^e_{ym1} \begin{Bmatrix} \sin(n\phi) \\ \cos(n\phi) \end{Bmatrix} \frac{nk_{y1}}{a\eta_1^{h2}} \cos(k_{y1} y)] \tag{3.61}$$

$$u_{32} = \int_{\frac{\pi}{2}}^{\frac{3\pi}{2}} d\phi \int_0^b dy e^{-\gamma_{m1} z} [e^h_{xm1} \cos(\phi) \begin{Bmatrix} \cos(n\phi) \\ -\sin(n\phi) \end{Bmatrix} \sin(k_{y1} y) + e^h_{ym1} \begin{Bmatrix} \sin(n\phi) \\ \cos(n\phi) \end{Bmatrix} \frac{nk_{y1}}{a\eta_1^{h2}} \cos(k_{y1} y)] \tag{3.62}$$

$$u_{33} = \int_{-\frac{\pi}{2}}^{\frac{\pi}{2}} d\phi \int_{0}^{b} dy e^{\gamma_{m1} z} [(e^{e}_{xm1} \cos(\phi) + e^{e}_{zm1} \sin(\phi)) \begin{Bmatrix} \cos(n\phi) \\ -\sin(n\phi) \end{Bmatrix} \sin(k_{y1} y) + e^{e}_{ym1} \begin{Bmatrix} \sin(n\phi) \\ \cos(n\phi) \end{Bmatrix} \frac{nk_{y1}}{a\eta_1^{h2}} \cos(k_{y1} y)] \tag{3.63}$$

$$u_{34} = \int_{-\frac{\pi}{2}}^{\frac{\pi}{2}} d\phi \int_{0}^{b} dy e^{\gamma_{m1} z} [e^{h}_{xm1} \cos(\phi) \begin{Bmatrix} \cos(n\phi) \\ -\sin(n\phi) \end{Bmatrix} \sin(k_{y1} y) + e^{h}_{ym1} \begin{Bmatrix} \sin(n\phi) \\ \cos(n\phi) \end{Bmatrix} \frac{nk_{y1}}{a\eta_1^{h2}} \cos(k_{y1} y)] \tag{3.64}$$

$$u_{35} = \int_{\frac{\pi}{2}}^{\frac{3\pi}{2}} d\phi \int_{0}^{b} dy e^{\gamma_{m1} z} [(e^{e}_{xm1} \cos(\phi) + e^{e}_{zm1} \sin(\phi)) \begin{Bmatrix} \cos(n\phi) \\ -\sin(n\phi) \end{Bmatrix} \sin(k_{y1} y) + e^{e}_{ym1} \begin{Bmatrix} \sin(n\phi) \\ \cos(n\phi) \end{Bmatrix} \frac{nk_{y1}}{a\eta_1^{h2}} \cos(k_{y1} y)] \tag{3.65}$$

$$u_{36} = \int_{\frac{\pi}{2}}^{\frac{3\pi}{2}} d\phi \int_{0}^{b} dy e^{\gamma_{m1} z} [e^{h}_{xm1} \cos(\phi) \begin{Bmatrix} \cos(n\phi) \\ -\sin(n\phi) \end{Bmatrix} \sin(k_{y1} y) + e^{h}_{ym1} \begin{Bmatrix} \sin(n\phi) \\ \cos(n\phi) \end{Bmatrix} \frac{nk_{y1}}{a\eta_1^{h2}} \cos(k_{y1} y)] \tag{3.66}$$

$$u_{37} = \int_{-\frac{\pi}{2}}^{\frac{\pi}{2}} d\phi \int_{0}^{b} dy e^{-\gamma_{m1} z} [(e^{e}_{xm1} \cos(\phi) - e^{e}_{zm1} \sin(\phi)) \begin{Bmatrix} \cos(n\phi) \\ -\sin(n\phi) \end{Bmatrix} \sin(k_{y1} y) + e^{e}_{ym1} \begin{Bmatrix} \sin(n\phi) \\ \cos(n\phi) \end{Bmatrix} \frac{nk_{y1}}{a\eta_1^{h2}} \cos(k_{y1} y)] \tag{3.67}$$

$$u_{38} = \int_{-\frac{\pi}{2}}^{\frac{\pi}{2}} d\phi \int_{0}^{b} dy e^{-\gamma_{m1}z} [e^{h}_{xm1} \cos(\phi) \begin{Bmatrix} \cos(n\phi) \\ -\sin(n\phi) \end{Bmatrix} \sin(k_{y1}y) + e^{h}_{ym1} \begin{Bmatrix} \sin(n\phi) \\ \cos(n\phi) \end{Bmatrix} \frac{nk_{y1}}{a\eta_1^{h2}} \cos(k_{y1}y)] \tag{3.68}$$

$$u_{41} = \int_{\frac{\pi}{2}}^{\frac{3\pi}{2}} d\phi \int_{0}^{b} dy \left[e^{-\gamma_{m1}z} h^{e}_{ym1} \begin{Bmatrix} \cos(n\phi) \\ -\sin(n\phi) \end{Bmatrix} \frac{1}{\eta_1^{h2}} \sin(k_{y1}y) \right] \tag{3.69}$$

$$u_{42} = \int_{\frac{\pi}{2}}^{\frac{3\pi}{2}} d\phi \int_{0}^{b} dy \left[e^{-\gamma_{m1}z} h^{h}_{ym1} \begin{Bmatrix} \cos(n\phi) \\ -\sin(n\phi) \end{Bmatrix} \frac{1}{\eta_1^{h2}} \sin(k_{y1}y) \right] \tag{3.70}$$

$$u_{43} = \int_{-\frac{\pi}{2}}^{\frac{\pi}{2}} d\phi \int_{0}^{b} dy \left[-e^{\gamma_{m1}z} h^{e}_{ym1} \begin{Bmatrix} \cos(n\phi) \\ -\sin(n\phi) \end{Bmatrix} \frac{1}{\eta_1^{h2}} \sin(k_{y1}y) \right] \tag{3.71}$$

$$u_{44} = \int_{-\frac{\pi}{2}}^{\frac{\pi}{2}} d\phi \int_{0}^{b} dy \left[-e^{\gamma_{m1}z} h^{h}_{ym1} \begin{Bmatrix} \cos(n\phi) \\ -\sin(n\phi) \end{Bmatrix} \frac{1}{\eta_1^{h2}} \sin(k_{y1}y) \right] \tag{3.72}$$

$$u_{45} = \int_{\frac{\pi}{2}}^{\frac{3\pi}{2}} d\phi \int_{0}^{b} dy \left[-e^{\gamma_{m1}z} h^{e}_{ym1} \begin{Bmatrix} \cos(n\phi) \\ -\sin(n\phi) \end{Bmatrix} \frac{1}{\eta_1^{h2}} \sin(k_{y1}y) \right] \tag{3.73}$$

$$u_{46} = \int_{\frac{\pi}{2}}^{\frac{3\pi}{2}} d\phi \int_{0}^{b} dy \left[-e^{\gamma_{m1}z} h^{h}_{ym1} \begin{Bmatrix} \cos(n\phi) \\ -\sin(n\phi) \end{Bmatrix} \frac{1}{\eta_1^{h2}} \sin(k_{y1}y) \right] \tag{3.74}$$

$$u_{47} = \int_{-\frac{\pi}{2}}^{\frac{\pi}{2}} d\phi \int_{0}^{b} dy \left[e^{-\gamma_{m1}z} h^{e}_{ym1} \begin{Bmatrix} \cos(n\phi) \\ -\sin(n\phi) \end{Bmatrix} \frac{1}{\eta_1^{h2}} \sin(k_{y1}y) \right] \tag{3.75}$$

$$u_{48} = \int_{-\frac{\pi}{2}}^{\frac{\pi}{2}} d\phi \int_{0}^{b} dy \left[e^{-\gamma_{m1} z} h_{ym1}^{h} \begin{Bmatrix} \cos(n\phi) \\ -\sin(n\phi) \end{Bmatrix} \frac{1}{\eta_1^{h2}} \sin(k_{y1} y) \right] \tag{3.76}$$

Chapter 4

Modal Analysis of Waveguide Bend and T- Junctions Loaded with A Partial Height Post

4.1 Introduction

The waveguide right angle bend and T- junctions loaded with a partial height post are two key modules in waveguide combline filters. They also find applications in many waveguide devices, such as diplexers [53], multiplexers [54][55], and antenna feed circuits [56]. Figure 4.1.1 shows a combline filter, which has four right angle bend junctions in the corners and two T-junctions in the middle. A rigorous modeling of the two key modules is a crucial step to realizing the full electromagnetic design of the complete combline filters. Because of the existence of the posts, the field distributions and the boundary conditions inside the waveguide junctions become much more

complicated than those inside a hollow bend or a hollow T-junction. In this chapter, a new method is introduced to characterize the waveguide bend and T-junctions loaded with a partial height post. This method will be called the technique of the extended eigenmode functions to distinguish from the traditional eigenmode functions used in the mode matching method.

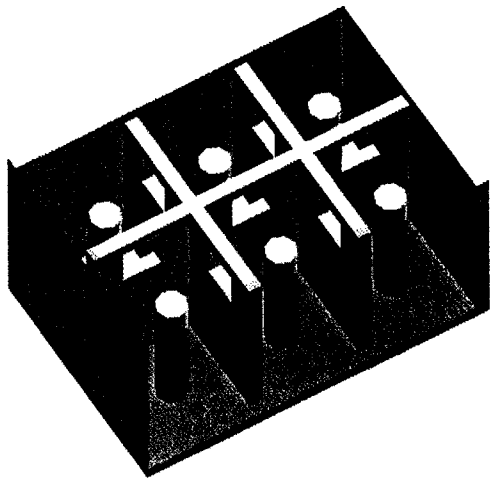

Fig. 4.1.1 A combline filter with six resonators (the input /output ports are not shown)

The hollow waveguide bend and T- junctions have been studied intensively using mode-matching methods [57][58][59][60][62]. In order to derive solutions for the discontinuity in the hollow waveguide junctions, the junction structures are decomposed into a number of straight one-port waveguides [57][59]. In this way, the eigenmode functions in each decomposed waveguide can be obtained directly by solving the Helmholtz equations in Cartesian coordinates.

In the case of the junctions with a post, each decomposed waveguide has a post in the waveguide. The eigenmode functions are obtained by solving the Helmholtz equations in a Cartesian-Cylindrical coordinate system. Similar to the case of the hollow waveguide, the basis functions in the waveguide regions are the eigenmode functions in the straight hollow waveguide. However, the basis functions in the cavity region are determined by using a group of the TE_{mn} and TM_{mn} modes. For any incident TE or TM mode in the decomposed straight waveguide, both the TE_{mn} and the TM_{mn} eigen modes will be excited to satisfy the boundary conditions on the surfaces of the waveguide walls and the post. The group of eigenmodes, including the corresponding incident mode, is used to construct a basis function for the field expression in the cavity region. The coefficients of the modes can be determined by using an approach introduced in [24]. To construct a complete set of the basis functions in the cavity region, two sets of extended eigenmodes in two perpendicular straight waveguides are required. Then, the total fields of the junctions are determined by summing up all the basis functions.

The method introduced in this chapter combines the classical mode matching method with the extended eigenmode functions to characterize the bend and T-junctions loaded with a partial height post. The generalized scattering matrices (GSM) of the bend junction and the T-junction are derived using the method of the extended eigenmode functions. In practice, the dimensions of the post have a large effect on the filter's performance and frequency responses. Using this method, one can accurately determine the dimensions of the posts and irises for the desired frequency responses.

Several concrete structures of the bend and T-junctions are analyzed with our new method. The simulation results are compared to the solutions obtained by using a commercial Finite Element Method software package. As will be shown, good agreement is achieved [63]. This method can also be used to derive the generalized scattering matrix (GSM) of the cross waveguide junctions with a post.

4.2 Right-Angle Bend Junction Loaded with a Partial Height Post

The resonators in the corners of a combline filter can be modeled as a right angle bend junction loaded with a partial height post. Then, the bend junction is cascaded with an iris at the aperture of each arm to form a resonator cavity. The three-dimensional structure of the bend junction is shown in Fig. 4.2.1.

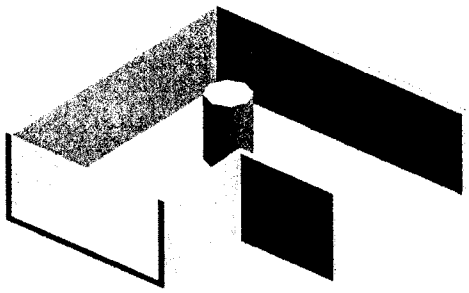

Fig. 4.2.1 A right angle bend junction loaded with a partial height cylindrical post

As shown in Fig. 4.2.2, the geometry of the bend junction with the post consists of a cavity region and two waveguide regions. The cylindrical post is located at the

center of the cavity region. The radius of the post is r_0 and the artificial region around the post has the radius of ρ = a. It is assumed that two waveguide arms have the same dimension 2a × b. The origin of the coordinates is located at the center of the post. The horizontal waveguide is along the z- axis and the vertical waveguide along the x-axis. The apertures of the arms are in the planes of z = a and x = a, respectively.

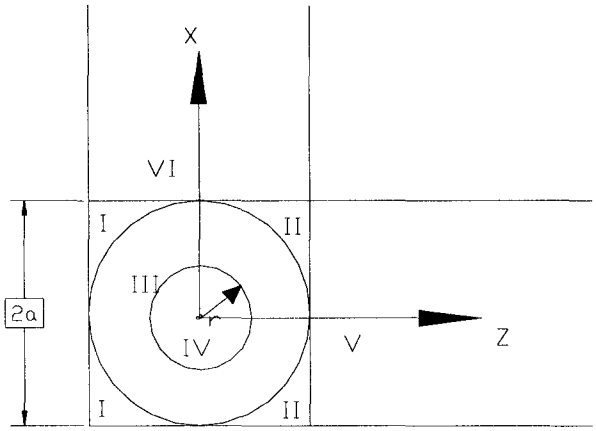

Fig. 4.2.2 Top view of a right angle bend junction loaded with a cylindrical post

To derive the generalized scattering matrix of a bend-junction, the extended eigenmode function method is developed in the following sections. To simplify the complex boundary problem, the bend-junction is decomposed into two parts. Each part is a one-port waveguide cavity loaded with a post so that the discontinuities of waveguide junction and the post can be solved separately. To deal with the discontinuity of the post, the extended eigenmode functions in the one-port cavity are determined by using the generalized scattering matrix of the straight waveguide loaded with a partial height post and then adding a short-plane at the end of the waveguide [24].

Two decomposed one-port waveguides are shown in Fig. 4.2.3 (a) and Fig. 4.2.3 (b). All the natural boundaries of the junction are parallel with the axes of the coordinates in the sub-regions. It ensures that every eigenmode function in the sub-regions satisfies the boundary conditions on the metal surfaces of the waveguides. The most noticeable feature of this structure is that the artificial cylindrical surface casts into the boundary of the two ports and is tangential to the waveguide walls.

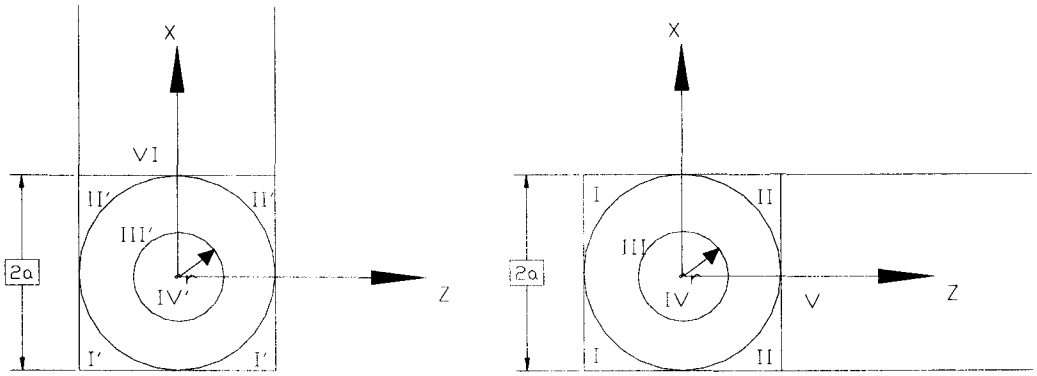

(a) vertical one port waveguide **(b) horizontal one port waveguide**

Fig. 4.2.3 Regions of analysis for a right angle bend junction loaded with a cylindrical post

4.2.1 Field Expressions in the Horizontal One-Port Waveguide

In the waveguide region V, where $-a \le x \le a$, $0 \le y \le b$, z $\ge a$, the transverse fields with respect to the z-direction are expressed in terms of the weighted modal functions,

$$\vec{\mathbf{E}}_t^V = \sum_m \sum_i [B_{mi}^{Vh} e^{-\gamma_{zmi} z} + A_{mi}^{Vh} e^{\gamma_{zmi} z}] \hat{e}_{tmi}^{hz} + \sum_m \sum_i [B_{mi}^{Ve} e^{-\gamma_{zmi} z} + A_{mi}^{Ve} e^{\gamma_{zmi} z}] \hat{e}_{tmi}^{ez}, \qquad (4.1)$$

$$\vec{\mathbf{H}}_t^V = \sum_m \sum_i [B_{mi}^{Vh} e^{-\gamma_{zmi} z} - A_{mi}^{Vh} e^{\gamma_{zmi} z}] \hat{h}_{tmi}^{hz} + \sum_m \sum_i [B_{mi}^{Ve} e^{-\gamma_{zmi} z} - A_{mi}^{Ve} e^{\gamma_{zmi} z}] \hat{h}_{tmi}^{ez}. \qquad (4.2)$$

In equation (4.1) and (4.2), $\hat{e}^{hz}_{tmi}$, $\hat{e}^{ez}_{tmi}$, $\hat{h}^{hz}_{tmi}$ and $\hat{h}^{ez}_{tmi}$ are the transverse mode fields, with the longitudinal mode fields e^{ez}_{zmi} and h^{hz}_{zmi}, given by

$$e^{ez}_{zmi} = \sin[k_{xm}(x+a)]\sin(k_{yi}y), \tag{4.3}$$

$$e^{pz}_{xmi} = \frac{1}{k^2_{cz}}\begin{Bmatrix} -\gamma_{zmi}k_{xm} & for\ \ p=e \\ k_{yi} & for\ \ p=h \end{Bmatrix}\cos[k_{xm}(x+a)]\sin(k_{yi}y), \tag{4.4}$$

$$e^{pz}_{ymi} = \frac{1}{k^2_{cz}}\begin{Bmatrix} -\gamma_{zmi}k_{yi} & for\ \ p=e \\ -k_{xm} & for\ \ p=h \end{Bmatrix}\sin[k_{xm}(x+a)]\cos(k_{yi}y), \tag{4.5}$$

$$j\omega\mu_0 h^{hz}_{zmi} = \cos[k_{xm}(x+a)]\cos(k_{yi}y), \tag{4.6}$$

$$j\omega\mu_0 h^{pz}_{xmi} = \frac{1}{k^2_{cz}}\begin{Bmatrix} -k_0^2 k_{yi} & for\ \ p=e \\ \gamma_{zmi}k_{xm} & for\ \ p=h \end{Bmatrix}\sin[k_{xm}(x+a)]\cos(k_{yi}y), \tag{4.7}$$

$$j\omega\mu_0 h^{pz}_{ymi} = \frac{1}{k^2_{cz}}\begin{Bmatrix} k_0^2 k_{xm} & for\ \ p=e \\ \gamma_{zmi}k_{yi} & for\ \ p=h \end{Bmatrix}\cos[k_{xm}(x+a)]\sin(k_{yi}y), \tag{4.8}$$

with

$$k^2_{cz} = k^2_{xm} + k^2_{yi} = \gamma^2_{zmi} + k_0^2, \tag{4.9}$$

where γ_{zmi} is the propagation/attenuation coefficient along the z-direction, k_{xm}, k_{yi} and k_0 are wave-numbers given by

$$k_{xm} = \frac{m\pi}{2a}, \qquad k_{yi} = \frac{i\pi}{b} \quad \text{and} \quad k_0^2 = \omega^2\mu_0\varepsilon_0. \tag{4.10}$$

In the cavity region I and II, the total fields are given by

$$\vec{\mathbf{E}}^{Iz} = \sum_j C^h_j \vec{\phi}^{hl}_j + \sum_j C^e_j \vec{\phi}^{el}_j, \tag{4.11}$$

$$\vec{\mathbf{H}}^{Iz} = \sum_j C^h_j \vec{\psi}^{hl}_j + \sum_j C^e_j \vec{\psi}^{el}_j, \tag{4.12}$$

$$\vec{\mathbf{E}}^{IIz} = \sum_j C_j^h \vec{\phi}_j^{hII} + \sum_j C_j^e \vec{\phi}_j^{eII}, \tag{4.13}$$

$$\vec{\mathbf{H}}^{IIz} = \sum_j C_j^h \vec{\psi}_j^{hII} + \sum_j C_j^e \vec{\psi}_j^{eII}, \tag{4.14}$$

where C_j^h and C_j^e are the eigenfield coefficients. The extended eigenmode functions $\vec{\phi}_j^{qi}$ and $\vec{\psi}_j^{qi}$ refer to the jth modal functions of the electric fields and the magnetic fields, respectively, superscripts q=h and q=e refer to the incident TE modes and TM modes, respectively, superscripts i = I, II refer to the waveguide region I and II. The extended eigenfunctions are given by

$$\vec{\phi}_j^{hI} = \sum_p^{ne}(A_{p,j}^{Ieh}e^{-\gamma_{zp}z} + B_{p,j}^{Ieh}e^{\gamma_{zp}z})\hat{e}_{tp}^{ez} + \sum_p^{nh}(A_{p,j}^{Ihh}e^{-\gamma_{zp}z} + B_{p,j}^{Ihh}e^{\gamma_{zp}z})\hat{e}_{tp}^{hz} + \sum_p^{ne}(A_{p,j}^{Ieh}e^{-\gamma_{zp}z} - B_{p,j}^{Ieh}e^{\gamma_{zp}z})\hat{e}_{zp}^{ez},$$

$$\vec{\phi}_j^{eI} = \sum_p^{ne}(A_{p,j}^{Iee}e^{-\gamma_{zp}z} + B_{p,j}^{Iee}e^{\gamma_{zp}z})\hat{e}_{tp}^{ez} + \sum_p^{nh}(A_{p,j}^{Ihe}e^{-\gamma_{zp}z} + B_{p,j}^{Ihe}e^{\gamma_{zp}z})\hat{e}_{tp}^{hz} + \sum_p^{ne}(A_{p,j}^{Iee}e^{-\gamma_{zp}z} - B_{p,j}^{Iee}e^{\gamma_{zp}z})\hat{e}_{zp}^{ez},$$

$$\vec{\psi}_j^{hI} = \sum_p^{ne}(A_{p,j}^{Ieh}e^{-\gamma_{zp}z} - B_{p,j}^{Ieh}e^{\gamma_{zp}z})\hat{h}_{tp}^{ez} + \sum_p^{nh}(A_{p,j}^{Ihh}e^{-\gamma_{zp}z} - B_{p,j}^{Ihh}e^{\gamma_{zp}z})\hat{h}_{tp}^{hz} + \sum_p^{nh}(A_{p,j}^{Ihh}e^{-\gamma_{zp}z} + B_{p,j}^{Ihh}e^{\gamma_{zp}z})\hat{h}_{zp}^{hz},$$

$$\vec{\psi}_j^{eI} = \sum_p^{ne}(A_{p,j}^{Iee}e^{-\gamma_{zp}z} - B_{p,j}^{Iee}e^{\gamma_{zp}z})\hat{h}_{tp}^{ez} + \sum_p^{nh}(A_{p,j}^{Ihe}e^{-\gamma_{zp}z} - B_{p,j}^{Ihe}e^{\gamma_{zp}z})\hat{h}_{tp}^{hz} + \sum_p^{nh}(A_{p,j}^{Ihe}e^{-\gamma_{zp}z} + B_{p,j}^{Ihe}e^{\gamma_{zp}z})\hat{h}_{zp}^{hz},$$

$$\vec{\phi}_j^{hII} = \sum_p^{ne}(B_{p,j}^{IIeh}e^{-\gamma_{zp}z} + A_{p,j}^{IIeh}e^{\gamma_{zp}z})\hat{e}_{tp}^{ez} + \sum_p^{nh}(B_{p,j}^{IIhh}e^{-\gamma_{zp}z} + A_{p,j}^{IIhh}e^{\gamma_{zp}z})\hat{e}_{tp}^{hz} + \sum_p^{ne}(B_{p,j}^{IIeh}e^{-\gamma_{zp}z} - A_{p,j}^{IIeh}e^{\gamma_{zp}z})\hat{e}_{zp}^{ez},$$

$$\vec{\phi}_j^{eII} = \sum_p^{ne}(B_{p,j}^{IIee}e^{-\gamma_{zp}z} + A_{p,j}^{IIee}e^{\gamma_{zp}z})\hat{e}_{tp}^{ez} + \sum_p^{nh}(B_{p,j}^{IIhe}e^{-\gamma_{zp}z} + A_{p,j}^{IIhe}e^{\gamma_{zp}z})\hat{e}_{tp}^{hz} + \sum_p^{ne}(B_{p,j}^{IIee}e^{-\gamma_{zp}z} - A_{p,j}^{IIee}e^{\gamma_{zp}z})\hat{e}_{zp}^{ez},$$

$$\vec{\psi}_j^{hII} = \sum_p^{ne}(B_{p,j}^{IIeh}e^{-\gamma_{zp}z} - A_{p,j}^{IIeh}e^{\gamma_{zp}z})\hat{h}_{tp}^{ez} + \sum_p^{nh}(B_{p,j}^{IIhh}e^{-\gamma_{zp}z} - A_{p,j}^{IIhh}e^{\gamma_{zp}z})\hat{h}_{tp}^{hz} + \sum_p^{nh}(B_{p,j}^{IIhh}e^{-\gamma_{zp}z} + A_{p,j}^{IIhh}e^{\gamma_{zp}z})\hat{h}_{zp}^{hz},$$

$$\vec{\psi}_j^{eII} = \sum_p^{ne}(B_{p,j}^{IIee}e^{-\gamma_{zp}z} - A_{p,j}^{IIee}e^{\gamma_{zp}z})\hat{h}_{tp}^{ez} + \sum_p^{nh}(B_{p,j}^{IIhe}e^{-\gamma_{zp}z} - A_{p,j}^{IIhe}e^{\gamma_{zp}z})\hat{h}_{tp}^{hz} + \sum_p^{nh}(B_{p,j}^{IIhe}e^{-\gamma_{zp}z} + A_{p,j}^{IIhe}e^{\gamma_{zp}z})\hat{h}_{zp}^{hz},$$

(4.15)

In the above equations, subscript p corresponds to a pair of subscripts m,i, $\hat{e}_{zp}^{ez}$, $\hat{e}_{tp}^{ez}$, $\hat{e}_{tp}^{hz}$, $\hat{h}_{zp}^{hz}$, $\hat{h}_{tp}^{ez}$ and $\hat{h}_{tp}^{hz}$ are normal mode functions with respect to the direction of the z-axis in the rectangular waveguide. They are given in equations (4.3) to (4.10). In equation (4.1) to (4.15), the superscripts e and h refer to TM and TE modes, respectively. The incident and reflected mode coefficients A_j^{ipq} and B_j^{ipq} have three superscripts, where i is for the region I or II, $p = e$ or $p = h$ corresponds to the TM or TE type mode functions, and $q = e$ or $q = h$ refers to the TM or TE type incident mode, respectively.

4.2.2 Coefficients for the Extended Eigen Mode Functions

In an infinite rectangular waveguide loaded with a post, a resonant mode function ϕ_j^{hII} in region II consists of two parts, an incident TE mode weighted by coefficient $A_{p,j}^{IIhh}$ from waveguide region II to the post region III, and corresponding reflected TE ($B_{p,j}^{IIhh}$) and TM ($B_{p,j}^{IIeh}$) modes from the post region. In the waveguide region I, the incident waves to the post region include the TE ($A_{p,j}^{Ihh}$) and TM ($A_{p,j}^{Ieh}$) modes, the reflected waves from the post region are the TE ($B_{p,I}^{Ihh}$) and TM ($B_{p,I}^{Ieh}$) modes. The waves in the two regions are related by the equation

$$\begin{Bmatrix} \mathbf{B}^I \\ \mathbf{B}^{II} \end{Bmatrix} = [\mathbf{S}]_2 \begin{Bmatrix} \mathbf{A}^I \\ \mathbf{A}^{II} \end{Bmatrix}, \tag{4.16}$$

where $[\mathbf{S}]_2$ is the generalized scattering matrix for a regular two port waveguide loaded with a post[24], and $\mathbf{A}^I$, $\mathbf{B}^I$, $\mathbf{A}^{II}$ and $\mathbf{B}^{II}$ are M × M matrices given by

$$\{\mathbf{B}^{II}\}=\begin{Bmatrix}\mathbf{B}^{IIhh}\\ \mathbf{B}^{IIeh}\end{Bmatrix},\quad \{\mathbf{A}^{I}\}=\begin{Bmatrix}\mathbf{A}^{Ihh}\\ \mathbf{A}^{Ieh}\end{Bmatrix}\qquad \text{and}\qquad \{\mathbf{B}^{I}\}=\begin{Bmatrix}\mathbf{B}^{Ihh}\\ \mathbf{B}^{Ieh}\end{Bmatrix}. \tag{4.17}$$

To ensure the linear independence of the extended eigen modes, the coefficient vector $\mathbf{A}^{II}{}_{p,j}$ is chosen as a set of linear independent vectors as

$$\{\mathbf{A}^{IIhh}_{p,1}\}=\begin{bmatrix}1\\0\\\vdots\\\vdots\\0\end{bmatrix},\quad \{\mathbf{A}^{IIhh}_{p,2}\}=\begin{bmatrix}0\\1\\0\\\vdots\\0\end{bmatrix},\quad \cdots\cdots,\quad \{\mathbf{A}^{IIee}_{p,m}\}=\begin{bmatrix}0\\\vdots\\\vdots\\0\\1\end{bmatrix}. \tag{4.18}$$

The dimension of the vectors is M × 1, where M is the total number of the TM and TE modes used in the rectangular waveguides. After obtaining $[\mathbf{S}]_2$, we move one of the reference planes from the center of the post to z = -a. The corresponding scattering matrix $[\mathbf{S}']_2$ can be obtained by

$$[\mathbf{S}']_2=[\mathbf{D}][\mathbf{S}]_2[\mathbf{D}]=\begin{bmatrix}\mathbf{D}_1 & \mathbf{0}\\ \mathbf{0} & \mathbf{I}\end{bmatrix}\begin{bmatrix}\mathbf{S}_{11} & \mathbf{S}_{12}\\ \mathbf{S}_{21} & \mathbf{S}_{22}\end{bmatrix}_2\begin{bmatrix}\mathbf{D}_1 & \mathbf{0}\\ \mathbf{0} & \mathbf{I}\end{bmatrix}. \tag{4.19}$$

In $\mathbf{D}$, $\mathbf{I}$ is the identity matrix, $\mathbf{D}_1$ is given by

$$[\mathbf{D}_1]=\begin{bmatrix}e^{-\gamma_1^I a} & & & \\ & e^{-\gamma_2^I a} & & \\ & & \ddots & \\ & & & e^{-\gamma_M^I a}\end{bmatrix}. \tag{4.20}$$

M is the total number of modes used in the waveguide region. The submatrices in $\mathbf{S}'$ are given by

$$\mathbf{S}'_{11}=\mathbf{D}_1\mathbf{S}_{11}\mathbf{D}_1,\qquad \mathbf{S}'_{12}=\mathbf{D}_1\mathbf{S}_{12}\mathbf{I}=\mathbf{D}_1\mathbf{S}_{12},$$

$$\mathbf{S}'_{21}=\mathbf{I}\mathbf{S}_{21}\mathbf{D}_1=\mathbf{S}_{21}\mathbf{D}_1,\qquad \mathbf{S}'_{22}=\mathbf{I}\mathbf{S}_{22}\mathbf{I}=\mathbf{S}_{22}. \tag{4.21}$$

Then, a short plane is placed at z = a. On the surface of the short plane, every pair of incident and reflected modes arriving at that plane cancel each other in order to satisfy the boundary condition. Substituting $\{\mathbf{B}^{I'}\} = -\{\mathbf{A}^{I'}\}$ and (4.21) into equation (4.16), the coefficient vectors of the extended eigenmode functions are expressed for a given incident wave $\{\mathbf{A}^{II}\}$ as

$$\begin{aligned}
\left\{\mathbf{B}^{II}\right\} &= [\mathbf{S'}_{22} - \mathbf{S'}_{21}(\mathbf{S'}_{11}+\mathbf{I})^{-1}\mathbf{S'}_{12}]\left\{\mathbf{A}^{II}\right\} = [\mathbf{S}]_1\left\{\mathbf{A}^{II}\right\}, \\
\left\{\mathbf{A}^{I}\right\} &= -\mathbf{D}_1(\mathbf{S'}_{11}+\mathbf{I})^{-1}\mathbf{S'}_{12}\left\{\mathbf{A}^{II}\right\}, \\
\left\{\mathbf{B}^{I}\right\} &= -\mathbf{D}_1^{-1}(\mathbf{S'}_{12} - \mathbf{S'}_{11}(\mathbf{I}+\mathbf{S'}_{11})^{-1}\mathbf{S'}_{12})\left\{\mathbf{A}^{II}\right. ,
\end{aligned} \tag{4.22}$$

where $[\mathbf{S}]_1$ is the generalized scattering matrix for a one port waveguide loaded with a post. The elements of the diagonal matrix $\mathbf{D}_1^{-1}$ are $e^{\gamma_p^I a}$, p=1,2,..., *M*.

4.2.3 Field Expressions in Vertical One Port Waveguide

In the waveguide region VI, the transverse fields with respect to the x-direction are expressed in terms of mode functions as

$$\vec{\mathbf{E}}_t^{VI} = \sum_m \sum_i [B_{mi}^{VIh} e^{-\gamma_{xmi}x} + A_{mi}^{VIh} e^{\gamma_{xmi}x}]\hat{e}_{tmi}^{hx} + \sum_m \sum_i [B_{mi}^{VIe} e^{-\gamma_{xmi}x} + A_{mi}^{VIe} e^{\gamma_{xmi}x}]\hat{e}_{tmi}^{ex}, \tag{4.23}$$

$$\vec{\mathbf{H}}_t^{VI} = \sum_m \sum_i [B_{mi}^{VIh} e^{-\gamma_{xmi}x} - A_{mi}^{VIh} e^{\gamma_{xmi}x}]\hat{h}_{tmi}^{hx} + \sum_m \sum_i [B_{mi}^{VIe} e^{-\gamma_{xmi}x} - A_{mi}^{VIe} e^{\gamma_{xmi}x}]\hat{h}_{tmi}^{ex}. \tag{4.24}$$

To reuse the scattering matrix of the straight waveguide in order to derive the eigenmode coefficients, the coordinate system is rotated 90° clockwise. Substituting $z = -x$ and $x = z$ into equation (4.1) to (4.8), the eigen-mode functions of the vertical waveguide in the general coordinate system are given by

$$e_{xmi}^{px} = \begin{cases} -\sin[k_{zm}(z+a)]\sin(k_{yi}y), & for\ \ p=e, \\ 0, & for\ \ p=h, \end{cases} \tag{4.25}$$

$$e_{ymi}^{px} = \frac{1}{k_{cx}^2}\begin{Bmatrix} \gamma_{xmi}k_{yi}, & for\ \ p=e \\ k_{zm}, & for\ \ p=h \end{Bmatrix}\sin[k_{zm}(z+a)]\cos(k_{yi}y), \tag{4.26}$$

$$e_{zmi}^{px} = \frac{1}{k_{cx}^2}\begin{Bmatrix} \gamma_{xmi}k_{zm}, & for\ \ p=e \\ -k_{yi}, & for\ \ p=h \end{Bmatrix}\cos[k_{zm}(z+a)]\sin(k_{yi}y), \tag{4.27}$$

$$j\omega\mu_0 h_{xmi}^{px} = \begin{cases} 0, & for\ \ p=e, \\ \cos[k_{zm}(z+a)]\cos(k_{yi}y), & for\ \ p=h, \end{cases} \tag{4.28}$$

$$j\omega\mu_0 h_{ymi}^{px} = \frac{1}{k_{cx}^2}\begin{Bmatrix} k_0^2 k_{zm}, & for\ \ p=e \\ \gamma_{xmi}k_{yi}, & for\ \ p=h \end{Bmatrix}\cos[k_{zm}(z+a)]\sin(k_{yi}y), \tag{4.29}$$

$$j\omega\mu_0 h_{zmi}^{px} = \frac{1}{k_{cx}^2}\begin{Bmatrix} -k_0^2 k_{yi}, & for\ \ p=e \\ \gamma_{xmi}k_{zm}, & for\ \ p=h \end{Bmatrix}\sin[k_{zm}(z+a)]\cos(k_{yi}y), \tag{4.30}$$

with

$$k_{cx}^2 = k_{zm}^2 + k_{yi}^2 = \gamma_{xmi}^2 + k_0^2, \tag{4.31}$$

$$k_{zm} = \frac{m\pi}{2a}, \qquad k_{yi} = \frac{i\pi}{b} \qquad \text{and} \qquad k_0^2 = \omega^2\mu_0\varepsilon_0. \tag{4.32}$$

In the cavity region I' and II', the electromagnetic fields are given by

$$\vec{\mathbf{E}}_t^{I'x} = \sum_j D_j^e \vec{\phi}_j^{eI'} + \sum_j D_j^h \vec{\phi}_j^{hI'}, \tag{4.33}$$

$$\vec{\mathbf{H}}_t^{I'x} = \sum_j D_j^e \vec{\psi}_j^{eI'} + \sum_j D_j^h \vec{\psi}_j^{hI'}, \tag{4.34}$$

$$\vec{\mathbf{E}}_t^{II'x} = \sum_j D_j^e \vec{\phi}_j^{eII'} + \sum_j D_j^h \vec{\phi}_j^{hII'}, \tag{4.35}$$

$$\vec{\mathbf{H}}_t^{II'x} = \sum_j D_j^e \vec{\psi}_j^{eII'} + \sum_j D_j^h \vec{\psi}_j^{hII'}. \tag{4.36}$$

Replacing z by x in equations (4.15), the extended eigenmodes in the above equations can be determined.

4.2.4 Generalized Scattering Matrix of a Bend Junction Loaded with a Post

A bend junction is formed by incorporating the two one-port structures, the vertical one and the horizontal one. The total field in the cavity region of the bend is the sum of the fields in the cavity region, which are derived for each one-port structure separately. At the boundary $z = a$, the total electromagnetic fields in the cavity region are given as follows

$$\vec{E}_t^{\,ztotal}\,|_{z=a} = \begin{cases} (\vec{E}_t^{\,IIz} + \vec{E}_x^{\,II'x} + \vec{E}_y^{\,II'x})_{z=a}, & 0 \le x \le a, \\ (\vec{E}_t^{\,IIz} + \vec{E}_x^{\,I'x} + \vec{E}_y^{\,I'x})_{z=a}, & -a \le x < 0. \end{cases} \tag{4.37}$$

In the cavity region, the tangential electric fields $\vec{E}_x^{\,I'x}$, $\vec{E}_y^{\,I'x}$, $\vec{E}_x^{\,II'x}$ and $\vec{E}_y^{\,II'x}$ in region I' and II' are equal to zero at $z = a$. Therefore, the total electric field in the cavity region is equal to $\vec{E}_t^{\,IIz}|_{z=a}$. However, the magnetic fields in region I' and II' are not equal to zero at $z = a$. Instead, they can be expressed as

$$\vec{H}_t^{\,ztotal}\,|_{z=a} = \begin{cases} (\vec{H}_t^{\,IIz} + \vec{H}_x^{\,II'x} + \vec{H}_y^{\,II'x})_{z=a}, & 0 \le x \le a, \\ (\vec{H}_t^{\,IIz} + \vec{H}_x^{\,I'x} + \vec{H}_y^{\,I'x})_{z=a}, & -a \le x < 0. \end{cases} \tag{4.38}$$

A similar relation can be found at the boundary $x = a$.

$$\vec{E}_t^{\,xtotal}\,|_{x=a} = \begin{cases} \vec{E}_t^{\,II'x}\,|_{x=a}, & 0 \le z \le a, \\ \vec{E}_t^{\,II'x}\,|_{x=a}, & -a \le z < 0, \end{cases} \tag{4.39}$$

$$\vec{H}_t^{\,xtotal}\,|_{x=a} = \begin{cases} (\vec{H}_t^{\,II'x} + \vec{H}_z^{\,IIz} + \vec{H}_y^{\,IIz})_{x=a}, & 0 \le z \le a, \\ (\vec{H}_t^{\,II'x} + \vec{H}_z^{\,Iz} + \vec{H}_y^{\,Iz})_{x=a}, & -a \le z < 0, \end{cases} \tag{4.40}$$

The continuity of the electromagnetic fields on the $z = a$ and $x = a$ planes implies that the tangential components of the fields satisfy the following equations

$$\vec{E}_t^V \mid_{z=a} = \vec{E}_t^{ztotal} \mid_{z=a}, \tag{4.41}$$

$$\vec{H}_t^V \mid_{z=a} = \vec{H}_t^{ztotal} \mid_{z=a}, \tag{4.42}$$

and

$$\vec{E}_t^{VI} \mid_{x=a} = \vec{E}_t^{xtotal} \mid_{x=a}, \tag{4.43}$$

$$\vec{H}_t^{VI} \mid_{x=a} = \vec{H}_t^{xtotal} \mid_{x=a}. \tag{4.44}$$

By taking inner products of equation (4.41) with $\hat{h}_t^{hz*}$ and $\hat{h}_t^{ez*}$, and equation (4.43) with $\hat{h}_t^{hx*}$ and $\hat{h}_t^{ex*}$, and substituting equations (4.1) into (4.41), and (4.23) into (4.43), respectively, one can obtain following four linear equations

$$(B_{kl}^{Vh} e^{-\gamma_{zkl} a} + A_{kl}^{Vh} e^{\gamma_{zkl} a}) < \hat{e}_{tkl}^{hz}, \hat{h}_{tkl}^{hz*} > = < \vec{E}_t^{ztotal}, \hat{h}_{tkl}^{hz*} >, \tag{4.45}$$

$$(B_{kl}^{Ve} e^{-\gamma_{zkl} a} + A_{kl}^{Ve} e^{\gamma_{zkl} a}) < \hat{e}_{tkl}^{ez}, \hat{h}_{tkl}^{ez*} > = < \vec{E}_t^{ztotal}, \hat{h}_{tkl}^{ez*} >, \tag{4.46}$$

$$(B_{kl}^{VIh} e^{-\gamma_{xkl} a} + A_{kl}^{VIh} e^{\gamma_{xkl} a}) < \hat{e}_{tkl}^{hx}, \hat{h}_{tkl}^{hx*} > = < \vec{E}_t^{xtotal}, \hat{h}_{tkl}^{hx*} >, \tag{4.47}$$

$$(B_{kl}^{VIe} e^{-\gamma_{xkl} a} + A_{kl}^{VIe} e^{\gamma_{xkl} a}) < \hat{e}_{tkl}^{ex}, \hat{h}_{tkl}^{ex*} > = < \vec{E}_t^{xtotal}, \hat{h}_{tkl}^{ex*} >, \tag{4.48}$$

where $\hat{h}_t^{hz*}$ and $\hat{h}_t^{ez*}$ are conjugates of tangential eigenfunctions in region V given by (4.7) (4.8), $\hat{h}_t^{hx*}$ and $\hat{h}_t^{ex*}$ are conjugates of tangential eigenfunctions in region VI given by (4.29) (4.30). The left side of equation (4.45) can be written as

$$(B_{kl}^{Vh} e^{-\gamma_{zkl} a} + A_{kl}^{Vh} e^{\gamma_{zkl} a}) < \hat{e}_{tkl}^{hz}, \hat{h}_{tkl}^{hz*} > = \mathbf{D}l_{11} (B_{kl}^{Vh} e^{-\gamma_{zkl} a} + A_{kl}^{Vh} e^{\gamma_{zkl} a}) \tag{4.49}$$

where $\mathbf{D}l_{11} = < \hat{e}_{tkl}^{hz}, \hat{h}_{tkl}^{hz*} >$. Substituting (4.13), (4.15) into (4.45), the right side of equation (4.45) can be written as

$$\begin{aligned} < \vec{E}_t^{ztotal}, \hat{h}_{tkl}^{hz*} > &= \sum_j C_j^h < \phi_j^{hII}, \hat{h}_{tkl}^{hz*} > + \sum_m C_j^e < \phi_j^{eII}, \hat{h}_{tkl}^{hz*} > \\ &= \sum_j C_j^h \{ \sum_m \sum_i [B_{mij}^{IIhh} e^{-\gamma_{mi} z} + A_{mij}^{IIhh} e^{\gamma_{mi} z}] < \hat{e}_{tmi}^{hz}, \hat{h}_{tkl}^{hz*} > \} \\ &+ \sum_j C_j^e \{ \sum_m \sum_i [B_{mij}^{IIhe} e^{-\gamma_{mi} z} + A_{mij}^{IIhe} e^{\gamma_{mi} z}] < \hat{e}_{tmi}^{hz}, \hat{h}_{tkl}^{hz*} > \}, \end{aligned} \quad (4.50)$$

Using orthogonality of the eigenmodes, when $m \neq k$ or $i \neq l$, the inner products are equal to zero. Since the incident wave is a TE mode, $A_{mij}^{IIhe} = 0$. We have

$$\mathbf{U}_{11}^h = < \phi_j^{hII}, , \hat{h}_{tkl}^{hz*} > = [B_{klj}^{IIhh} e^{-\gamma_{mi} z} + A_{klj}^{IIhh} e^{\gamma_{mi} z}] < \hat{e}_{tkl}^{hz}, \hat{h}_{tkl}^{hz*} > \quad (4.51)$$

$$\mathbf{U}_{12}^e = < \phi_j^{eII}, \hat{h}_{tkl}^{hz*} > = B_{klj}^{IIhe} e^{-\gamma_{mi} z} < \hat{e}_{tkl}^{hz}, \hat{h}_{tkl}^{hz*} > \quad (4.52)$$

$\mathbf{D}l_{11}$, $\mathbf{U}_{11}^h$ and $\mathbf{U}_{12}^e$ are diagonal matrices. In the same way, we can obtain other elements from equation (4.46), (4.47) and (4.48). The results can be expressed as a matrix equation.

$$\begin{bmatrix} \mathbf{U}_{11}^h & \mathbf{U}_{12}^e & \mathbf{0} & \mathbf{0} \\ \mathbf{U}_{21}^h & \mathbf{U}_{22}^e & \mathbf{0} & \mathbf{0} \\ \mathbf{0} & \mathbf{0} & \mathbf{U}_{33}^h & \mathbf{U}_{34}^e \\ \mathbf{0} & \mathbf{0} & \mathbf{U}_{43}^h & \mathbf{U}_{44}^e \end{bmatrix} \begin{bmatrix} \mathbf{C}^h \\ \mathbf{C}^e \\ \mathbf{D}^h \\ \mathbf{D}^e \end{bmatrix} = \begin{bmatrix} \mathbf{D}l_{11} & \mathbf{0} & \mathbf{0} & \mathbf{0} \\ \mathbf{0} & \mathbf{D}l_{22} & \mathbf{0} & \mathbf{0} \\ \mathbf{0} & \mathbf{0} & \mathbf{D}l_{33} & \mathbf{0} \\ \mathbf{0} & \mathbf{0} & \mathbf{0} & \mathbf{D}l_{44} \end{bmatrix} \begin{bmatrix} \mathbf{B}^{Vh} e^{-\gamma_z a} + \mathbf{A}^{Vh} e^{\gamma_z a} \\ \mathbf{B}^{Ve} e^{-\gamma_z a} + \mathbf{A}^{Ve} e^{\gamma_z a} \\ \mathbf{B}^{Vlh} e^{-\gamma_x a} + \mathbf{A}^{Vlh} e^{\gamma_x a} \\ \mathbf{B}^{Vle} e^{-\gamma_x a} + \mathbf{A}^{Vle} e^{\gamma_x a} \end{bmatrix} . \quad (4.53)$$

Taking inner products of equation (4.42) with mode functions $\hat{e}_t^{hz*}$ and $\hat{e}_t^{ez*}$, equation (4.44) with $\hat{e}_t^{hx*}$ and $\hat{e}_t^{ex*}$, we have the matrix equation

$$\begin{bmatrix} \mathbf{M}_{11} & \mathbf{M}_{12} & \mathbf{M}_{13} & \mathbf{M}_{14} \\ \mathbf{M}_{21} & \mathbf{M}_{22} & \mathbf{M}_{23} & \mathbf{M}_{24} \\ \mathbf{M}_{31} & \mathbf{M}_{32} & \mathbf{M}_{33} & \mathbf{M}_{34} \\ \mathbf{M}_{41} & \mathbf{M}_{42} & \mathbf{M}_{43} & \mathbf{M}_{44} \end{bmatrix} \begin{bmatrix} \mathbf{C}^h \\ \mathbf{C}^e \\ \mathbf{D}^h \\ \mathbf{D}^e \end{bmatrix} = \begin{bmatrix} \mathbf{D}l_{11}^* & \mathbf{0} & \mathbf{0} & \mathbf{0} \\ \mathbf{0} & \mathbf{D}l_{22}^* & \mathbf{0} & \mathbf{0} \\ \mathbf{0} & \mathbf{0} & \mathbf{D}l_{33}^* & \mathbf{0} \\ \mathbf{0} & \mathbf{0} & \mathbf{0} & \mathbf{D}l_{44}^* \end{bmatrix} \begin{bmatrix} \mathbf{B}^{Vh} e^{-\gamma_z a} - \mathbf{A}^{Vh} e^{\gamma_z a} \\ \mathbf{B}^{Ve} e^{-\gamma_z a} - \mathbf{A}^{Ve} e^{\gamma_z a} \\ \mathbf{B}^{Vlh} e^{-\gamma_x a} - \mathbf{A}^{Vlh} e^{\gamma_x a} \\ \mathbf{B}^{Vle} e^{-\gamma_x a} - \mathbf{A}^{Vle} e^{\gamma_x a} \end{bmatrix}. \quad (4.54)$$

The generalized scattering matrix can be obtained by combining equation (4.53) and (4.54). From (4.53), we have

$$\begin{bmatrix} \mathbf{C}^h \\ \mathbf{C}^e \\ \mathbf{D}^h \\ \mathbf{D}^e \end{bmatrix} = \begin{bmatrix} \mathbf{U}_{11}^h & \mathbf{U}_{12}^e & \mathbf{0} & \mathbf{0} \\ \mathbf{U}_{21}^h & \mathbf{U}_{22}^e & \mathbf{0} & \mathbf{0} \\ \mathbf{0} & \mathbf{0} & \mathbf{U}_{33}^h & \mathbf{U}_{34}^e \\ \mathbf{0} & \mathbf{0} & \mathbf{U}_{43}^h & \mathbf{U}_{44}^e \end{bmatrix}^{-1} \begin{bmatrix} \mathbf{D}l_{11} & \mathbf{0} & \mathbf{0} & \mathbf{0} \\ \mathbf{0} & \mathbf{D}l_{22} & \mathbf{0} & \mathbf{0} \\ \mathbf{0} & \mathbf{0} & \mathbf{D}l_{33} & \mathbf{0} \\ \mathbf{0} & \mathbf{0} & \mathbf{0} & \mathbf{D}l_{44} \end{bmatrix} \begin{bmatrix} \mathbf{B}^{Vh} e^{-\gamma_z a} + \mathbf{A}^{Vh} e^{\gamma_z a} \\ \mathbf{B}^{Ve} e^{-\gamma_z a} + \mathbf{A}^{Ve} e^{\gamma_z a} \\ \mathbf{B}^{Vlh} e^{-\gamma_x a} + \mathbf{A}^{Vlh} e^{\gamma_x a} \\ \mathbf{B}^{Vle} e^{-\gamma_x a} + \mathbf{A}^{Vle} e^{\gamma_x a} \end{bmatrix}. \quad (4.55)$$

Substituting (4.55) into (4.54) results in

$$[\mathbf{M}][\mathbf{U}]^{-1}[\mathbf{D}l]\left[\mathbf{B}e^{-\gamma a} + \mathbf{A}e^{\gamma a}\right] = \left[\mathbf{D}l^*\right]\left[\mathbf{B}e^{-\gamma a} - \mathbf{A}e^{\gamma a}\right]. \quad (4.56)$$

The generalized scattering matrix [S] can be derived from (4.56)

$$[\mathbf{S}] = ([\mathbf{I}] - [\mathbf{G}])^{-1}([\mathbf{I}] + [\mathbf{G}]), \quad (4.57)$$

where

$$[\mathbf{G}] = \left[\mathbf{D}l^*\right]^{-1}[\mathbf{M}][\mathbf{U}]^{-1}[\mathbf{D}l], \quad (4.58)$$

and [I] is the identity matrix.

Note that the reference planes are at the center of the post for **A** and **B** coefficients. For generalized scattering matrix [S] in (4.57), the reference plane is moved to the apertures of the arms since **A** multiplies phase shift $e^{\gamma a}$ and **B** multiplies $e^{-\gamma a}$.

4.2.5 Simulation Results of a Bend Junction Loaded with a Conducting Post

Simulation results for three examples are given in Fig. 4.2.4 to Fig. 4.2.6. The first example is the S parameters of a hollow waveguide bend with the width of $2a$=0.75 inches and the height of b=0.375 inches. In Fig. 4.2.4(a) and (b), the magnitude and phase of the S parameters for the dominant mode in the bend calculated using the formula described in this chapter and using a commercial software which incorporates the Finite Element Method are superimposed. Excellent agreement can be observed.

In a full height post case, the dimensions of the bend are given as follows: the width of the waveguide $2a$=0.75 inches, the height of the waveguide b= 0.375 inches, the radius of the post r_0=0.1inches, and the height of the post is 0.375 inches. The real part and imaginary part of the S_{11} of the dominant mode are plotted in Fig. 4.2.5 (a). Fig. 4.2.5 (b) gives the real and imaginary parts of S_{12} for the bend loaded with a full height post.

For the partial height post case, $a = b = 0.375$ inches, $r_0 = 0.1$inches, the height of the post $l_a = 0.3$ inches. The real part and imaginary part of S_{11} are given in Fig. 4.2.6 (a). Those of S_{12} are shown in Fig. 4.2.6 (b). In all plots, solid lines are the results of finite element method, square points are the results of our new formulas. Excellent agreement between the results of the modal analysis and the finite element methods is observed.

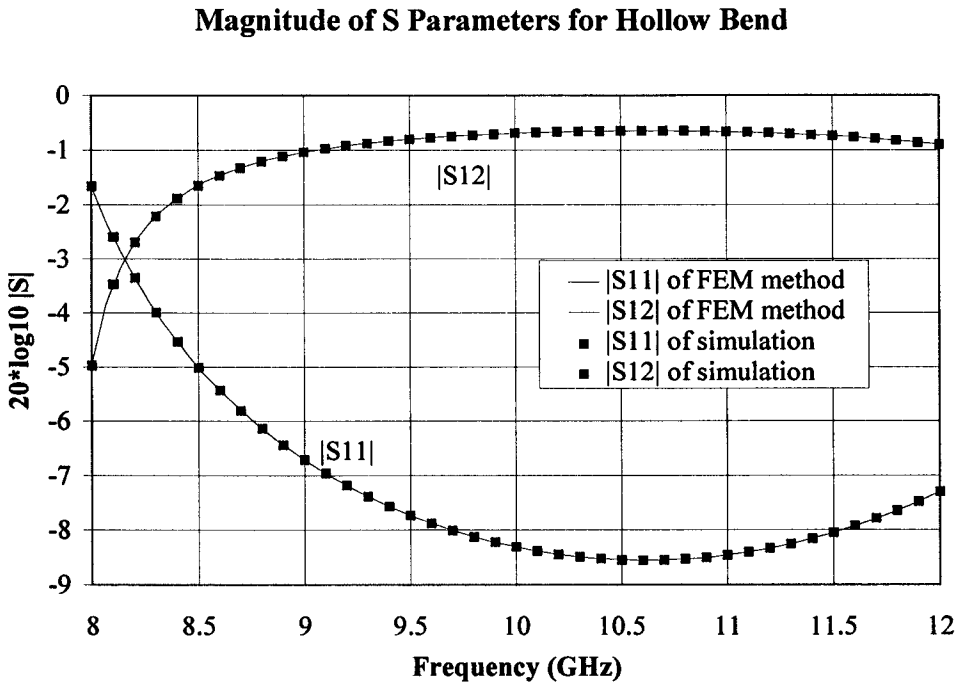

Fig. 4.2.4 (a) Magnitude of the S parameters of the dominant mode in a right angle waveguide bend

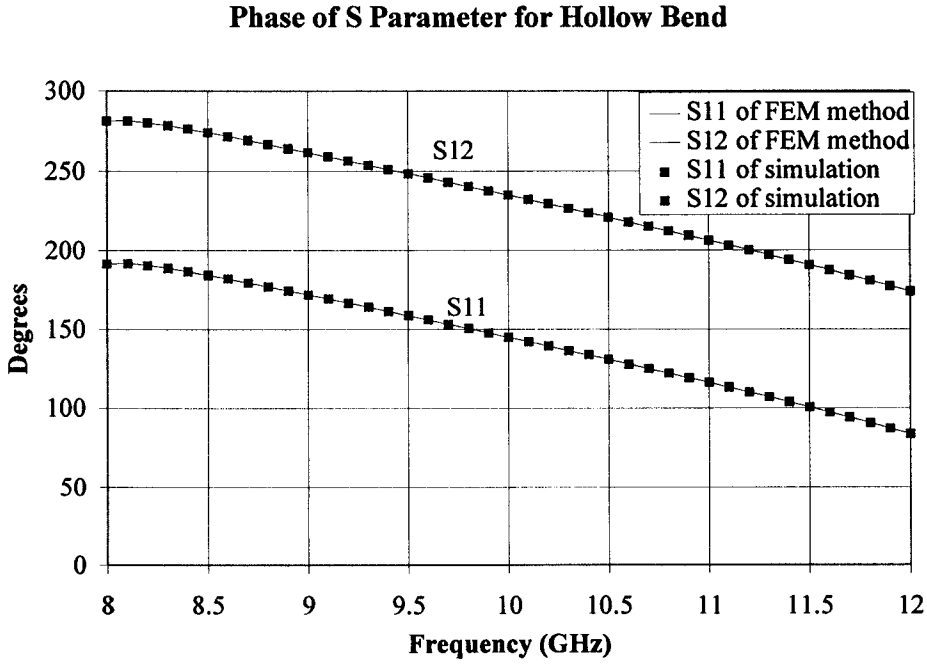

Fig. 4.2.4 (b) The phase of the S parameters of the dominant mode in a right angle waveguide bend

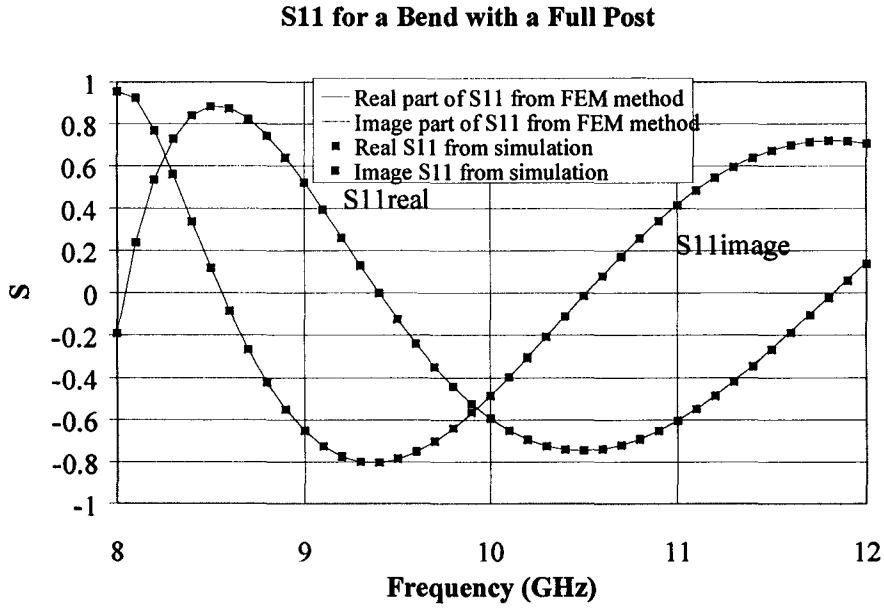

Fig. 4.2.5 (a) S11 of the dominant mode in a bend junction with a full height post

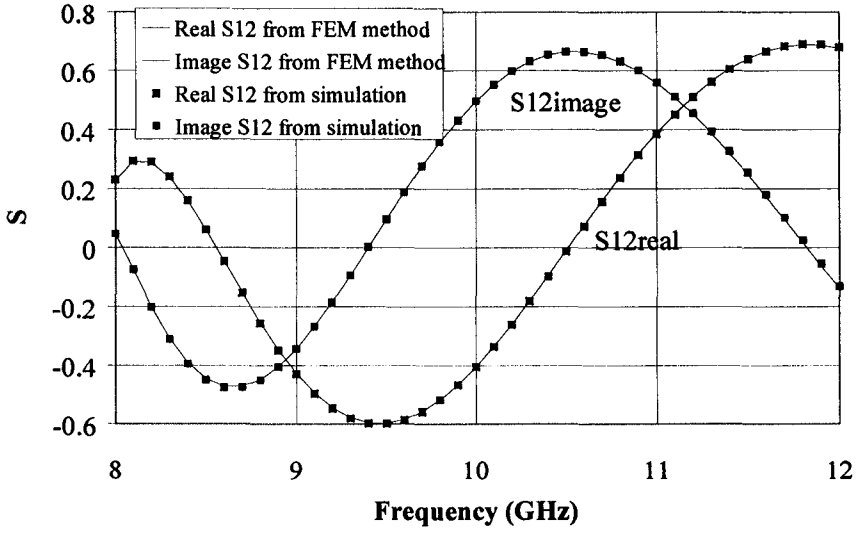

Fig. 4.2.5 (b) S12 of the dominant mode in a bend junction with a full height post

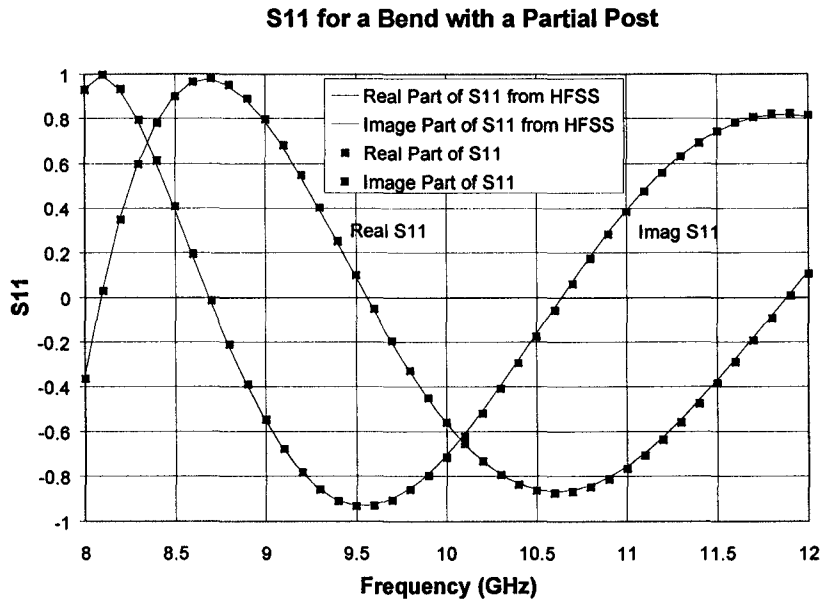

Fig. 4.2.6 (a) S11 of the dominant mode in a bend junction with a partial height post

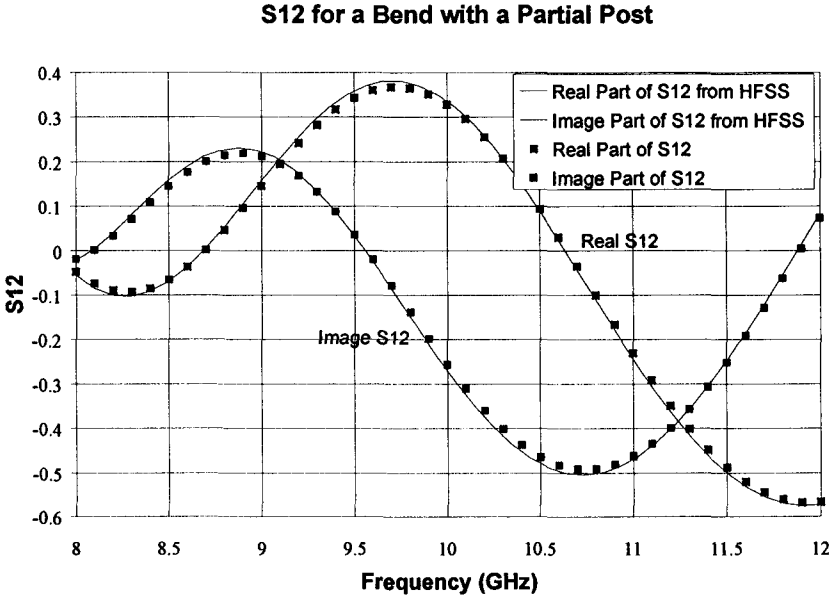

Fig. 4.2.6 (b) S12 of the dominant mode in a bend junction with a partial height post

4.3 Modeling a T Junction Loaded with a Partial Height Post

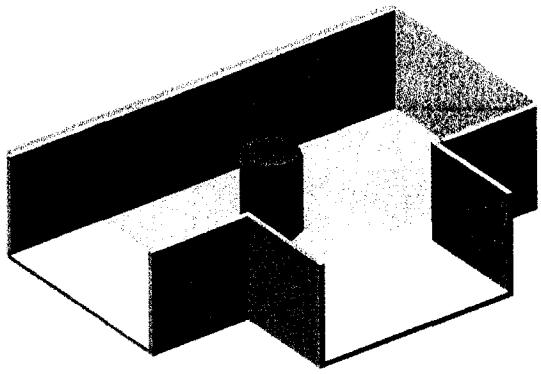

Fig. 4.3.1 The structure of a T junction loaded with a partial height post

The structure of the T-junction loaded with a partial height conducting post is shown in Fig. 4.3.1. The modeling of the T-junction can be derived in the same way as that of the right angle bend. The T-junction is sensitive to different sets of the mode functions in the vertical waveguide. In the approach used here, special attention is paid to choosing the correct set of eigenmodes in the vertical straight waveguide, which will determine the accuracy of the results and the succinctness of the equations.

First, we decompose a T-junction into three parts. By adding perfect electric walls at each aperture of the right and the upper arms, the left arm and cavity region will form a one-port cavity as shown in Fig. 4.3.2. The field expressions in a one-port waveguide were given in the last section. The total field in each arm remains the same as that in the

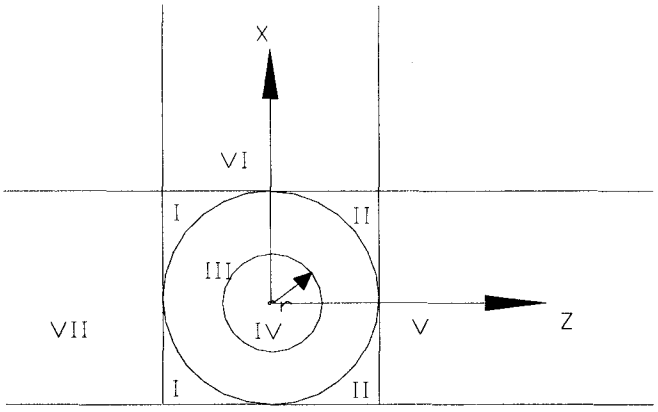

Fig. 4.3.2 Top view of a waveguide T-junction loaded with a post

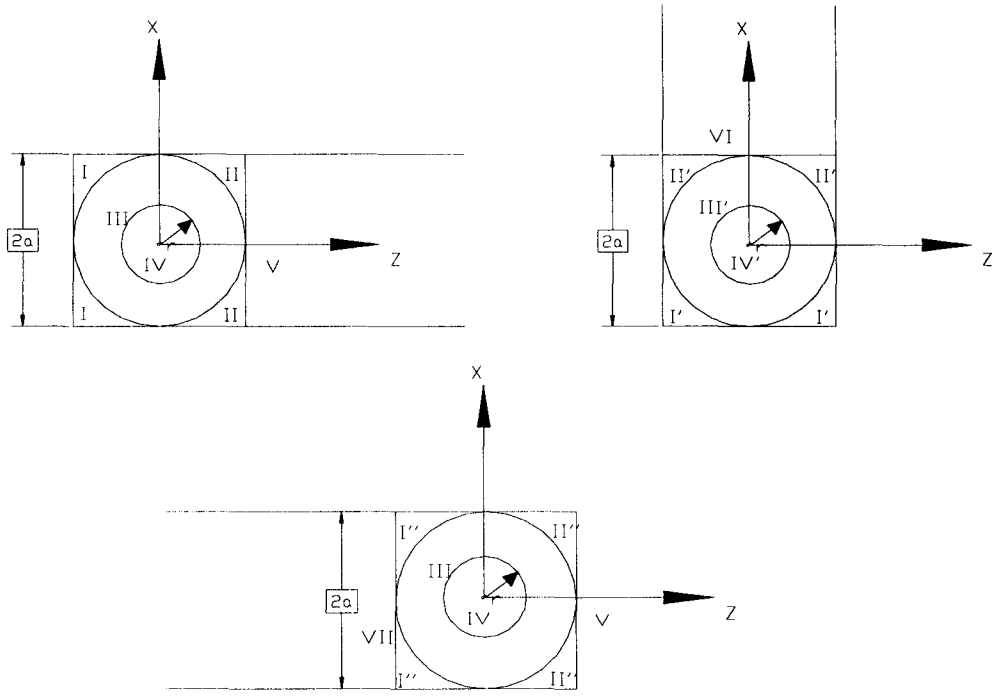

Fig. 4.3.3 Separated regions for T-junction loaded with a post

one-port waveguide. The fields in the cavity region are the sums of the fields in three cavity regions of the one-port waveguides. After applying the boundary conditions to each aperture of the arms, a set of linear equations are obtained. The generalized scattering matrix is derived from these equations.

4.3.1 Field Expressions in the Left One-Port Waveguide

The expressions of electromagnetic fields in the right horizontal one-port waveguide are given in section 4.2.1. Section 4.2.3 gives the field expressions in vertical one port waveguide. The field in region VII of the one port waveguide is expanded in terms of mode functions as

$$\bar{\mathbf{E}}_t^{VII} = \sum_m \sum_i [A_{mi}^{VIIh} e^{-\gamma_{zmi} z} + B_{mi}^{VIIh} e^{\gamma_{zmi} z}] \hat{e}_{tmi}^{hz} + \sum_m \sum_i [A_{mi}^{VIIe} e^{-\gamma_{zmi} z} + B_{mi}^{VIIe} e^{\gamma_{zmi} z}] \hat{e}_{tmi}^{ez}, \tag{4.59}$$

$$\bar{\mathbf{H}}_t^{VII} = \sum_m \sum_i [A_{mi}^{VIIh} e^{-\gamma_{zmi} z} - B_{mi}^{VIIh} e^{\gamma_{zmi} z}] \hat{h}_{tmi}^{hz} + \sum_m \sum_i [A_{mi}^{VIIe} e^{-\gamma_{zmi} z} - B_{mi}^{VIIe} e^{\gamma_{zmi} z}] \hat{h}_{tmi}^{ez}. \tag{4.60}$$

The total fields in the cavity region I" and II" are given by

$$\bar{\mathbf{E}}_t^{I"z} = \sum_j F_j^h \phi_j^{hI"} + \sum_j F_j^e \phi_j^{eI"}, \tag{4.61}$$

$$\bar{\mathbf{H}}_t^{I"z} = \sum_j F_j^h \psi_j^{hI"} + \sum_j F_j^e \psi_j^{eI"}, \tag{4.62}$$

$$\bar{\mathbf{E}}_t^{II"z} = \sum_j F_j^h \phi_j^{hII"} + \sum_j F_j^e \phi_j^{eII"}, \tag{4.63}$$

$$\bar{\mathbf{H}}_t^{II"z} = \sum_j F_j^h \psi_j^{hII"} + \sum_j F_j^e \psi_j^{eII"}, \tag{4.64}$$

where F_j^h and F_j^e are eigenfield coefficients, the extended eigenmode functions $\phi_j^{eI"}$, $\phi_j^{hI"}$, $\psi_j^{eI"}$ and $\psi_j^{hI"}$ are the same as those given in equation (4.15). And the eigenmode

functions are given by multiplying –1 with the right sides of the equations (4.3) – (4.8). The coefficients $A_{p,j}^{I'',II''}$ and $B_{p,j}^{I'',II''}$ can be obtained in the same way as that given in section 4.2.2.

4.3.2 Boundary Conditions and Generalized Scattering Matrix

At the boundaries z = a, z = -a and x = a, the tangential components of the electromagnetic field are continuous.

$$\vec{E}_t^{V}|_{z=a} = \vec{E}_t^{II}|_{z=a}, \tag{4.65}$$

$$\vec{E}_t^{VI}|_{x=a} = \vec{E}_t^{II'}|_{x=a}, \tag{4.66}$$

$$\vec{E}_t^{VII}|_{z=-a} = \vec{E}_t^{I''}|_{z=-a}, \tag{4.67}$$

$$\vec{H}_t^{V}|_{z=a} = \vec{H}_t^{II}|_{z=a} + \vec{H}_t^{II''}|_{z=a} + \begin{cases} (H_x^{II'} + H_y^{II'})_{z=a}, & 0 \le x \le a, \\ (H_x^{I'} + H_y^{I'})_{z=a}, & -a \le x < 0, \end{cases} \tag{4.68}$$

$$\vec{H}_t^{VI}|_{x=a} = \vec{H}_t^{II'}|_{x=a} + \begin{cases} (H_z^{II} + H_y^{II} + H_z^{II''} + H_y^{II''})_{x=a}, & 0 \le z \le a, \\ (H_z^{I} + H_y^{I} + H_z^{I''} + H_y^{I''})_{x=a}, & -a \le z < 0, \end{cases} \tag{4.69}$$

$$\vec{H}_t^{VII}|_{z=-a} = \vec{H}_t^{I''}|_{z=-a} + \vec{H}_t^{I}|_{z=-a} + \begin{cases} (H_x^{II'} + H_y^{II'})_{z=-a}, & 0 \le x \le a, \\ (H_x^{I'} + H_y^{I'})_{z=-a}, & -a \le x < 0. \end{cases} \tag{4.70}$$

Substituting the series expressions of electric field and magnetic field into above equations, then taking inner products of equation (4.65) with $\hat{h}_t^{hz*}$ and $\hat{h}_t^{ez*}$, (4.66) with $\hat{h}_t^{hx*}$ and $\hat{h}_t^{ex*}$, and (4.67) with $\hat{h}_t^{hz*}$ and $\hat{h}_t^{ez*}$, we obtain the matrix equation

$$\begin{bmatrix} \mathbf{U}_{11} & \mathbf{U}_{12} & \mathbf{0} & \mathbf{0} & \mathbf{0} & \mathbf{0} \\ \mathbf{U}_{21} & \mathbf{U}_{22} & \mathbf{0} & \mathbf{0} & \mathbf{0} & \mathbf{0} \\ \mathbf{0} & \mathbf{0} & \mathbf{U}_{33} & \mathbf{U}_{34} & \mathbf{0} & \mathbf{0} \\ \mathbf{0} & \mathbf{0} & \mathbf{U}_{43} & \mathbf{U}_{44} & \mathbf{0} & \mathbf{0} \\ \mathbf{0} & \mathbf{0} & \mathbf{0} & \mathbf{0} & \mathbf{U}_{55} & \mathbf{U}_{56} \\ \mathbf{0} & \mathbf{0} & \mathbf{0} & \mathbf{0} & \mathbf{U}_{65} & \mathbf{U}_{66} \end{bmatrix} \begin{bmatrix} \mathbf{C}^h \\ \mathbf{C}^e \\ \mathbf{D}^h \\ \mathbf{D}^e \\ \mathbf{F}^h \\ \mathbf{F}^e \end{bmatrix} = \begin{bmatrix} \mathbf{D}l_{11} & \cdots & \mathbf{0} \\ \vdots & \ddots & \vdots \\ \mathbf{0} & \cdots & \mathbf{D}l_{66} \end{bmatrix} \begin{bmatrix} \mathbf{B}^{Vh} e^{-\gamma_z a} + \mathbf{A}^{Vh} e^{\gamma_z a} \\ \mathbf{B}^{Ve} e^{-\gamma_z a} + \mathbf{A}^{Ve} e^{\gamma_z a} \\ \mathbf{B}^{Vlh} e^{-\gamma_x a} + \mathbf{A}^{Vlh} e^{\gamma_x a} \\ \mathbf{B}^{Vle} e^{-\gamma_x a} + \mathbf{A}^{Vle} e^{\gamma_x a} \\ \mathbf{B}^{Vllh} e^{-\gamma_z a} + \mathbf{A}^{Vllh} e^{\gamma_z a} \\ \mathbf{B}^{Vlle} e^{-\gamma_z a} + \mathbf{A}^{Vlle} e^{\gamma_z a} \end{bmatrix}, \tag{4.71}$$

where **Dl** matrix is a diagonal matrix, **A**, **B**, **C**, **D** and **F** are coefficient vectors. $\mathbf{U}_{ij}$ and $\mathbf{Dl}_{ii}$ are diagonal submatrices.

Taking inner products of equation (4.68) with $\hat{e}_t^{hz*}$ and $\hat{e}_t^{ez*}$, equation (4.69) with $\hat{e}_t^{hx*}$ and $\hat{e}_t^{ex*}$, and equation (4.70) with $\hat{e}_t^{hz*}$ and $\hat{e}_t^{ez*}$, we have the matrix expression

$$\begin{bmatrix} \mathbf{M}_{11} & \mathbf{M}_{12} & \mathbf{M}_{13} & \mathbf{M}_{14} & \mathbf{M}_{15} & \mathbf{M}_{16} \\ \mathbf{M}_{21} & \mathbf{M}_{22} & \mathbf{M}_{23} & \mathbf{M}_{24} & \mathbf{M}_{25} & \mathbf{M}_{26} \\ \mathbf{M}_{31} & \mathbf{M}_{32} & \mathbf{M}_{33} & \mathbf{M}_{34} & \mathbf{M}_{35} & \mathbf{M}_{36} \\ \mathbf{M}_{41} & \mathbf{M}_{42} & \mathbf{M}_{43} & \mathbf{M}_{44} & \mathbf{M}_{45} & \mathbf{M}_{46} \\ \mathbf{M}_{51} & \mathbf{M}_{52} & \mathbf{M}_{53} & \mathbf{M}_{54} & \mathbf{M}_{55} & \mathbf{M}_{56} \\ \mathbf{M}_{61} & \mathbf{M}_{62} & \mathbf{M}_{63} & \mathbf{M}_{64} & \mathbf{M}_{65} & \mathbf{M}_{66} \end{bmatrix} \begin{bmatrix} \mathbf{C}^h \\ \mathbf{C}^e \\ \mathbf{D}^h \\ \mathbf{D}^e \\ \mathbf{F}^h \\ \mathbf{F}^e \end{bmatrix} = \begin{bmatrix} \mathbf{D}l_{11}^* & \cdots & \mathbf{0} \\ \vdots & \ddots & \vdots \\ \mathbf{0} & \cdots & \mathbf{D}l_{66}^* \end{bmatrix} \begin{bmatrix} \mathbf{B}^{Vh} e^{-\gamma_z a} - \mathbf{A}^{Vh} e^{\gamma_z a} \\ \mathbf{B}^{Ve} e^{-\gamma_z a} - \mathbf{A}^{Ve} e^{\gamma_z a} \\ \mathbf{B}^{Vlh} e^{-\gamma_x a} - \mathbf{A}^{Vlh} e^{\gamma_x a} \\ \mathbf{B}^{Vle} e^{-\gamma_x a} - \mathbf{A}^{Vle} e^{\gamma_x a} \\ \mathbf{B}^{Vllh} e^{-\gamma_z a} - \mathbf{A}^{Vllh} e^{\gamma_z a} \\ \mathbf{B}^{Vlle} e^{-\gamma_z a} - \mathbf{A}^{Vlle} e^{\gamma_z a} \end{bmatrix} \tag{4.72}$$

Combining two matrix equations (4.71) and (4.72), the generalized scattering matrix obtained is given by

$$[\mathbf{S}] = ([\mathbf{I}] - [\mathbf{G}])^{-1}([\mathbf{I}] + [\mathbf{G}]), \tag{4.73}$$

where

$$[\mathbf{G}] = \left[\mathbf{Dl}^*\right]^{-1}[\mathbf{M}][\mathbf{U}]^{-1}[\mathbf{Dl}], \tag{4.74}$$

and [I] is the identity matrix. Like the right angle bend, the reference planes are located at the apertures of the waveguide arms since the coefficient vectors **A** and **B** are multiplied by an exponential factor.

4.3.3 Simulation Results

The generalized scattering matrices of T-junctions loaded with a partial height post are calculated in this section. Two examples of simulated results are presented.

In Fig. 4.3.4, the magnitudes and the phases of the S parameters of the T-junction are plotted. The dimensions of the junction are given as: the half width of the waveguide a = 0.375 inches, the height of the waveguide b = 0.375 inches, the radius of the post r_0=0.05 inches, the height of the post l_a=0.1 inches. The solid lines are the results of the finite element method using a commercial software. The points are the values calculated using the proposed formulae. The frequency range is 8 GHz to 12 GHz.

The magnitudes and phases of the scattering parameters of the second T-junction are plotted in Fig. 4.3.5. The dimensions of the junction are: a = 0.14 inches, b = 0.14 inches, r_0 = 0.025 inches, l_a=0.12 inches. The frequency range is 24GHz to 38 GHz.

The method can be applied to derive the generalized scattering matrix for a cross waveguide junction loaded with a partial height post. The additional step is to add a one-port waveguide to the T-junction.

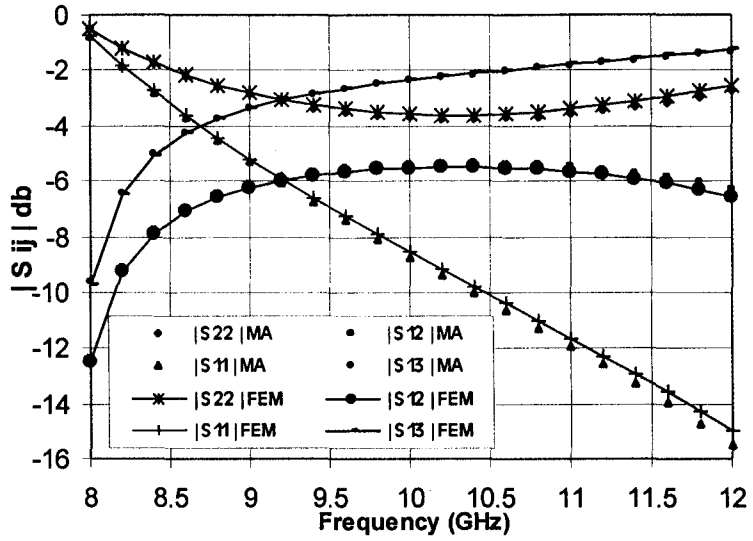

(a) **Magnitude of S_{11}, S_{22}, S_{12} and S_{13} of the dominant mode in a T-junction**

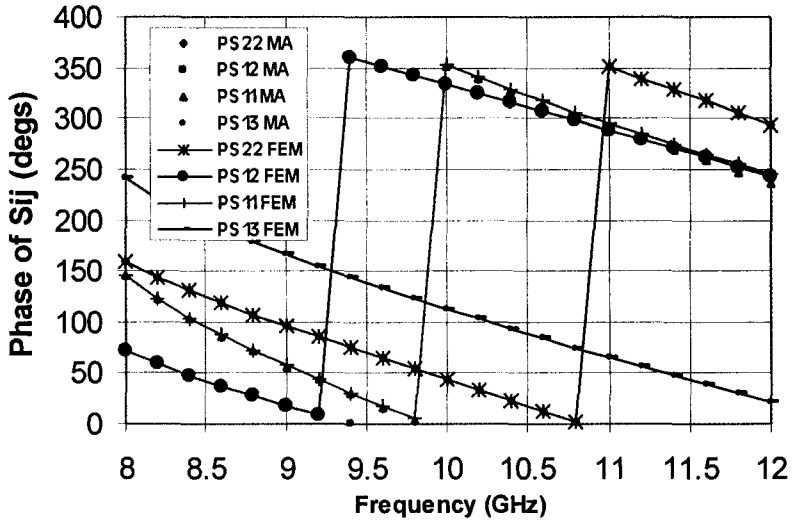

(b) Phase of S_{11}, S_{12} and S_{13} of the dominant mode in a T-junction

Fig. 4.3.4 Magnitude and phase of S_{11}, S_{22}, S_{12} and S_{13} for a T-junction

a = 0.375 inch, b = 0.375 inch, r_0 = 0.05 inch, l_a = 0.1 inch.

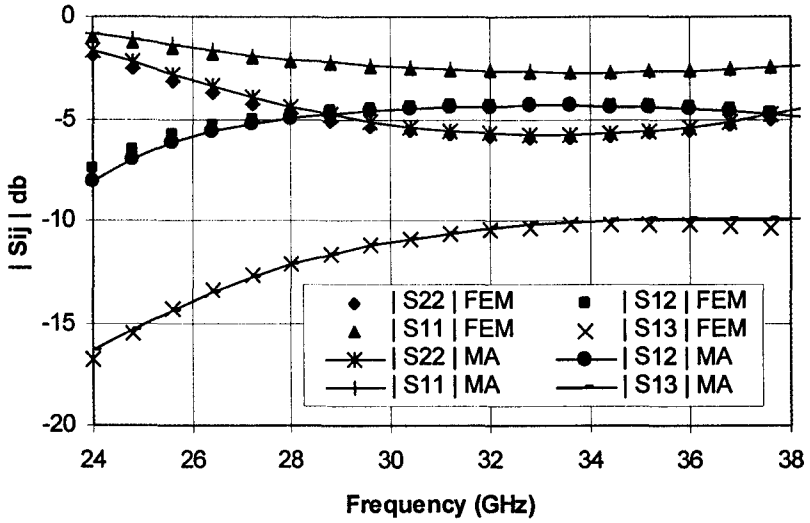

(a) Magnitude of S_{11}, S_{22}, S_{12} and S_{13} of the dominant mode in a T-junction

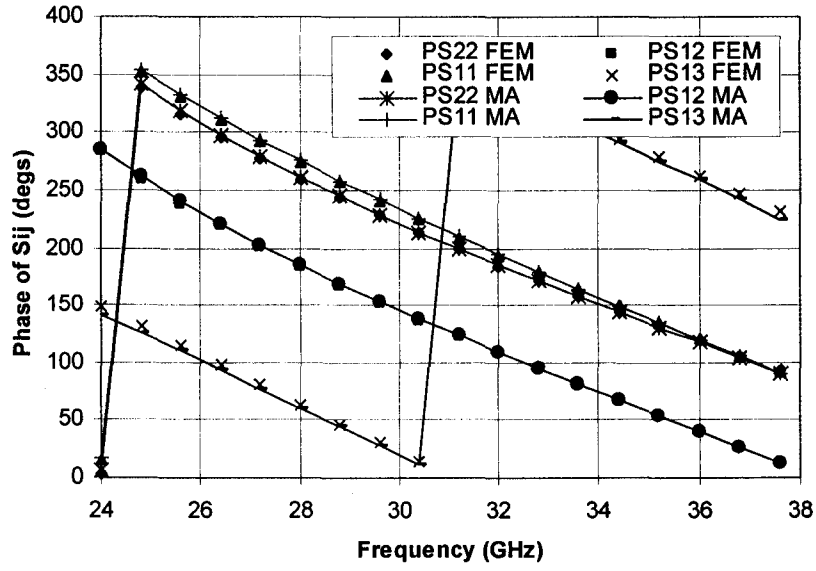

(b) Phase of S_{11}, S_{22}, S_{12} and S_{13} of the dominant mode in a T-junction

Fig. 4.3.5 Magnitude and phase of S_{11}, S_{22}, S_{12} and S_{13} for a T-junction

a = 0.14 inch, b = 0.14 inch, r_0 = 0.025 inch, l_a = 0.12 inch.

4.4 Appendix

4.4.1 The expressions of elements in matrix [Dl], [Dl*], [U] and [M] in section 4.2.4

The elements in the matrices [**Dl**] and [**Dl***] are self inner products of the mode functions in each arm, defined at the end of this appendix.

$$\mathbf{Dl}_{ii} = < \hat{e}_{tkl}^{pu}, \hat{h}_{tkl}^{pu*} >, \qquad \mathbf{Dl}_{ii}^{*} = < \hat{e}_{tkl}^{pu*}, \hat{h}_{tkl}^{pu} >,$$

$$\begin{cases} p = h, & \text{for } i = 1,\ 3, \\ p = e, & \text{for } i = 2,\ 4, \end{cases} \quad \text{and} \quad \begin{cases} u = z, & \text{for } i = 1,\ 2, \\ u = x, & \text{for i} = 3,\ 4. \end{cases} \tag{4.75}$$

The matrices [**Dl**] and [**Dl***] are diagonal matrices.

The elements of matrix [**U**] are given by

$$(\mathbf{U}_{ik}^{p})_{qj} = < \phi_{j}^{pII}, \hat{h}_{tq}^{ru*} >, \tag{4.76}$$

$$\begin{cases} p = h, & \text{for } k = 1,\ 3, \\ p = e, & \text{for } k = 2,\ 4, \end{cases} \quad \begin{cases} r = h, & \text{for } i = 1,\ 3, \\ r = e, & \text{for } i = 2,\ 4, \end{cases} \quad \text{and} \quad \begin{cases} u = z, & \text{for } i = 1,\ 2, \\ u = x, & \text{for } i = 3,\ 4, \end{cases}$$

where ϕ_j^{pII}'s are extended eigenmode functions given in equation (4.15), the inner products are integrations on the cross sections of the waveguides.

The elements of the matrix [**M**] are given by

$$(\mathbf{M}_{i1})_{q,j} = < \hat{e}_{tq}^{pz*}, \psi_{j}^{hII} |_{z=a} >_{-a}^{a}, \qquad (\mathbf{M}_{i2})_{q,j} = < \hat{e}_{tq}^{pz*}, \psi_{j}^{eII} |_{z=a} >_{-a}^{a}, \tag{4.77}$$

$$(\mathbf{M}_{i3})_{q,j} = < \hat{e}_{tq}^{pz*}, \underset{x,y}{\psi_{j}^{hII'}} |_{z=a} >_{0}^{a} + < \hat{e}_{tq}^{pz*}, \underset{x,y}{\psi_{j}^{hI'}} |_{z=a} >_{-a}^{0}, \tag{4.78}$$

$$(\mathbf{M}_{i4})_{q,j} = < \hat{e}_{tq}^{pz*}, \underset{x,y}{\psi_{j}^{eII'}} |_{z=a} >_{0}^{a} + < \hat{e}_{tq}^{pz*}, \underset{x,y}{\psi_{j}^{eI'}} |_{z=a} >_{-a}^{0}, \tag{4.79}$$

$$\begin{cases} p = h, & \text{for } i = 1, \\ p = e, & \text{for } i = 2. \end{cases}$$

$$(\mathbf{M}_{i1})_{q,j} = < \hat{e}_{tq}^{px*}, \psi_j^{hII'} |_{x=a} >_{-a}^{a}, \qquad (\mathbf{M}_{i2})_{q,j} = < \hat{e}_{tq}^{px*}, \psi_j^{eII'} |_{x=a} >_{-a}^{a}, \tag{4.80}$$

$$(\mathbf{M}_{i3})_{q,j} = < \hat{e}_{tq}^{px*}, \underset{y,z}{\psi_j^{hII}} |_{x=a} >_{0}^{a} + < \hat{e}_{tq}^{px*}, \underset{y,z}{\psi_j^{hI}} |_{x=a} >_{-a}^{0}, \tag{4.81}$$

$$(\mathbf{M}_{i4})_{q,j} = < \hat{e}_{tq}^{px*}, \underset{y,z}{\psi_j^{eII}} |_{x=a} >_{0}^{a} + < \hat{e}_{tq}^{px*}, \underset{y,z}{\psi_j^{eI}} |_{x=a} >_{-a}^{0}, \tag{4.82}$$

$$\begin{cases} p = h, & \text{for } i = 3, \\ p = e, & \text{for } i = 4, \end{cases}$$

where $\psi_j^{pI,II}$'s are extended eigenmode functions given in (4.15), the upper and lower limits of the integration are given by superscripts and subscripts outside the sign <>, respectively. The subscripts of ψ, x, y and z = a, signify the x and y components of ψ waves at the reference plane z = a.

4.4.2 The expressions of the matrices [Dl], [Dl*], [U] and [M] in section 4.3.2

The elements in the matrices [**Dl**] and [**Dl***] are given by

$$\mathbf{Dl}_{ii} = < \hat{e}_{tkl}^{pu}, \hat{h}_{tkl}^{pu*} >, \quad \mathbf{Dl}_{ii}^{*} = < \hat{e}_{tkl}^{pu*}, \hat{h}_{tkl}^{pu} >, \tag{4.83}$$

$$\begin{cases} p = h, & \text{for } i = 1,\ 3,\ 5, \\ p = e, & \text{for } i = 2,\ 4,\ 6, \end{cases} \quad \text{and} \quad \begin{cases} u = z, & \text{for } i = 1,\ 2,\ 5,\ 6, \\ u = x, & \text{for } i = 3,\ 4. \end{cases}$$

The matrices [**Dl**] and [**Dl***] are diagonal matrices.

The elements of matrix [**U**] are given by

$$(\mathbf{U}_{ik}^{p})_{qj} = < \phi_j^{pII}, \hat{h}_{tq}^{ru*} >, \tag{4.84}$$

$$\begin{cases} r = h, & \text{for } i = 1,\ 3,\ 5, \\ r = e, & \text{for } i = 2,\ 4,\ 6, \end{cases} \quad \begin{cases} p = h, & \text{for } k = 1,\ 3,\ 5, \\ p = e, & \text{for } k = 2,\ 4,\ 6, \end{cases} \quad \text{and} \quad \begin{cases} u = z, & \text{for } i = 1,\ 2,\ 5,\ 6, \\ u = x, & \text{for } i = 3,\ 4, \end{cases}$$

where the inner products are integrated from -a to a.

The elements of the matrix [M] are given by

$$(\mathbf{M}_{i1})_{q,j} = < \hat{e}_{tq}^{pz*}, \psi_j^{hII} |_{z=a} >_{-a}^{a}, \qquad (\mathbf{M}_{i2})_{q,j} = < \hat{e}_{tq}^{pz*}, \psi_j^{eII} |_{z=a} >_{-a}^{a}, \tag{4.85}$$

$$(\mathbf{M}_{i3})_{q,j} = < \hat{e}_{tq}^{pz*}, \underset{x,y}{\psi_j^{hII'}} |_{z=a} >_{0}^{a} + < \hat{e}_{tq}^{pz*}, \underset{x,y}{\psi_j^{hI'}} |_{z=a} >_{-a}^{0}, \tag{4.86}$$

$$(\mathbf{M}_{i4})_{q,j} = < \hat{e}_{tq}^{pz*}, \underset{x,y}{\psi_j^{eII'}} |_{z=a} >_{0}^{a} + < \hat{e}_{tq}^{pz*}, \underset{x,y}{\psi_j^{eI'}} |_{z=a} >_{-a}^{0}, \tag{4.87}$$

$$(\mathbf{M}_{i5})_{q,j} = < \hat{e}_{tq}^{pz*}, \psi_j^{hII''} |_{z=a} >_{-a}^{a}, \qquad (\mathbf{M}_{i6})_{q,j} = < \hat{e}_{tq}^{pz*}, \psi_j^{eII''} |_{z=a} >_{-a}^{a}, \tag{4.88}$$

$$\begin{cases} p = h, & \text{for } i = 1, \\ p = e, & \text{for } i = 2, \end{cases}$$

$$(\mathbf{M}_{i1})_{q,j} = < \hat{e}_{tq}^{px*}, \psi_j^{hII'} |_{x=a} >_{-a}^{a}, \qquad (\mathbf{M}_{i2})_{q,j} = < \hat{e}_{tq}^{px*}, \psi_j^{eII'} |_{x=a} >_{-a}^{a}, \tag{4.89}$$

$$(\mathbf{M}_{i3})_{q,j} = < \hat{e}_{tq}^{px*}, \underset{y,z}{\psi_j^{hII}} |_{x=a} >_{0}^{a} + < \hat{e}_{tq}^{px*}, \underset{y,z}{\psi_j^{hI}} |_{x=a} >_{-a}^{0}, \tag{4.90}$$

$$(\mathbf{M}_{i4})_{q,j} = < \hat{e}_{tq}^{px*}, \underset{y,z}{\psi_j^{eII}} |_{x=a} >_{0}^{a} + < \hat{e}_{tq}^{px*}, \underset{y,z}{\psi_j^{eI}} |_{x=a} >_{-a}^{0}, \tag{4.91}$$

$$(\mathbf{M}_{i5})_{q,j} = < \hat{e}_{tq}^{px*}, \underset{y,z}{\psi_j^{hII''}} |_{x=a} >_{0}^{a} + < \hat{e}_{tq}^{px*}, \underset{y,z}{\psi_j^{hI''}} |_{x=a} >_{-a}^{0}, \tag{4.92}$$

$$(\mathbf{M}_{i6})_{q,j} = < \hat{e}_{tq}^{px*}, \underset{y,z}{\psi_j^{eII''}} |_{x=a} >_{0}^{a} + < \hat{e}_{tq}^{px*}, \underset{y,z}{\psi_j^{eI''}} |_{x=a} >_{-a}^{0}, \tag{4.93}$$

$$\begin{cases} p = h, & \text{for } i = 3, \\ p = e, & \text{for } i = 4, \end{cases}$$

$$(\mathbf{M}_{i1})_{q,j} = < \hat{e}_{tq}^{pz*}, \psi_j^{hI} |_{z=-a} >_{-a}^{a}, \qquad (\mathbf{M}_{i2})_{q,j} = < \hat{e}_{tq}^{pz*}, \psi_j^{eI} |_{z=-a} >_{-a}^{a}, \tag{4.94}$$

$$(\mathbf{M}_{i3})_{q,j} = < \hat{e}_{tq}^{pz*}, \underset{x,y}{\psi_j^{hII'}} |_{z=-a} >_{0}^{a} + < \hat{e}_{tq}^{pz*}, \underset{x,y}{\psi_j^{hI'}} |_{z=-a} >_{-a}^{0}, \tag{4.95}$$

$$(\mathbf{M}_{i4})_{q,j} = < \hat{e}_{tq}^{pz*}, \underset{x,y}{\psi_j^{ell'}} |_{z=-a} >_0^a + < \hat{e}_{tq}^{pz*}, \underset{x,y}{\psi_j^{el'}} |_{z=-a} >_{-a}^0, \tag{4.96}$$

$$(\mathbf{M}_{i5})_{q,j} = < \hat{e}_{tq}^{pz*}, \psi_j^{hl''} |_{z=-a} >_{-a}^a, \qquad (\mathbf{M}_{i6})_{q,j} = < \hat{e}_{tq}^{pz*}, \psi_j^{el''} |_{z=-a} >_{-a}^a, \tag{4.97}$$

$$\begin{cases} p = h, & \text{for } i = 5, \\ p = e, & \text{for } i = 6. \end{cases}$$

In this chapter, the inner products are defined as [22]

$$< \hat{e},\ \hat{h} > = \int_{-a}^{a} (\int_{0}^{b} (\hat{e} \times \hat{h}) \cdot \hat{n}\, dy) dx$$

for the horizontal waveguide, and

$$< \hat{e},\ \hat{h} > = \int_{-a}^{a} (\int_{0}^{b} (\hat{e} \times \hat{h}) \cdot \hat{n}\, dy) dz$$

for the vertical waveguide, where $\hat{n}$ is the normal vector perpendicular to the surface of integration.

Chapter 5

Conclusions

This dissertation is devoted to the analytical development of models that are used in waveguide designs. The problems investigated include the analyses of the TE, TM, and TEM modes in a circular-rectangular (CR) waveguide, and the generalized scattering matrices (GSM) of a waveguide bend and a T-junction loaded with a partial height circular post.

In chapter 2, a rigorous analysis for the higher order modes in a circular-rectangular waveguide is introduced. Mathematical expressions of the TE and TM modes are derived using the Galerkin method based on two different coordinate systems. The derived formula can be easily used to determine the eigenvalue spectrum of the higher order modes. The cutoff frequencies and eigenmode fields are solved by means of SVD technique. The numerical results agree with the results obtained by using the finite element method (FEM).

A modal solution for the TEM mode of the circular-rectangular coaxial waveguide is presented in chapter 3. An analytical expression of the characteristic impedance of the waveguide is derived. Three typical C-R waveguides are considered as examples to test this expression, and excellent results are observed. The attenuation coefficient of the waveguide is also derived to calculate the power loss. An optimal dimension aspect ratio for the minimum power loss is determined, which is a critical parameter in designs of the combline type filters and diplexers.

There are two remarkable advantages of using the modal analyses of higher-order modes and TEM mode. (i) Only a few waveguide modes are needed for doing analyses, which makes computations much more efficient than using other technologies. (ii) The module of the C-R waveguide can be easily cascaded with other waveguide modules, such as a waveguide step junction, so that more complicated transmission line structures can be analyzed. It is worth pointing out that the solutions of both higher order modes and the TEM mode in asymmetric C-R waveguides can be obtained by using the addition theorems of Bessel functions.

In Chapter 4, the processing of the modal analysis for a waveguide right-angle bend and a T-junction was explored. A new concept called the method of extended eigenmode functions is introduced to solve the complex boundary problems caused by the existence of the partial height posts inside the waveguides. The generalized scattering matrices (GMS) for the bend and T-junctions are obtained. Concrete examples of the bend and T-junctions with partial height posts are calculated, and the numerical results are verified by comparing to results obtained using the finite element method. It has been

demonstrated that the modal analysis techniques have great potential to become a design tool for waveguide combline filters and diplexers due to the advantages of both accuracy and calculation efficiency.

References

[1] C. Wang, H. Yao and K. A. Zaki, "Modeling of conductor-loaded resonators and filters in rectangular enclosures," *IEEE Trans. Microwave Theory Tech.*, vol. MTT-45, pp. 2479-2485, Dec. 1997.

[2] Y. Rong and K. A. Zaki, "Full-wave analysis of coupling between cylindrical combline resonators," *IEEE Trans. Microwave Theory Tech.*, vol. MTT-47, pp. 1721-1729, Sept. 1999.

[3] C. Wang *et al*, "Mixed modes cylindrical planar dielectric resonator filters with rectangular enclosure," *IEEE Trans. Microwave Theory Tech.*, vol. MTT-43, pp. 2817-2823, Dec. 1995.

[4] R. Levy, H. Yao and K. A. Zaki, "Transitional combline/ evanescent-mode microwave filters," *IEEE Trans. on Microwave Theory Tech.*, vol. MTT-45, pp. 2094-2099, Dec. 1997.

[5] K. Hano, H. Kohriyama and K. I. Sawamoto, "A direct-coupled λ/4 coaxial resonator bandpass filter for land mobile communications," *IEEE Trans. on Microwave Theory Tech.*, vol. MTT-34, pp. 972-976, Sept. 1986.

[6] C. Wang *et al.*, "Coaxial and combline elliptic function filters for base station applications," *Wireless Technology' 95 Conference Proceedings.* pp. 319-323, Sept. 1995.

[7] A. Fukasawa, "Analysis and composition of a new microwave filter configuration with inhomogeneous dielectric medium," *IEEE Trans. on Microwave Theory Tech.,* vol. MTT-30, pp.1367-1375, Sept. 1982.

[8] M. Sugawara, M. Makimoto and S. Yamashita, "A design mathod of bandpass filters using dielectric-filled coaxial resonators," *IEEE Trans. on Microwave Theory Tech.,* vol. MTT-33, pp. 152-157, 1985.

[9] R. Levy, "Simplified analysis of inhomogeneous dielectric block combline filters," *in 1990 IEEE MTT-S, Int. Microwave Symp. Dig.,* pp. 135-138.

[10] C. You, C. Huang and C. Wei, "Single-block ceramic microwave bandpass filters," *Microwave J.,* pp.24-35, Nov. 1994.

[11] C. Wang, K. A. Zaki, A.E. Atia and T.G. Dolan, "Dielectric combline resonators and filters," *IEEE Trans. on Microwave Theory Tech.,* vol. MTT-46, pp.2501-2506, Dec. 1998.

[12] K.-L. Wu, R. R. Mansour and H. Wang, "A full wave analysis of a conductor post insert reentrant coaxial resonator in rectangular waveguide combline filters," 1996 *IEEE MTT-S Int. Microwave Symp. Digest,* vol. 3, pp. 1639-1642.

[13] C. Wang and K. A. Zaki, "Temperature compensation of combline resonators and filters," 1999 *IEEE MTT-S Int. Microwave Symp. Digest,* vol. 3, pp. 1041-1044.

[14] H. Yao *et al*, "Improvement of spurious performance of combline filters," 1997 *IEEE MTT-S Int. Microwave Symp. Digest,* vol. 3, pp. 1099-1102.

[15] G. L. Matthaei, "Combline band-pass filters of narrow or moderate bandwidth," *The Microwave J.,* vol. 6, pp. 82-91, 1963.

[16] S. Cohn, "Direct-coupled-resonator filters," *Proc. IRE,* vol.45, pp. 187-196, Feb. 1957.

[17] L. Matthaei, L. Young and E. M. *Jones, Microwave Filters Impedance Matching Networks, and Coupling Structures.* New York: McGraw-Hill, 1964.

[18] R. M. Kurzrok, "Design of combline band-pass filters," *IEEE Trans. on Microwave Theory Tech.,* vol. MTT-14, pp. 351-353, Sept. 1966.

[19] R. M. Kurzrok, "General four-resonator filters at microwave frequencies," *IEEE Trans. on Microwave Theory Tech.,* vol. MTT-14, pp. 295-297, 1966.

[20] R. M. Kurzrok, "General three-resonator filters in waveguide," *IEEE Trans. on Microwave Theory Tech.,* vol. MTT-14, pp. 46-47, Jan. 1966.

[21] X. Liang and K. A. Zaki, "Modeling of cylindrical dielectric resonators in rectangular waveguide," *IEEE Trans. on Microwave Theory Tech.,* vol. MTT-41, pp. 2174-2181, Dec. 1993.

[22] X. Liang, *Modeling of Dual Mode Dielectric resonator Filters and Multiplexers,* Chapter 3, Ph. D. dissertation, The University of Maryland, 1993.

[23] R. Gesche and N. Löchel, "Scattering by a lossy dielectric cylinder in a rectangular waveguide," *IEEE Trans. on Microwave Theory Tech.,* vol. MTT-36, pp. 137-144, Jan. 1988.

[24] H. Yao *et al.,* " Full wave modeling of conducting posts in rectangular waveguides and its applications to slot coupled combline filters," *IEEE Trans. on Microwave Theory Tech.,* vol. MTT-43, pp. 2824-2829, Dec. 1995.

[25] H. Yao, *EM Simulation of Resonant and Transmission Structures – Applications to Filters and Multiplexers,* Chapt. 3, Ph. D. dissertation, The University of Maryland, 1995.

[26] G. Mur, "Finite difference method for the solution of electromagnetic waveguide discontinuity problem," *IEEE Trans. Microwave Theory Tech.,* vol. MTT-22, pp. 54-57, Jan. 1974.

[27] M. Koshiba and M. Suzuki, "Finite-element analysis of H-plane waveguide junction with arbitrarily shaped ferrite post," *IEEE Trans. Microwave Theory Tech.,* vol. MTT-34, pp. 103-109, Jan. 1986.

[28] F. Moglie, T. Rozzi and P. Marcozzi, "Wideband matching of waveguide discontinuities by FDTD methods," *IEEE Trans. on Microwave Theory Tech.,* vol. MTT-42, pp. 2093-2098, Nov. 1994.

[29] J. Ritter and F. Arndt, "Efficient FDTD/ matrix-pencil method for the full-wave scattering parameter analysis of waveguide structures," *IEEE Trans. on Microwave Theory Tech.,* vol. MTT-44, pp. 2450-2456, Dec. 1996.

[30] H. Yao and K. A. Zaki, "Modeling of generalized coaxial probes in rectangular waveguides," *IEEE Trans. on Microwave Theory Tech.,* vol. MTT-43, pp. 2805-2811, Dec. 1995.

[31] H. Yao, J. Liang and K. A. Zaki, "Accuracy of coupling computation and its application to DR filter design," *1994 IEEE MTT-S Int. Microwave Symp. Digest,* pp. 723-726.

[32] K. Shamsaifar, "Designing iris coupled waveguide filters using the mode matching technique," *Microwave Journal,* vol. 35, pp. 156-164, Jan. 1992.

[33] C. Wang and K. A. Zaki, "Modeling of coupling between double-ridge waveguide and dielectric-loaded resonator", *IEEE Trans. Microwave Theory Tech.,* vol. MTT-46, pp. 2404-24, Dec. 1998.

[34] R. Mittra and S. W. Lee, *Analytical techniques in the theory of guided waves,* The Macmillan Company, New York, 1971.

[35] R. F. Harrington, *Time-Harmonic electromagnetic fields,* McGraw-Hill Book Co., 1961.

[36] T. Itoh, *Numerical techniques for microwave and millimeter-wave passive structures,* John Wiley & Sons, Inc., 1989.

[37] H. Patzelt and F. Arndt, "Double planar steps in rectangular waveguides and their application for transformers, irises and filters," *IEEE Trans. on Microwave Theory Tech.,* vol. MTT-30, pp. 771-776, 1982.

[38] H. Wang, K.-L. Wu and J. Litva, "The higher order modal characteristics of circular-rectangular coaxial waveguides", *IEEE Trans. Microwave Theory Tech.,* vol. 45, pp. 414-419, Mar. 1997.

[39] L. Gruner, "Higher order modes in rectangular coaxial waveguides," *IEEE Trans. Microwave Theory Tech.*, vol. MTT-15, pp. 483-485, Aug. 1967.

[40] Q. C. Tham, "Modes and cutoff frequencies of crossed rectangular waveguides," *IEEE Trans. Microwave Theory Tech.,* vol. MTT-25, pp. 585-588, July 1977.

[41] F. Alessadri, M. Mongiardo, and R. Sorrentino, "Computer-aided design of beam forming networks for modern satellite antennas," *IEEE Trans. Microwave Theory Tech.*, vol. 40, pp. 1117-1127, June 1992.

[42] K.-L. Wu and R. H. Macphie, "A rigorous analysis of a cross waveguide to large circular waveguide junction and its application in waveguide filter design," *IEEE Trans. Microwave Theory Tech.*, to be published.

[43] A. S. Omar and K. F. Schünemann, "Application of the generalized spectral-domain technique to the analysis of rectangular waveguides with rectangular and circular metal inserts," *IEEE Trans. Microwave Theory Tech.*, vol. 39, pp. 944-952, June 1991.

[44] V. A. Labay and J. Bornemann, "Singular value decomposition improves accuracy and reliability of T-septum waveguide field-matching analysis," *Int. J. Microwave Millimeter-Wave Computer-Aided Eng.*, vol. 2, no. 2, pp. 82-88, 1992.

[45] C. T. Carson, "The Numerical solution of TEM mode transmission lines with curved boundaries", *IEEE Trans. Microwave Theory Tech.*, vol. 15, pp. 269-270, April 1967.

[46] M. M. Taheri and D. Mirshekar-Syahkal, "Accurate determination of modes in dielectric loaded cylindrical cavities using a one-dimensional finite element method," *IEEE Trans. on Microwave Theory Tech.*, vol. 37, pp. 1536-1541, Oct. 1989.

[47] S. Frankel, "Characteristic impedance of parallel wires in rectangular troughs," *Proc. I.R.E.*, vol. 30, pp. 182-190, April 1942.

[48] R. M. Chisholm : "The characteristic impedance of trough and slab lines", *IRE Trans. Microwave Theory Tech.,* vol. 4, pp. 166-173, July 1956.

[49] W. Lin, "A critical study of the coaxial transmission line utilizing conductors of both circular and square cross section", *IEEE Trans. Microwave Theory Tech.,* vol. 30, No. 11, pp. 1981-1988, Nov. 1982.

[50] H. A. Wheeler, "Transmission-line properties of a round wire in a polygon shield", *IEEE Trans. Microwave Theory Tech.,* vol. 27, No. 8, pp. 717-721, Aug. 1979.

[51] E. G. Cristal, "Characteristic impedance of coaxial lines of circular inner and rectangular outer conductors", *Proc. IEEE,* vol. 52, pp. 1265-1266, Oct. 1964.

[52] E. G. Cristal, "Coupled circular cylindrical rods between parallel ground planes ", *IEEE Trans. Microwave Theory Tech.,* vol. 12, pp. 428-439, July 1964.

[53] J. Bornemann, S. Amari and R. Vahldieck, "A combined mode-matchine and coupled-integral-equations technique for the design of narrow-band H-plane waveguide diplexers." IEEE International Antenna & Propag. Symposium, vol.2, pp.950-953, 1999.

[54] A. A. Kirilenko, S. L. Senkevich, V. I. Tkachenko, and B. G. Tysik, "Waveguide diplexer and multiplexer design," IEEE Trans. Microwave Theory Tech., vol. MTT-42, pp.1393-1194, July, 1994.

[55] J. D. Rhodes and R. Levy, "Design of general manifold multiplexers," IEEE Trans. Microwave Theory Tech., vol. MTT-27, pp.111-123, Feb. 1979.

[56] J. Hirokawa, K. Sakruai, M. Ando and N. Goto, "An analysis of a waveguide T junction with an inductive post," IEEE Trans. Microwave Theory Tech., vol. MTT-39, pp563-566, March 1991.

[57] E. K*ü*hn, " A mode-matching method for solving field problems in waveguide and resonator circuits," *Arch. Elek. Ü bertragung.,* vol.. 27, pp. 511-518, Dec. 1973.

[58] F. Arndt *et al.*, "Optimized E-plane T-junction series power dividers," *IEEE Trans. on Microwave Theory Tech.,* vol. MTT-35, pp. 1052-1059, Nov. 1987.

[59] E. D. Sharp, "An exact calculation for a T-junction of rectangular waveguide having arbitrary cross sections," *IEEE Trans. on Microwave Theory Tech.,* vol. MTT-15, pp. 109-116, Feb. 1967.

[60] J. M. Rebollar, J. Esteban and J. E. Page, "Fullwave analysis of three and four-port rectangular waveguide junctions," *IEEE Trans. on Microwave Theory Tech.,* vol. MTT-42, pp. 256-263, Feb. 1994.

[61] H. Wang, K. Wu and J. Litva, "A modal analysis of TEM mode in circular-rectangular coaxial waveguides," *IEEE Trans. on Microwave Theory Tech.,* vol. MTT-47, pp. 356-359, March 1999.

[62] X. Liang, K. A. Zaki and A. E. Atia, "A rigorous three plane mode-matching technique for characterizing waveguide T-junctions, and its application in multiplexer design," *IEEE Trans. on Microwave Theory Tech.,* vol. MTT-39, pp. 2138-2146, Dec. 1991.

[63] K. Wu and H. Wang, "A rigorous modal analysis of H-plane waveguide T-junction loaded with a partial height post for wide band application," *IEEE Trans. on Microwave Theory Tech.*, vol. MTT-49, pp. 893-901, May 2001.

[64] A. S. Omar and K. Schünemann, "Analysis of waveguides with metal inserts," *IEEE Trans. Microwave Theory Tech.*, vol. 37, pp. 1924-1932, Dec. 1989.

[65] D. M. Pozar *Microwave Engineering, Addison Wesley,* 1993. chapter 3 and chapter 4, pp. 71 – 172.

Publications:

1. Haiyin Wang, Ke-Li Wu and John Litva, "The higher order modal characteristics of circular-rectangular coaxial waveguides", *IEEE Trans. Microwave Theory Tech.,* vol. 45, pp. 414-419, Mar. 1997.
2. Haiyin Wang, Ke-Li Wu and John Litva, "A modal analysis of TEM mode in circular-rectangular coaxial waveguides," *IEEE Trans. on Microwave Theory Tech.,* vol. MTT-47, pp. 356-359, March 1999.
3. K-L.Wu and H. Wang, "A rigorous modal analysis of H-plane waveguide T-junction loaded with a partial height post for wide band application," *IEEE Trans. on Microwave Theory Tech.,* vol. MTT-49, pp. 893-901, May 2001.
4. K-L. Wu, R. R. Mansour and H. Wang, "A full wave analysis of a conductor post insert reentrant coaxial resonator in rectangular waveguide combline filters," 1996 *IEEE MTT-S Int. Microwave Symp. Digest,* vol. 3, pp. 1639-1642.
5. H. Wang, K. Wu and J. Litva, "A modal solution of TEM mode in circular-rectangular waveguides", International Symposium on Antenna and EM Theory, Xian, China , Aug. 1997.
6. H. Wang, K. Wu and J. Litva, "The analysis of higher-order modes and cutoff frequencies in circular-rectangular coaxial waveguides using SVD technique," *IEEE* 1998 *APS International Symposium*, vol.3, pp. 1500-1503.